# Nanoparticle-Stabilized $CO_2$ Foam for $CO_2$ EOR Application

Final Report

Submitted by

New Mexico Petroleum Recovery Research Center,
New Mexico Institute of Mining and Technology
Socorro, New Mexico 87801

**Ning Liu**

Prepared for

U.S. Department of Energy
National Energy Technology Laboratory
(Project Number: DE-FE-0005979)

Report Date: April 30, 2015

## Disclaimer

# Acknowledgement

This research was sponsored by the U.S. Department of Energy through the National Energy Technology Laboratory (grant # DE-FE-0005979).

The contributions of the project team members and graduate students are greatly appreciated. They are Dr. Robert Lee, Dr. Jianjia Yu, Dr. Liangxiong Li, Ms. Liz Bustamante, Mr. Munawar Khalil, Mr. Di Mo, Mr. Bao Jia, Mr. Sai Wang, Mr. Jingshan San, Mr. Cheng An. We would like to thank Elizabeth Bustamante for aiding in the preparations of this manuscript.

# Abstract

The practice of injecting $CO_2$ for oil recovery was initiated in the 1950s. Today, $CO_2$ flooding is an established technique to improve oil production, and $CO_2$ capture and storage in deep geologic formations is being studied for mitigating carbon emissions. Ultimate incremental oil recovery from $CO_2$ floods in the U.S. is estimated to be 8 to 15 billion bbl, depending on oil prices and economic incentives. However, because the mobility of $CO_2$ is high compared to that of oil, $CO_2$ channeling and early breakthrough often occur in $CO_2$ enhanced oil recovery (EOR) processes, which results in increased gas processing costs and/or reduced oil production. Thus, the need for mobility control during $CO_2$ flooding is highly desirable. A basic principle of mobility control during $CO_2$ flooding is that the mobility of $CO_2$ flowing through a porous medium is lowered when $CO_2$ is dispersed within a surfactant solution, forming foam. However, surfactant-stabilized $CO_2$ foams have some potential weaknesses. Because foam is by nature ultimately unstable, its long-term stability during a field application is difficult to maintain.[2] This is especially true when the foam contacts the resident oil. Under high-temperature reservoir conditions, surfactants generally tend to degrade before they fulfill their long-term duty, even the expensive specialty surfactants that are available. In addition, surfactant loss in a reservoir due to adsorption in the porous medium results in a large consumption of chemicals in $CO_2$ foam flooding, and is thus a major feature governing the economic viability of $CO_2$ foam flooding.

New technologies developing in nanoscience provided an alternative for the generation of stable $CO_2$ foam. It is known that small solid particles can adsorb at fluid/fluid interfaces to stabilize drops in emulsions and bubbles in foams without surfactant molecules. The solid-stabilized dispersions may stay stable for years upon storage. Nanoparticle-stabilized $CO_2$ foam is a new

technology in $CO_2$-EOR, in which solid nanoparticles instead of surfactants adsorb at the water–$CO_2$ interface and create a rigid protective barrier around each dispersed drop.

The purpose of this project was to develop nanoparticle-stabilized $CO_2$ foam for $CO_2$ -EOR application, in which nanoparticles instead of surfactants are used for stabilizing $CO_2$ foam to improve the $CO_2$ sweep efficiency and increase oil recovery. The studies included: (1) investigation of $CO_2$ foam generation nanoparticles, such as silica nanoparticles, and the effects of particle concentration and surface properties, $CO_2$/brine ratio, brine salinity, pressure, and temperature on foam generation and foam stability; (2) coreflooding tests to understand the nanoparticle-stabilized $CO_2$ foam for waterflooded residual oil recovery, which include: oil-free coreflooding experiments with nanoparticle-stabilized $CO_2$ foam to understand the transportation of nanoparticles through the core; measurements of foam stability and $CO_2$ sweep efficiency under reservoir conditions to investigate temperature and pressure effects on the foam performance and oil recovery as well as the sweep efficiency in different core samples with different rock properties; and (3) long-term coreflooding experiments with the nanoparticle-stabilized $CO_2$ foam for residual oil recovery. Finally, the technical and economical feasibility of this technology was evaluated.

Our completed research has resulted in deep understanding of $CO_2$ flooding and mobility control. $CO_2$ foam could be generated with the aid of nanosilica dispersion in both static and dynamic conditions. The selected nanosilica dispersion in this project displayed excellent ion and temperature resistivity. The silica nanoparticles could easily pass through the sandstone and limestone cores without changing the core permeability.

It was observed that changing the surface properties of particles resulted in more stable $CO_2$ foam being generated, with the aid of some hydrophobic particles. Coreflooding tests indicated

that stable $CO_2$-foams were generated at reservoir conditions as liquid $CO_2$ and nanosilica mixture flowed through a porous media. $CO_2$ foam could be generated with the nanosilica concentration as low as 500 ppm. With the increase of nanosilica concentration, foam mobility decreased and the foam resistance factor increased. The $CO_2$ foam mobility remained almost constant as the foam quality increased from 20% to 60% and then increased with further increase in foam quality. A synergistic interaction between the surfactant and nanosilica particles was observed as $CO_2$/nanosilica dispersion + surfactant flowed through porous media for $CO_2$ foam generation. This result indicates that low-concentration nanoparticle and surfactant mixture can be used in the future for $CO_2$ mobility control. Nanoparticle-stabilized $CO_2$ foam was observed to improve the residual oil recovery. The residual oil recovery (percent of waterflooded residual oil) by $CO_2$/nanosilica flooding increased when the pressure was increased from 1,200 psi to 2,500 psi and decreased when the temperature increased from 25°C to 60°C. Nanoparticle-stabilized $CO_2$ foam also improved residual oil recovery from limestone and dolomite after waterflooding. Core permeability was observed to decrease for dolomite after the test. Long-term coreflooding test of nanoparticle-stabilized $CO_2$ foam for residual oil recovery indicated that after 20 PV of $CO_2$/nanosilica dispersion were injected into the core, total nanoparticles recovery during $CO_2$/nanosilica dispersion flooding was ~95.3%. No significant core permeability change was observed, indicating no particle plugging occurred during the long-term coreflooding. Small-volume $CO_2$/nanosilica dispersion coreflooding tests displayed that ~32% oil was recovered when the core was flooded with 1 PV $CO_2$/nanosilica dispersion.

# Table of Contents

# List of Figures

# List of Tables

## Executive Summary

This document is the Final Report for the U.S. Department of Energy under contract No. DE-FE-0005979, a three-year contract with a no-cost extension entitled: "Nanoparticle-Stabilized $CO_2$ Foam for $CO_2$ EOR Application." The research improved our knowledge and understanding of $CO_2$ flooding and includes work in the areas of $CO_2$ foam generation and foam stability, mobility control, and residual oil recovery. The bulk of this work has been performed by the New Mexico Petroleum Recovery Research Center, a research division of New Mexico Institute of Mining and Technology. This report covers the reporting period of October 1, 2010 through January 31, 2015.

This report summarizes the work completed under the above-mentioned contract. This document does not attempt to detail all the work that has been completed. Much of the work from this project has been reported in the previous quarterly reports and various publications, and thus will not be duplicated here, but generally only summarized for the previously published work.

Chapter 1 introduces the background of this project and a brief summary of the statement of work.

Chapter 2 summarizes $CO_2$ foam generation at static conditions with the aid of nanosilica particles. Coarse CO2 bubbles were formed as liquid $CO_2$ slowly passed through a nanosilica dispersion. Particle concentration, brine salinity, pressure, and temperature effects on the $CO_2$ foam generation were discussed.

Chapter 3 summarizes the results of nanoparticle-stabilized $CO_2$ foam generation at dynamic conditions. A series of flow experiments on the simultaneous injection of $CO_2$ and nanosilica solution through a porous glass beads column were conducted. Stable and dense $CO_2$ foam was

generated at dynamic conditions. Particle surface properties such as the effect of wettability on $CO_2$ foam generation and foam stability were investigated.

Chapter 4 summarizes the transport behavior of nanoparticle in three different rocks: sandstone, limestone, and dolomite. Silica nanoparticles could easily pass through the sandstone core without changing the core permeability. Little adsorption was observed as nanosilica particles flooded the limestone core, but the core permeability was not changed. Core plugging occurred and core permeability was changed as the particles flowed through dolomite core.

Chapter 5 summarizes nanosilica-stabilized $CO_2$ foam generation during the coreflooding tests. Very stable and dense $CO_2$ foam was formed as liquid $CO_2$ and nanosilica dispersion were flowed through a sandstone core. $CO_2$ foam could be generated with the nanosilica concentration as low as 500 ppm. With the increase of nanosilica concentration, foam mobility decreased and the foam resistance factor increased. $CO_2$ foam mobility increased as the foam quality increased from 70% to 95%. As the total flow rate increased, the $CO_2$ foam mobility decreased first and then leveled off.

Chapter 6 summarizes the effects of different surfactants (cationic, anionic, and non-ionic surfactants) on nanosilica-stabilized $CO_2$ foam generation and foam stability. A synergistic interaction between the surfactant and nanosilica particles was observed as $CO_2$/nanosilica dispersion + surfactant flowed through porous media for $CO_2$ foam generation.

Chapters 7 and 8 summarize nanosilica-stabilized $CO_2$ foam for waterflooded residual oil recovery. Nanoparticle-stabilized $CO_2$ foam was observed to improve the residual oil recovery. The residual oil recovery (percent of waterflooded residual oil) by $CO_2$/nanosilica flooding increased when the pressure was increased from 1,200 psi to 2,500 psi and decreased when the temperature increased from 25°C to 60°C. Large and small volume $CO_2$/nanosilica dispersion coreflooding tests indicated that 30–39% oil could be recovered by the $CO_2$ foam.

Chapter 9, “Technology Transfer,” summarizes the numerous papers, reports, and presentations as a result of research performed under this contract.

# 1. INTRODUCTION

## 1.1 $CO_2$ flooding for enhanced oil recovery

The practice of injecting $CO_2$ for oil recovery was initiated in the 1950s. Today, $CO_2$ flooding is an established technique to improve oil production, and $CO_2$ capture and storage in deep geologic formations is being studied for mitigating carbon emissions. Ultimate incremental oil recovery from $CO_2$ floods in the U.S. is estimated to be 8 to 15 billion bbl, depending on oil prices and economic incentives.[1] However, because the mobility of $CO_2$ is high compared to that of oil, $CO_2$ channeling and early breakthrough often occur in $CO_2$ enhanced oil recovery (EOR) processes, which results in increased gas processing costs and/or reduced oil production. Thus, the need for mobility control during $CO_2$ flooding is highly desirable. A basic principle of mobility control during $CO_2$ flooding is that the mobility of $CO_2$ flowing through a porous medium is lowered when $CO_2$ is dispersed within a surfactant solution, forming foam. However, surfactant-stabilized $CO_2$ foams have some potential weaknesses. Because foam is by nature ultimately unstable, its long-term stability during a field application is difficult to maintain.[2] This is especially true when the foam contacts the resident oil. Under high-temperature reservoir conditions, surfactants generally tend to degrade before they fulfill their long-term duty, even the expensive specialty surfactants that are available. In addition, surfactant loss in a reservoir due to adsorption in the porous medium results in a large consumption of chemicals in $CO_2$ foam flooding, and is thus a major feature governing the economic viability of $CO_2$ foam flooding.

## 1.2 Nanoparticles as $CO_2$ foam stabilizer

New technologies developing in nano-science may provide an alternative for the generation of stable $CO_2$ foam. It is known that small solid particles can adsorb at fluid/fluid interfaces to stabilize drops in emulsions and bubbles in foams without surfactant molecules.[3-6] The solid-stabilized dispersions may stay stable for years upon storage. A wide variety of mineral powders can be employed to stabilize such emulsions, e.g., iron oxide, hydroxides, metal sulfates, silica, clays and carbon. As schematically shown in Fig. 1.1,[7] the solid particles can adsorb at an interface between aqueous and nonaqueous phases, becoming surface-active. For hydrophilic particles, e.g. metal oxides, the contact angle ($\theta$) that the nonaqueous/aqueous phase interface makes with the particle surface is normally $< 90^o$ and a larger fraction of the particle surface

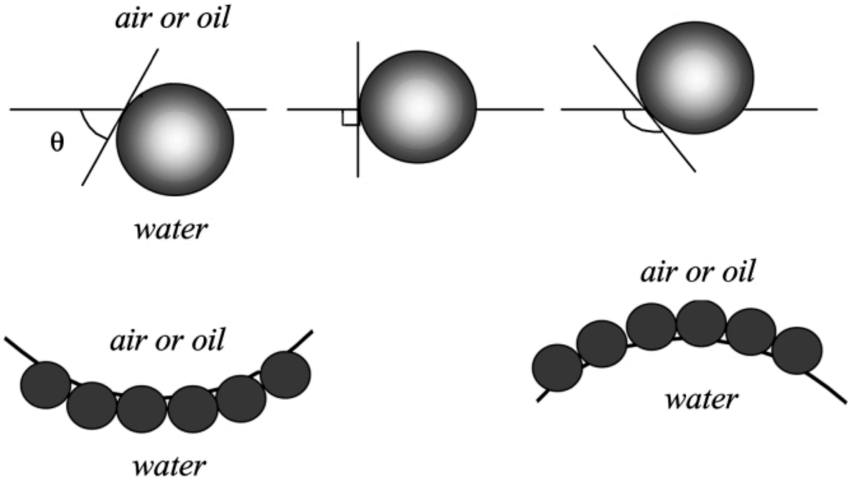

**Fig. 1.1 (Upper) Position of a small spherical particle at a planar fluid-water interface For a contact angle less than 90° (left), equal to 90° (center) and greater than 90° (right). (Lower) Corresponding probable positioning of particles at a curved fluid-water interface. For θ<90°, solid-stabilized aqueous foams or w/o emulsions may form (left). For θ>90°, Solid-stabilized aerosols or w/o emulsions may form (right).**

resides in water than in the nonaqueous phase so that stable water–external emulsions are formed. For hydrophobic particles, such as suitably surface-treated silica, $\theta$ is normally greater than $90^o$ and the particle resides more in air or oil than in water, so that water–internal emulsions are formed.

Nanoparticle-stabilized $CO_2$ foam, compared with conventional surfactant-induced $CO_2$ foam, has several critical advantages:

1. The most important advantage of using nanoparticles to stabilize $CO_2$ foam is the good long-term foam stability that will be achieved, due to the high adhesion energy for particle adsorption at the foam interface. When a particle is adsorbed and held at a nonaqueous/aqueous phase interface, the energy of adhesion for the particle is calculated[8] as $\Delta G_{ad} = \pi\alpha^2\gamma_{ow}(1-|cos\theta|)^2$, where $\alpha$ is the particle radius; $\gamma_{ow}$ is the interfacial tension; and $\theta$ is the contact angle through the aqueous phase. Simple calculations with typical particle parameters show that the adhesion energy is of the order of several thousands of $k_BT$, which is much larger than the adsorption and desorption energy for a typical surfactant molecule at an oil-water interface (which is of the order of $k_BT$).

2. As nanoparticles are solid, the nanoparticle-stabilized $CO_2$ foams also have potential to withstand high-temperature and/or high-salinity reservoir conditions for extended periods.

3. The high retention of surfactant in reservoir rock is a problem for surfactant-stabilized $CO_2$ foam, but the retention of nanoparticles with an appropriate surface coating in reservoir rock appears to be slight.[9]

### 1.3 Statement of Work

The purpose of this project is to develop nanoparticle-stabilized $CO_2$ foam for $CO_2$ -EOR application, in which nanoparticles instead of surfactants are used for stabilizing $CO_2$ foam to improve the $CO_2$ sweep efficiency and increase oil recovery. The studies in Phase 1 of this project included: Investigate $CO_2$ foam generation nanoparticles, such as silica nanoparticles, and the effects of particle concentration and surface properties, $CO_2$/brine ratio, brine salinity, pressure, and temperature on foam generation and foam stability. In Phase 2, research focused on coreflooding tests to understand the nanoparticle-stabilized $CO_2$ foam for waterflooded residual oil recovery, which included: perform oil-free coreflooding experiments with nanoparticle-stabilized $CO_2$ foam to understand the transportation of nanoparticles through the core; measure foam stability and $CO_2$ sweep efficiency under reservoir conditions to investigate temperature and pressure effects on the foam performance and oil recovery as well as the sweep efficiency in different core samples with different rock properties. In Phase 3, long-term coreflooding experiments with the nanoparticle-stabilized $CO_2$ foam for residual oil recovery were carried out and evaluation of the technical and economical feasibility of this technology for future field application was performed.

### 1.4 Layout of the Report

This research aims to develop nanoparticle-stabilized $CO_2$ foam for $CO_2$ –EOR. The research improved our knowledge and understanding of $CO_2$ flooding and includes work in the areas of $CO_2$ foam generation and foam stability, mobility control, and residual oil recovery.

Chapter 1 introduces the background of this project and a brief summary of the statement of work.

Chapter 2 summarizes $CO_2$ foam generation at static conditions with the aid of nanosilica particles. Coarse $CO_2$ bubbles were formed as liquid $CO_2$ slowly passed through a nanosilica dispersion. Particle concentration, brine salinity, pressure, and temperature effects on the $CO_2$ foam generation were discussed.

Chapter 3 summarizes the results of nanoparticle-stabilized $CO_2$ foam generation at dynamic conditions. A series of flow experiments on the simultaneous injection of $CO_2$ and nanosilica solution through a porous glass beads column were conducted. Stable, dense $CO_2$ foam was generated at dynamic conditions. Particle surface property such as the effect of wettibility on $CO_2$ foam generation and foam stability was investigated.

Chapter 4 summarizes the transport behavior of nanoparticle in three different rocks —sandstone, limestone, and dolomite. Silica nanoparticles could easily pass through the sandstone core without changing the core permeability. Little adsorption was observed as nanosilica particles flooded the limestone core, but the core permeability was not changed. Core plugging occurred and core permeability was changed as the particles flowed through dolomite core.

Chapter 5 summarizes nanosilica-stabilized $CO_2$ foam generation during the coreflooding tests. Very stable and dense $CO_2$ foam was formed as liquid $CO_2$ and nanosilica dispersion were flowed through a sandstone core. $CO_2$ foam could be generated with the nanosilica concentration as low as 500 ppm. With the increase of nanosilica concentration, foam mobility decreased and the foam resistance factor increased. The $CO_2$ foam mobility increased as the foam quality increased from 70% to 95%. As the total flow rate increased, the $CO_2$ foam mobility decreased first and then leveled off.

Chapter 6 summarizes different surfactants (cationic, anionic, and non-ionic surfactants) effects on nanosilica-stabilized $CO_2$ foam generation and foam stability. A synergistic interaction between the surfactant and nanosilica particles was observed as $CO_2$/nanosilica dispersion + surfactant flowed through a porous media for $CO_2$ foam generation.

Chapters 7 and 8 summarize nanosilica-stabilized $CO_2$ foam for waterflooded residual oil recovery. Nanoparticle-stabilized $CO_2$ foam was observed to improve the residual oil recovery. The residual oil recovery (percent of waterflooded residual oil) by $CO_2$/nanosilica flooding increased when the pressure was increased from 1,200 psi to 2,500 psi and decreased when the temperature increased from 25°C to 60°C. Large and small volume $CO_2$/nanosilica dispersion coreflooding tests indicated that 30–39% oil could be recovered by $CO_2$ foam.

Chapter 9, "Technology Transfer," summarizes the numerous papers, reports, and presentations as a result of research performed under this contract.

# 2, Nanoparticle-stabilized $CO_2$ foam generated at static conditions

This chapter describes how $CO_2$ foam generation at static condition was investigated. Here the static condition refers to liquid $CO_2$ bubbles passing through static nanoparticle dispersion at a slow flow rate. Factors such as particle concentration, brine salinity, pressure, and temperature effects on the foam generation and foam stability were addressed.

## 2.1 Materials and equipment

### *2.1.1 Preparation of nanosilica dispersions*

Silica powder purchased from Sigma was used for this study. To prepare the dispersion phase, a quantity of water was poured into a blender and some silica particles (different concentration) were placed on top. This was mixed at high speed for 5 min, then moved to an ultrasonic bath for 1 hour of dispersion. Finally, the solution was placed in a vacuum chamber overnight to remove the soluble air.

### *2.1.2 Silica nanoparticle characterization*

Different techniques were deployed to characterize nanosilica particle morphology and size distribution. An X-ray diffraction study of the nanoparticles was carried out using a PANalytical X'Pert Pro diffractometer equipped with PIXcel detector (PANalytical B.V., Almelo, Netherlands). The measurements were performed on zero-background silicon plates with the diffraction angle from 6° to 70° using Cu K$\alpha$ radiation. Data were collected using X'Pert Data Collector software and processed using X'Pert HighScore Plus (PANalytical B.V.). The morphology of the particle was characterized by scanning electron microscope (SEM, JEOL 5800LV) and Hi-Resolution Transmission Electron Microscope (HRTEM, JEOL 2010). The hydrodynamic particle size was determined by Microtrac Zetatrac (Model NPA152-31A), a dynamic light scattering (DLS) analyzer.

### *2.1.3 $CO_2$ foam generation at static condition*

An experiment setup for $CO_2$ foam generation was constructed in the laboratory. The apparatus includes a $CO_2$ tank, an ISCO pump, a sapphire observation tube, temperature and pressure controllers, and valves. Figure 2.1 shows the schematic diagram of the $CO_2$ foam generation apparatus. Before the test, the tubing was cleaned by opening valves 5, 6, and 7. Then the sapphire observation cell was filled with test solution. The heating loop was checked and the water bath temperature set at 25°C. After the temperature reached the set point, the system was allowed to sit for at least 10 minutes. The ISCO $CO_2$ refill pump was used to adjust $CO_2$ pressure to 1500 psi and the pressure differential gauge was set to zero, as the pressure in the aqueous phase and $CO_2$ were equalized. Valve 10 at the bottom of the water tank was opened to allow $CO_2$ to flow into the test solution. The Ruska pump was then run backward, causing the withdrawal of the test solution from the sapphire cell into the solution storage cylinder. As the solution was withdrawn from the sapphire cell, a liquid $CO_2$ bubble was produced and drawn upward through a needle at the bottom of the cell. The $CO_2$ bubbles either formed a layer of foam at the top of the sapphire tube or coalesced into a clear layer of dense $CO_2$ depending on the test solution. After a standard volume of $CO_2$ was introduced, the pump was stopped. At the same time, the initial height of the $CO_2$ foam was measured. The stability of the $CO_2$ foam was also evaluated by measuring the decrease in foam height every 30 min. At the end of the experiment, the silica suspensions were removed from the system by partially releasing $CO_2$ pressure. The sapphire tube was then thoroughly cleaned with distilled water to prepare it for the next test.

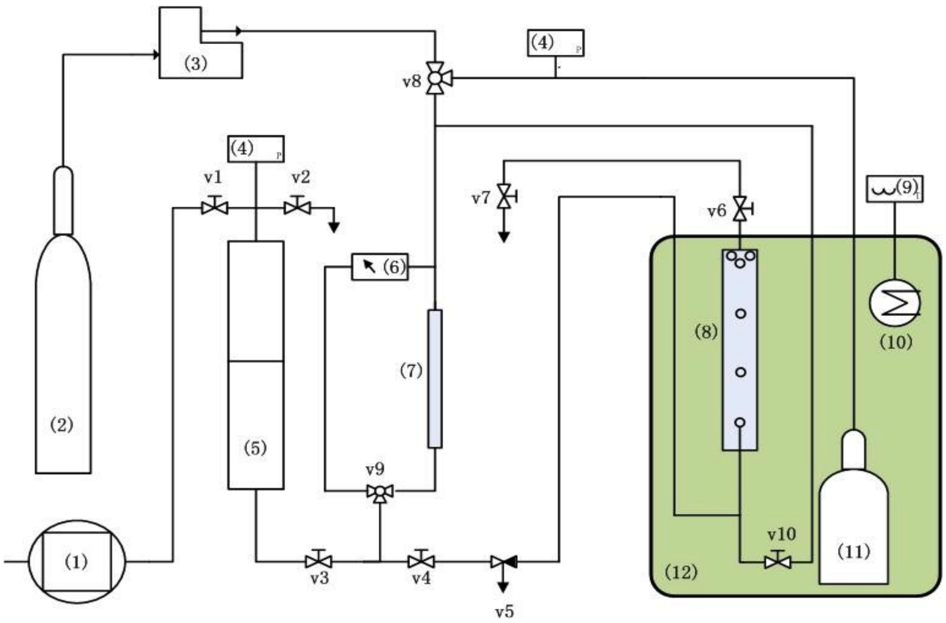

(1) Ruska pump; (2) $CO_2$ cylinder; (3) ISCO pump; (4) Pressure gauge; (5) Storage cylinder;
(6) Pressure transducer; (7) Storage cylinder, (8) Sapphire observation tube,
(9) Temperature indictor; (10) Heater control, (11) $CO_2$ tank, (12) Water bath.

**Fig. 2.1 Schematic diagram of the $CO_2$ foam generation apparatus.**

## 2.2 Results and discussion

### *2.2.1 Characterization of silica nanoparticle in dispersion*

Figure 2.2 gives the DLS results of the prepared nanosilica dispersions with silica powder from Sigma, showing that the particle diameters in were in the range of 100–150 nm. Comparing the particle size in the powder sample (10–12 nm as received), we believe that particle aggregation occurred as the particles dispersed in water. It is known that silanol (SiOH) groups are generated on the silica surface as silica particles disperse in water.[10] When the nanosilica solution is prepared, adjacent aggregates can interact via silanol-silanol hydrogen bonding giving rise to larger structures called flocs or agglomerates. On the other hand, the electrostatic repulsion (Coulombic pair interactions)[11] between silica particles prevents the particles' further aggregation. The final equilibrium between the hydrogen bonding and Coulombic interaction resulted in particle size in the dispersion of around 100–150 nm, which is consistent with other reports.[10,12] Figure 2.3 displays the TEM image of the nanosilica solution, where the network of aggregates is clearly seen.

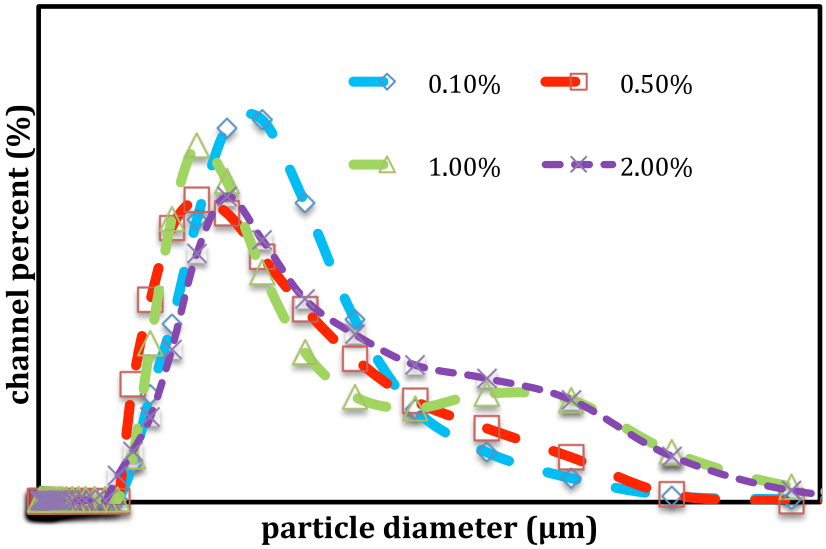

**Fig. 2.2 Particle size distribution in different nanosilica solutions.**

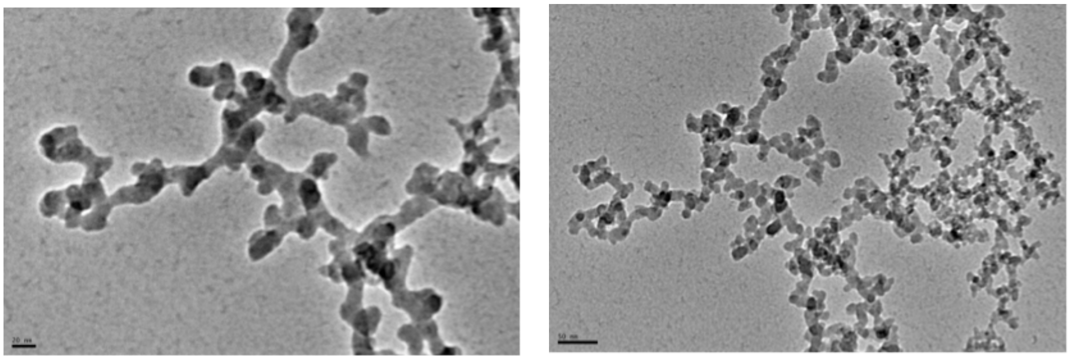

(a) (b)

**Fig. 2.3 Transmission Electron Microscope (TEM) images of nanosilica particles dispersed in water; scale bar=20 nm (a) and 50 nm (b).**

### *2.2.2 $CO_2$ foam generation with silica nanoparticles at static conditions*

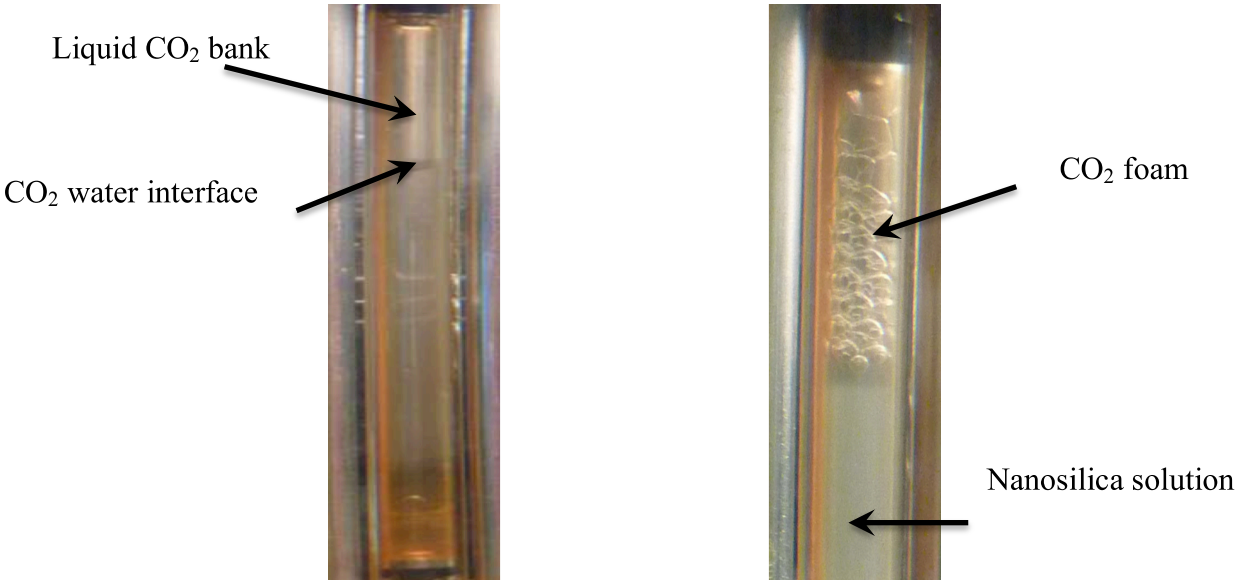

(a) DI water (b) Nanosilica solution

**Fig. 2.4 Pictures of $CO_2$ foam generated in water and nanosilica solution.**

It is known that $CO_2$ foam can be generated as nanoparticles adsorb onto the interface between $CO_2$ and water. In our experiments, as the $CO_2$ bubbles rise from the bottom of the sapphire tube, nanosilica particles can be adsorbed onto the $CO_2$/water interface. The adsorbed nanosilica decreases the surface interaction energy and stabilizes the foam. Figure 2.4 shows $CO_2$ foam generated in DI water and 0.5% nanosilica solution. No $CO_2$ foam was generated in DI water alone. We noticed that, during the experiment, as the $CO_2$ bubbles formed in the DI water, they immediately coalesced together and a $CO_2$ bank formed on the top of the sapphire tube (as seen in Fig. 2.4a). On the other hand, when nanosilica particles were introduced in the solution, the $CO_2$ bubbles were stabilized by the particle and $CO_2$ foam was formed on the top of the tube. The height of the $CO_2$ foam, which indicates the stability of the foam, was 1.25 cm when it was first generated and 0.97 cm after 90 min. The results indicate that stable $CO_2$ foam can be generated by 0.5% nanosilica solution.

### *2.2.3 Effect of particle concentration on $CO_2$ foam generation at static condtion*

To study the effects of particle concentration on $CO_2$ foam, different concentration of nanosilica solutions were prepared by dispersing nanosilica powder in deionized water (DI). Figure 2.5 shows the results of $CO_2$ foam generated in different nanosilica solutions. We observed that, as the nanosilica concentration was less than 4,000 ppm, little $CO_2$ foam was generated. When the particle concentration increased to 4,000 ppm 6,000 ppm, more $CO_2$ foam was observed in the sapphire tube. The explanation for this is, that, as the particle concentration was low, there were not enough particles to be attached completely at the interface around the $CO_2$ bubbles. When particle concentration increased, more particles could be adsorbed at the $CO_2$ bubble interface, which stabilized the produced $CO_2$ foam. We also observed that, with further increased nanoparticle concentration, the height of the generated $CO_2$ foam decreased (refer to Fig. 2.5g). By measured the particle size distribution, we found that the particle size profile was distributed more widely in high-concentration solutions (refer to Fig. 2.6). Thus, we believe that particle aggregation occurred in the highly concentrated nanoparticle solution, which inhibited $CO_2$ foam generation.

To evaluate foam stability, we measured the height of the foam remaining in the observation cell at every interval time. Figure 2.7 displays the remaining foam volume relative to the beginning produced foam volume in a 4,000 ppm nanosilica solution. The results demonstrated that, after 150 min, the generated $CO_2$ foam volume reduced only 7.0%, which revealed that the produced $CO_2$ foam with the nanoparticle was very stable.

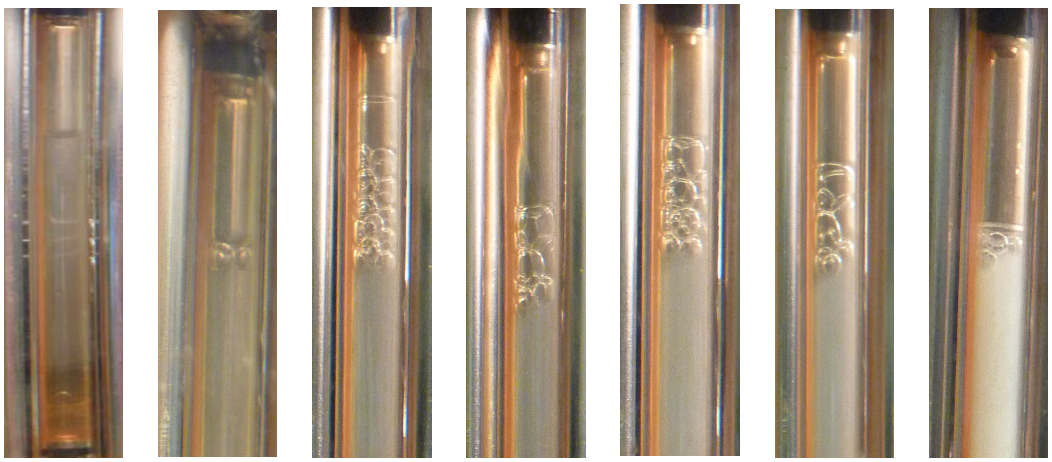

(a) 0 ppm (b) 1,000 ppm (c) 4,000ppm (d) 4,500 ppm(e) 5,500 ppm(f) 6,000 ppm (g)50,000ppm

Fig. 2.5. The effect of silica concentration on $CO_2$ foam generation at 25 °C, 1500 psi.

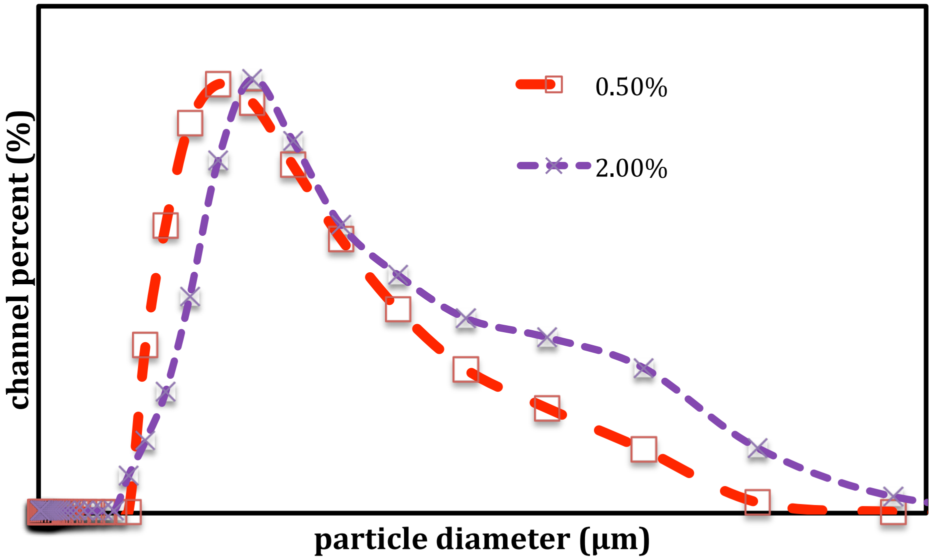

Fig. 2.6 Particle size distribution in different nanosilica solutions.

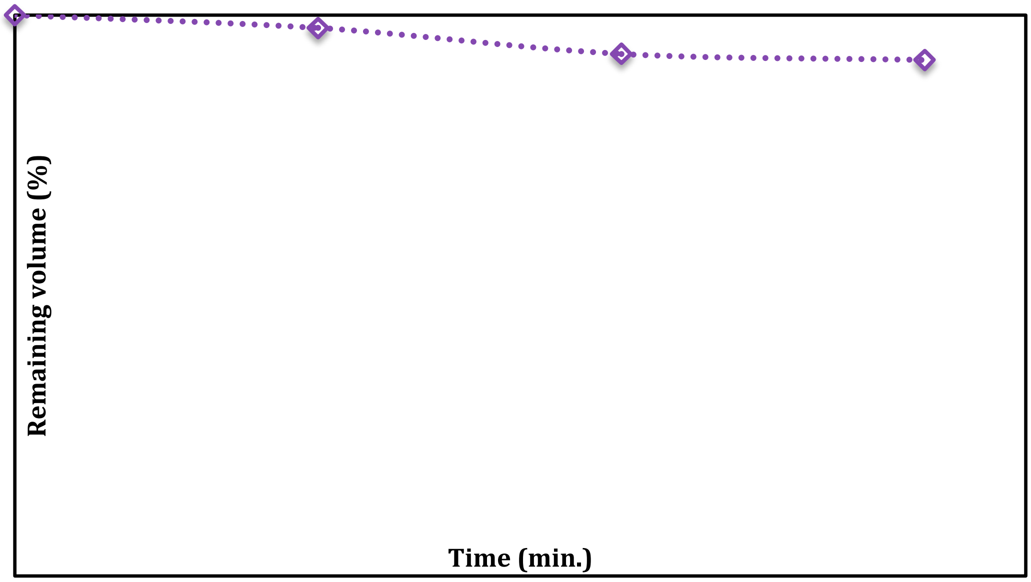

**Fig. 2.7 $CO_2$ foam volume reduction in 4,000 ppm nanosilica solution.**

### *2.2.4 Effect of brine salinity on $CO_2$ foam generation at static condition*

To investigate the effect of brine salinity on $CO_2$ foam generation, different concentrations of NaCl solutions were used to prepare nanosilica dispersions. Figure 2.8 shows the results of $CO_2$ foam generated in different brine solutions, in which the nanosilica concentration is 5,000 ppm. It can be seen that, at a low concentration of brine (<2.0% NaCl), the generation of $CO_2$ foam is insensitive to brine concentration. However, as the brine concentration increases, the process of generating $CO_2$ foam is inhibited by the brine salinity. It is well known that adding salt to an aqueous nanosilica dispersion can reduce the particle zeta potential, hence decreasing the particles' electrostatic repulsion and leading to particle aggregation[13,14]. Figure 2.9 shows the particle size distribution in different brine contents. The particle sizes are 140 nm, 153 nm, 364 nm, and 193–5,600 nm for brine content of 0, 5,000 ppm, 20,000 ppm and 50,000 ppm, respectively.

(a) DI water (b) 0.5% NaCl (c) 2% NaCl (d) 5% NaCl

**Fig. 2.8 The effect of brine salinity on $CO_2$ foam generation.**

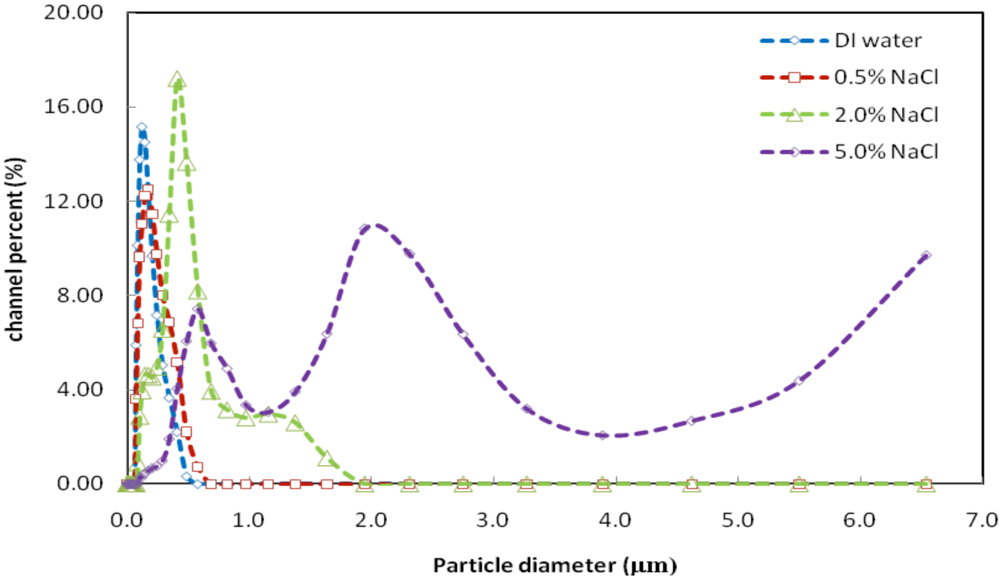

**Fig. 2.9 Particle size distribution in different brine solutions.**

### *2.2.5 Effects of pressure on $CO_2$ foam generation*


(a) 1200 psi (b) 1500 psi (c) 2000 psi

**Fig. 2.10 $CO_2$ foam generated at different pressures.**

The experiments for study of the effects of pressure on $CO_2$ foam generation were conducted with 5,000 ppm nanosilica solution at room temperature. The nanosilica solutions were prepared by dispersing the nanoparticles in 2.0% NaCl solution. The pressure at which the experiments were conducted ranged from 1200 psi to 2000 psi. Figure 2.10 shows the results of the effects of different pressures on $CO_2$ foam generation. It was observed that, as the pressure increased, more $CO_2$ foam was generated in the sapphire tube. The heights of $CO_2$ foam in the observation cell were 0.65 cm, 1.79 cm, and 2.49 cm for pressures of 1200 psi, 1500 psi, and 2000 psi, respectively. It is known that, as the pressure increases, the interfacial tension (IFT) between $CO_2$ and brine decreases[15]. IFT represents the surface or interface energy level. The high value of IFT at low pressures means that the interfacial energy between $CO_2$ bubbles and the water solution is high and the system is not stable. Thus the $CO_2$ bubbles collapse and hinder $CO_2$ foam generation.

### *2.2.6 Effects of temperature on CO2 foam generation*

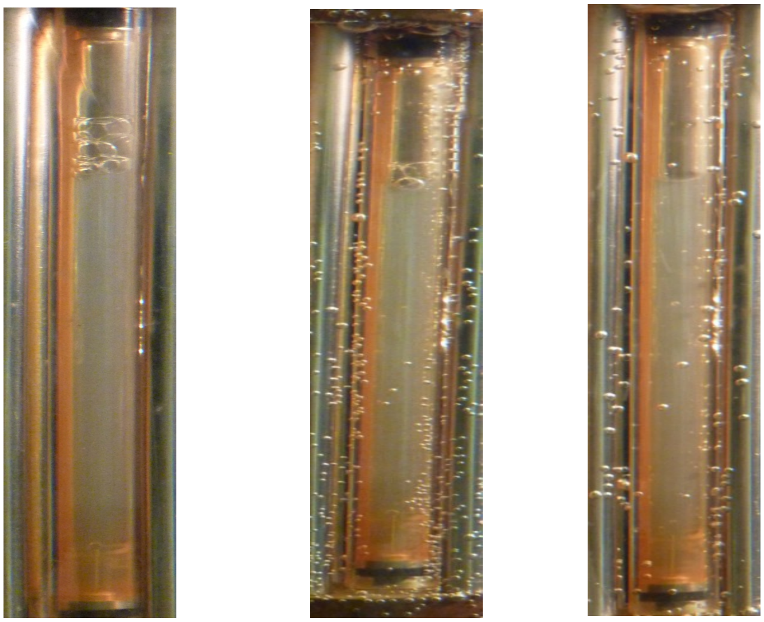
(a) 25°C (b) 45°C (c) 60°C

**Fig. 2.11 Temperature effects on $CO_2$ foam generation.**

Temperature is an important parameter for foam applications in the petroleum industry. To investigate effects of temperature effect $CO_2$ foam generation, the experiments were conducted at 1500 psi with temperatures in the range of $25^oC$ to $60^oC$ with nanosilica concentration of 5,000 ppm, dispersed in 2.0% NaCl. Figure 2.11 shows the results of $CO_2$ foam generated at different temperatures. The results revealed that the height of the $CO_2$ foam decreased with increased temperature. As the temperature reached $60^oC$, no $CO_2$ foam was observed in the sapphire tube. It is well-proven that the IFT between $CO_2$ and water increases with temperature increase[15]. For example, our previous study indicated that the IFT between $CO_2$ and brine increased from 20 mN/m to 30 mN/m as temperature increased from $20^oC$ to $40^oC$ under a pressure of 1500 psi. The high IFT at high temperature led to $CO_2$ bubble collapse and hindered $CO_2$ foam generation. On the other hand, the high mobility of the nanoparticle at high temperature also inhibited the particle adsorption at the interface of $CO_2$/water.

# 3, Nanoparticle-stabilized $CO_2$ foam generated at dynamic conditions

In previous studies, systematical investigation the generation $CO_2$ foam with nanosilica at static conditions were performed. This chapter describes the study of $CO_2$ foam generation at dynamic conditions. A series of flow experiments on the simultaneous injection of $CO_2$ and nanosilica solution through a porous glass beads column was conducted.

## 3.1 Materials and equipment

### *3.1.1 Silica nanoparticles*

Two kinds of silica nanoparticle powder, or nanopowder, were obtained from Sigma-Aldrich (AS-silica) and Wacker Silicones, respectively. The silica nanoparticles obtained from Wacker Silicones (AW-silica) were coated with dimethylsiloxy, with particle size around 10 nm. Silica nanocrystals (C-silica) were prepared by hydrothermal synthesis in a lab-made autoclave.[16] To prepare the silica nanocrystals, 1.40g NaOH was dissolved in 100 ml 1M tetrapropyl ammonium hydroxide (TPAOH, Sigma-Aldrich). Then, 20g fumed silica was added into the solution at 80°C under continuous magnetic stirring until a clear solution was obtained. The prepared solution stood at room temperature for at least 4 hours. After that, the solution was transferred to a lab-made autoclave and put into a preheated oven. The hydrothermal reaction for silica crystal synthesis was continued for 72 hours at 120°C. Finally, the particles were washed with de-ionized water until pH reached 7.

### *3.1.2 Measurement of particle hydrophobicity*

The aqueous silica dispersions were prepared by mixing the silica nanopowder/nanocrystal into 2.0% NaCl: the NaCl solution was placed in a high speed blender into which silica particles were added, then blended on high speed for five minutes, followed by an hour of sonication. This silica nanoparticle dispersion had an average particle size ~100 nm.

The silica nanoparticle hydrophobicity was determined by contact angle measurement (OCA 30, FDS Inc.). To measure the contact angle, several drops of the silica nanoparticle dispersion were dispersed on a glass slide and dried at room temperature. Then a water drop was placed on the modified glass slide. Using the CCD camera, the shape of the water drop was recorded and the image was analyzed using a software package from Dataphysics Company to estimate the air/water/nanosilica contact angle.

### ***3.1.3 $CO_2$ foam generation and characterization***

#### *3.1.3.1 $CO_2$ foam generation*

The apparatus used to generate nanoparticle-stabilized $CO_2$ foam is shown in Fig. 3.1. Two ISCO syringe pumps (model 260D) inject silica nanoparticle dispersion and liquid $CO_2$ into the glass beads-packed column. Three floating piston accumulators reserve nanosilica dispersion, liquid $CO_2$, and the effluent, respectively. Three TEMCO backpressure regulators (BPR) maintain the required operation pressure. The injected liquid $CO_2$ and the silica nanoparticle dispersion are mixed within the glass beads column by a strong shearing force. Pressure drop across the glass beads column is measured by a Honeywell 3000 differential pressure transducer connected to a Daq56 data acquisition system, which records pressure response with time. The mixture then flows out from the glass beads column into a capillary tube. The differential pressure across the capillary tube is measured by another differential pressure transducer. After leaving the capillary tube, the fluid flows into the sapphire observation tube (Fig. 3.2), which is designed for observing $CO_2$ foam morphology and foam bubble size. The entire apparatus, except for the syringe pumps, is placed in an air bath to maintain a constant temperature throughout the experiment.

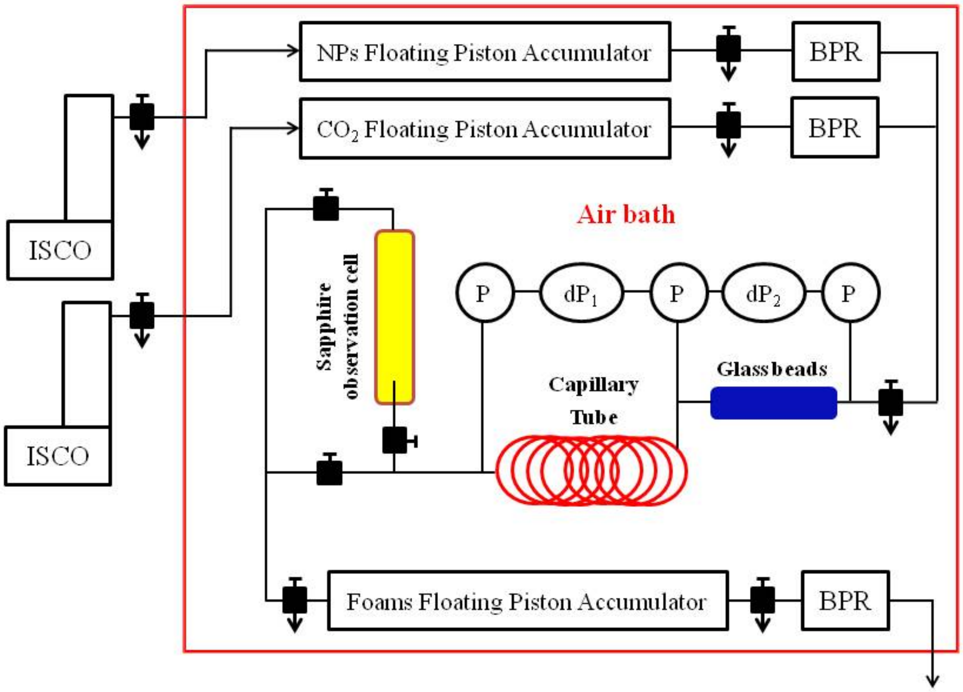

**Fig. 3.1 Schematic diagram of dynamic foam generation and the mobility test setup.**

Foam generation and mobility measurements were conducted at 25°C and 1200 psig. In order to evaluate the effect of silica nanoparticles on $CO_2$ foam generation and mobility reduction, a series of baseline experiments (base) were performed at various flow rates by simultaneously injecting $CO_2$ and 2.0% NaCl (without silica nanoparticles) into the glass beads column and capillary tube. Each baseline experiment was continued until a steady-state pressure drop across the glass beads column was achieved. Following the baseline experiment, the $CO_2$ foam generation experiments were performed by simultaneously injecting $CO_2$ and nanosilica dispersion into the glass beads column and capillary tube at flow rates and phase ratios similar to those used in the baseline experiments.

**Fig. 3.2 Diagram and image of the sapphire observation tube.**

*3.1.3.2 Foam characterization*

***Determine the mixture mobility*** During $CO_2$ foam generation, a lab-made, glass bead-packed column was used to mix $CO_2$ and nanosilica dispersion to generate $CO_2$ foam. The properties of the glass beads column are listed in Table 3.1. The pressure drop across the column was used to estimate the total mobility of the $CO_2$ /nanosilica dispersion (foam mobility). The mobility can be calculated by equation 1:

$$\lambda = \frac{\left(\frac{q}{A}\right)}{\left(\frac{\Delta p}{L}\right)} \tag{1}$$

where $q$ is the flow rate of the fluids in the glass bead column; $A$ and $L$ are the length and diameter of the glass bead column, respectively; and $\Delta p$ is the pressure drop along the glass bead column.

***Measurement of the mixture's apparent viscosity*** After $CO_2$ foam was generated in the glass bead column, it flowed into the capillary tube. The apparent viscosity of the $CO_2$ foam/$CO_2$+brine in the capillary tube can be calculated from the shear rate and measured pressure drop across the capillary tube according to equation 2:[17]

$$\eta = \frac{\tau}{\dot{\gamma}} = \frac{\lambda R_{cap}^2 \Delta P}{LU} \tag{2}$$

where $\Delta P$ is the pressure difference across the capillary tube; $L$ and $R_{cap}$ are the length (3048 mm) and radius (0.381 mm) of the capillary tube, respectively; U is the average velocity of the mixture flow through the capillary tube; and $\lambda$ is the geometric scale of 0.5.

**Table 3.1 Properties of glass bead-packed column**

| | |
|---|---|
| Length (inch) | 3.94 |
| Diameter (inch) | 0.18 |
| Porosity (%) | 36.82 |
| Pore volume (ml) | 0.60 |
| Permeability (D) | 25.04 |

## 3.2 Results and discussion

### ***3.2.1 Nanosilica crystal***

The morphology and particle size distribution for AS-silica and AW-silica were discussed in Chapter 2 of this report. Here we first discussed the morphology and particle size distribution of the lab-made silica nanocrystals. Figure 3.3 shows the x-ray diffraction pattern (XRD) of the synthesized particles. The appearance peaks at 7.9°, 8.9°, and 23.1° showing that MFI type silica crystals were obtained. The TEM images in Fig. 3.4 show that the synthesized silica crystals were around 60 nm. Dynamic light scattering particles size analysis (DLS) was employed to measure particle size distribution in solution. The DLS result in Fig. 3.5 confirms that the diameter of the lab-synthesized silica particle is around 65 nm.

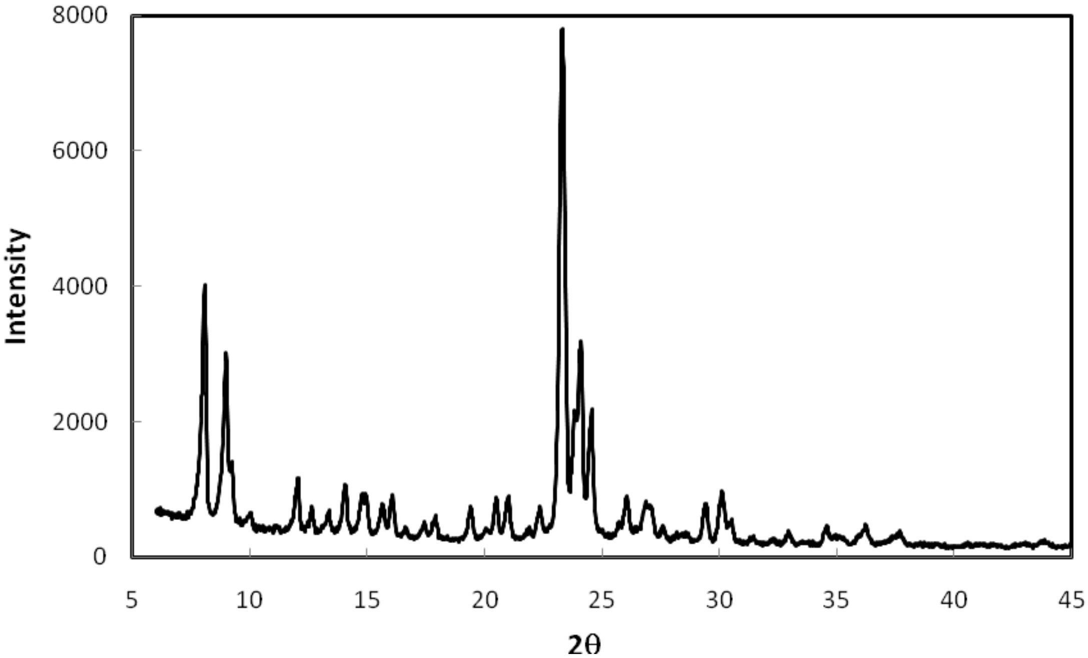

**Fig. 3.3 X-ray diffraction pattern of the synthesized silica crystal.**

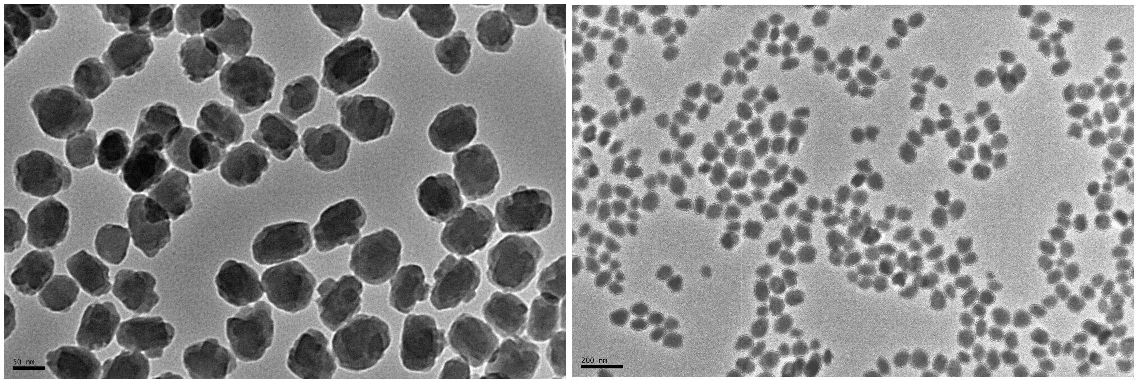

(a) (b)

**Fig. 3.4 TEM images of the synthesized silica crystal; scale bar = 50 nm (a) and 200 nm (b).**

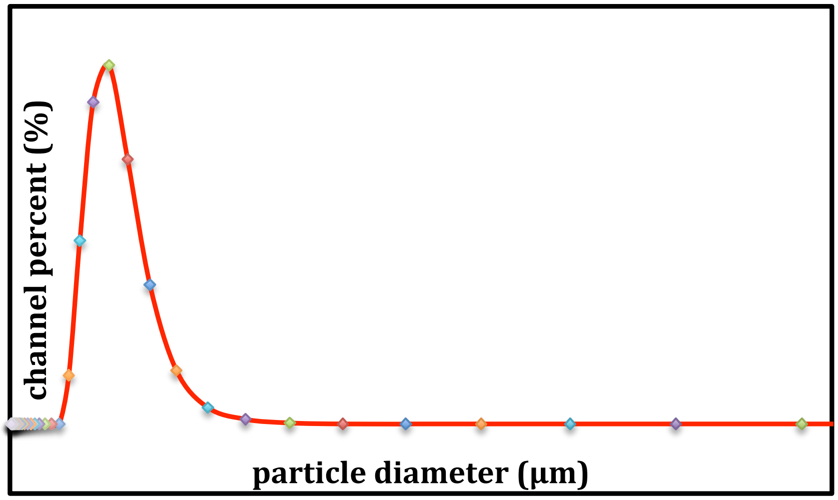

**Fig. 3.5 Particle size distribution of the synthesized silica crystal.**

### *3.2.2 $CO_2$ foam generation with nanosilica particles*

It is well known that small solid particles can have surfactant-like properties. They have a strong tendency to adhere to fluid interfaces, mainly due to the reduction of the total interfacial energy upon replacing part of the liquid-liquid or liquid-vapor interface by a liquid-particle interface.[3,7] Figure 3.6 shows images of $CO_2$ foam from an observation cell, in the presence and absence of nanosilica particles (C-silica particle dispersion with concentration of 5,000 ppm). In the presence of nanosilica particles, uniform $CO_2$ foam was generated and observed on the top of the observation cell. The size of the bubbles, packed on top of the observation cell, was around several millimeters. Water was present between the bubbles, forming lamellae. However, in the absence of nanosilica particles, no $CO_2$ foam was observed in the observation cell, although a $CO_2$ bank was formed on its top. During the experiments, we also observed that, when the injected $CO_2$ bubbles rose from the bottom of the cell, they contacted and merged immediately in the absence of nanosilica particles. In addition, the generated $CO_2$ foam was very stable in the presence of nanosilica particles. It is known that small particles, such as nanosilica, can be adsorbed at $CO_2$-brine interface; these formed a rigid protective barrier to prevent bubble coalescence when $CO_2$ and nanosilica dispersion were co-injected into the glass beads column. The energy, $G$, required to remove a spherical particle of radius $R$ from the $CO_2$–water interface of tension $Y$ is given by $G=\gamma R2\pi(1\pm\cos\theta)$, where $R$ is the radius of the particles and $\theta$ is the contact angle at the $CO_2$–water interface.[7] The sign inside the bracket is negative for removal into water and positive for removal into $CO_2$. Simple calculations with typical parameters show that the adhesion energy is of the order of several thousands of $k_bT$, which is much larger than the adsorption energy for a typical surfactant molecule at an oil–water interface (which is of the order of $k_bT$)[7].

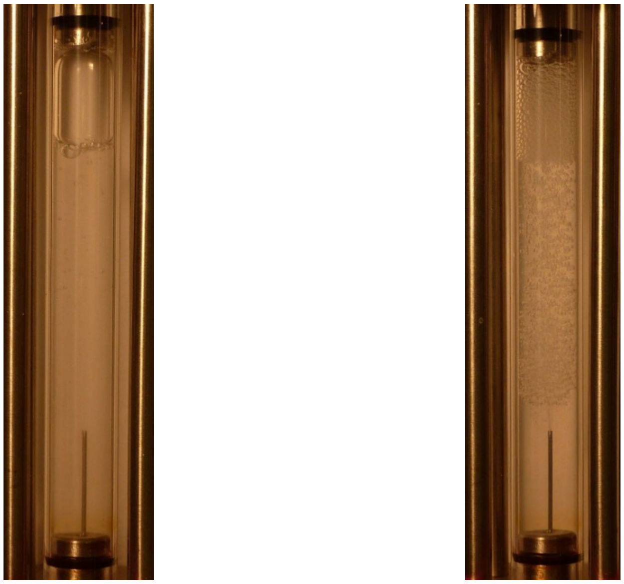
(a) (b)

**Fig. 3.6 The images of $CO_2$ foam generated in the absence of (a) and in presence of (b) nanosilica particles (particle concentration=5,000 ppm).**

### *3.2.3 Effects of particle hydrophobicity on $CO_2$ foam generation*

Three kinds of nanosilica particles (AW-silica; C-silica; AS-silica) were used to investigate the effect of nanosilica hydrophobicity on $CO_2$ foam generation and foam stability. The hydrophobicity of the nanosilica particles was demonstrated by measuring the contact angle of the particles at the water–air interface. Figure 3.7 shows the measured contact angles for these three nanosilica particles. The contact angles are 59.5°, 20.8°, and 8.6° for AW-silica, C-silica, and AS-silica, respectively. The contact angle measurements demonstrated that the hydrophobicity of the particles changed from strongly hydrophilic to varying degrees of hydrophobicity; that is, strongly hydrophilic for AS-silica, moderately hydrophilic for C-silica, and somewhat hydrophobic for AW-silica. The results of $CO_2$ foam generation with the three different nanosilica particles are displayed in Fig. 3.8. These indicate that the amount of $CO_2$ foam generated by the nanosilica particles increased in the order of AS-silica, C-silica, and AW-silica. At the same time, the bubble size of the $CO_2$ foam decreased in the same order. According to findings of this experiment, the adhesion energy of particles at the $CO_2$/water interface is related to their contact angles. When a particle has a strong hydrophilic surface, such as AS-silica, the adsorbed particles are easy to remove from the $CO_2$/water interface into water and the generated $CO_2$ foam collapses. The amount of $CO_2$ foam (the height of the foam) in Fig. 3.8 indicates that AS-silica particles generated the least amount of foam, implying that the $CO_2$ foam is not stable and the foams are easy to collapse. On the other hand, AW-silica particles, which have a more hydrophobic surface, displayed more inclination to generate stable $CO_2$ foam. Uniform $CO_2$ foam that almost filled the cell was observed. C-silica particles, which have more hydrophobicity than AS-silica and less than AW-silica, generated more foam than AS-silica particles and less than AW-silica. Furthermore, the bubble size of the generated $CO_2$ foam was observed to differ according to the different nanosilica particles used. Due to bubble coalescence, AS-silica stabilized $CO_2$ foam had the biggest bubble size, followed by C-silica stabilized $CO_2$ foam. AW-silica stabilized $CO_2$ foam had the smallest bubble size. Our results were also consistent with the conclusion that the size of bubbles decreased progressively with an increase in hydrophobicity of the particles.[3]

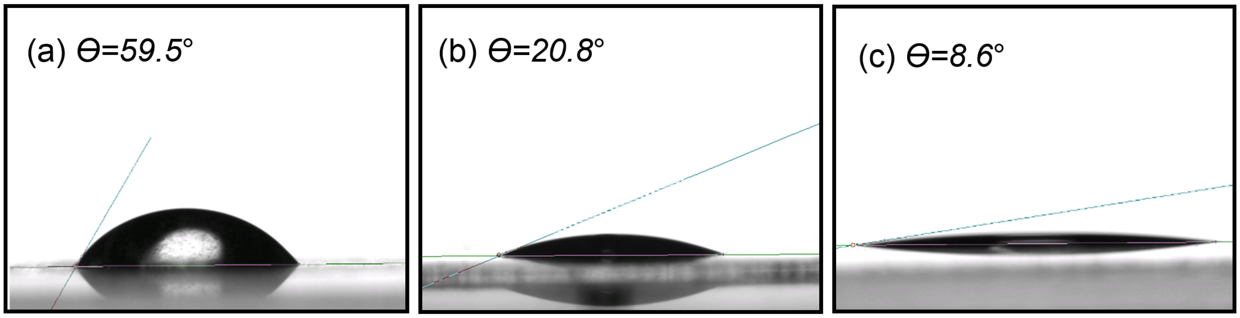

**Fig. 3.7 Contact angle measurement of three types of silica: (a) AW-silica; (b) C-silica; (c) AS-silica.**

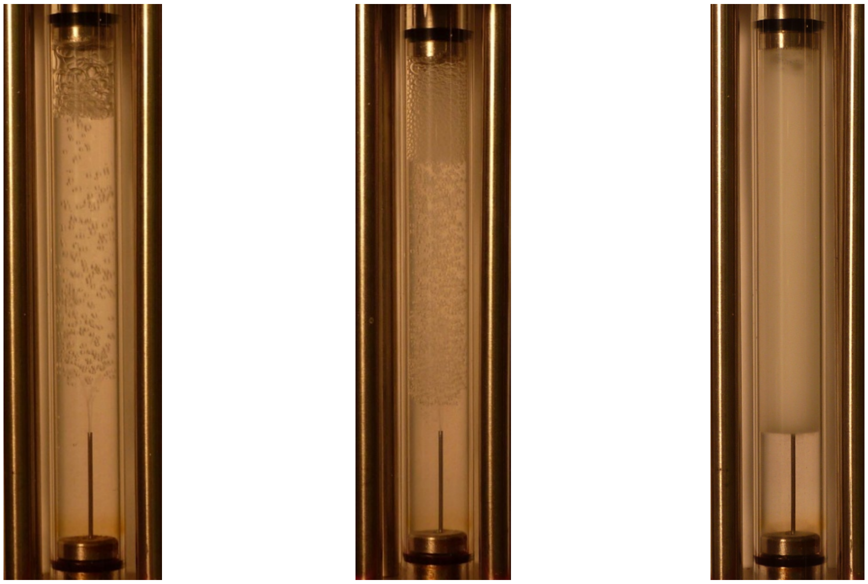

(a) (b) (c)

**Fig. 3.8 Images of $CO_2$ foam generated with different nanosilica particles; (a) AS-silica; (b) C-silica; (c) AW-silica; experimental conditions: Total flow rate = 6ml/min, nanosilica concentration=5,000 ppm, nanosilica dispersion/$CO_2$ ratio = 5:1.**

### *3.2.4 Effect of particle hydrophobicity on $CO_2$ foam flow behaviors in porous media*

$CO_2$ foam for enhanced oil recovery is one of the most import applications of $CO_2$ foam in industry. The purpose of using $CO_2$ foam in enhanced oil recovery is to reduce $CO_2$ mobility and improve $CO_2$ sweep efficiency. In order to demonstrate nanosilica-stabilized $CO_2$ foam for $CO_2$ mobility control and the application in $CO_2$ enhanced oil recovery, nanosilica (AS-silica, C-silica, AW-silica)-stabilized $CO_2$ foam flow behavior in porous media was investigated.

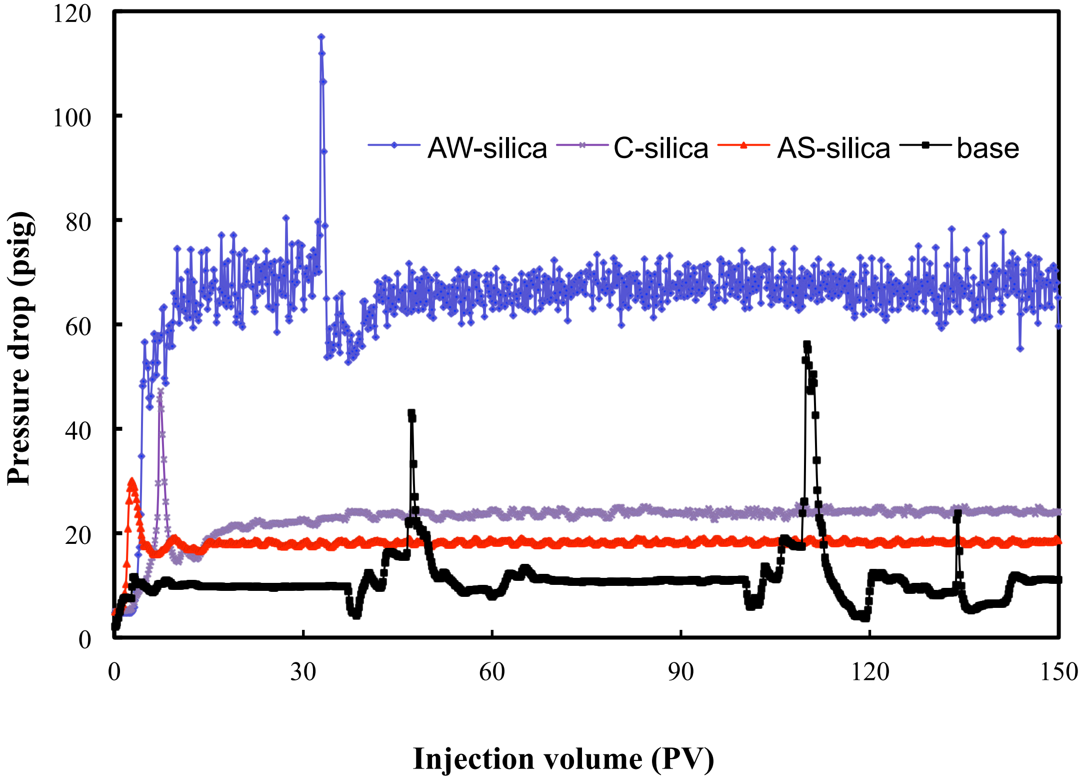

**Fig. 3.9 Pressure drop across the glass beads column for different nanosilica-stabilized $CO_2$ foams; Total flow rate = 6 ml/min, nanosilica concentration=5,000 ppm, nanosilica dispersion/$CO_2$ ratio = 3:1.**

Figure 3.9 shows the pressure drop along the glass bead column for three different nanosilica particles during $CO_2$ foam generation. The injection volume, measured as pore volume (PV), is the total injection of liquid $CO_2$ and nanosilica dispersion volume. It is clearly indicated that, in the absence of nanosilica particles, the pressure drop is lower than in all cases where nanosilica particles are present. As discussed in Section 4.2, when nanosilica dispersion was co-injected with $CO_2$, foam was generated in the glass beads column and $CO_2$ mobility was reduced, resulting in higher pressure drop across the glass beads column. Among the three types of nanosilica particles, the AW-silica dispersion had the highest pressure drop. That was consistent with the results of the amounts of the $CO_2$ foam generation and foam stability discussed in Section 3.2.3. Figure 3.9 also shows that, in the presence of nanosilica particles of C- and AS-silica, the pressure drop reached a maximum at the beginning and then decreased and leveled off. The maximum pressure drop corresponds to the foam breakthrough at the outlet.[18] The pressure decreases after breakthrough because of the coalescence of the bubbles due to diffusion or breaking of the foam films. However, the decrease of the pressure drop after the foam breakthrough for AW-silica-stabilized $CO_2$ foam was very small, indicating that the AW-silica-stabilized $CO_2$ foam was very stable and little foam coalescence occurred.

Figure 3.10 shows the AW-silica, C-silica and AS-silica-stabilized $CO_2$ foam mobilities at different phase ratios. Here, *phase ratio* is defined as the ratio of injection volume of liquid phase (nanosilica dispersion or brine) to the volume of liquid $CO_2$. As a comparison, Fig. 3.10 also displays the mobility of $CO_2$ and brine (in the absence of the nanosilica particles) at the same phase ratio. These results indicated two trends of mobility change in the injected $CO_2$. First, for both the $CO_2$-foam and $CO_2$-brine processes, the mobility of the $CO_2$ rich phase is reduced with increasing $CO_2$ quality. Similar results were also reported by Khalil and Asgari when they studied surfactant-induced foam flowed through a porous medium.[19] Second, the mobility of the $CO_2$-foam system was lower than that of the $CO_2$-brine system through all the phase ratios. For example, at the phase ratio of 2, the mobility of the base ($CO_2$-brine) was $6.99\times10^3$ mD/cp, which was reduced to $6.53\times10^3$ mD/cp, $3.50\times10^3$ mD/cp, and $1.08\times10^3$ mD/cp with the assistance of AS-silica, C-silica and AW-silica as foam stabilizers, with correlated mobility reduction of 6.6%, 49.9% and 84.5%, respectively. As the phase ratio increased to 11, the mobility reduction was 8.5%, 36.1% and 84.1% for AS-silica, C-silica, and AW-silica-stabilized $CO_2$ foam, respectively. The $CO_2$ foam stabilized by AW-silica nanoparticles displayed a much better performance in $CO_2$ mobility reduction than that for C-silica and AS-silica. When the phase ratio increased from 2 to 11, the mobility of AW-silica-stabilized $CO_2$ foam increased slightly, indicating AW-silica can be used as a $CO_2$ foam stabilizer over a wide range of phase ratios.

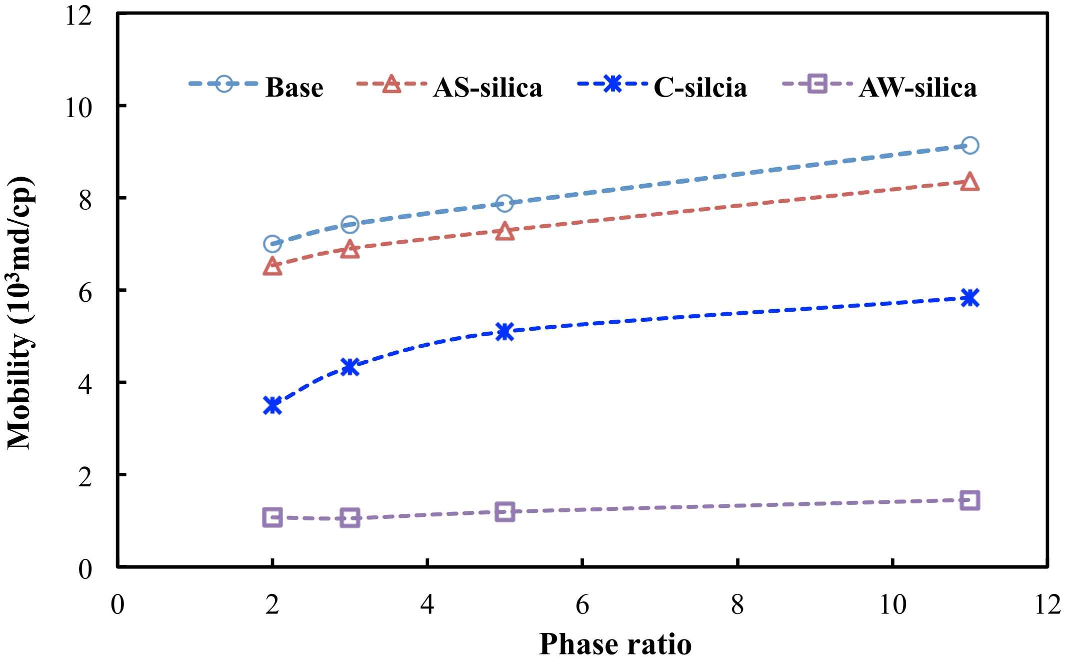

**Fig. 3.10 Mobility of $CO_2$ foams stabilized by different types of silica nanoparticles; the total flow rate = 6 ml/min, nanosilica concentration=5,000 ppm.**

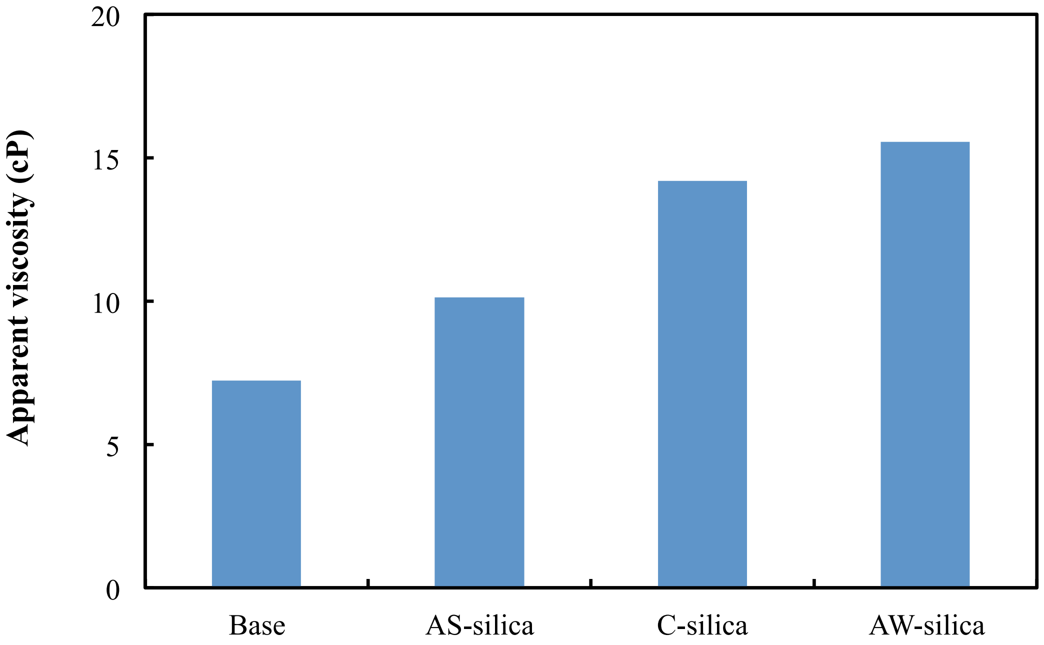

**Fig. 3.11 Apparent viscosity measured in the capillary tube of $CO_2$ foam stabilized with different nanosilica particles; the total flow rate = 6 ml/min, nanosilica concentration=5,000 ppm, nanosilica dispersion/$CO_2$ ratio = 2:1.**

After the $CO_2$ foam flowed out from the glass beads column, it traveled through a capillary tube. To better understand $CO_2$ foam behavior under different conditions, the apparent viscosity of the mixture was measured. Figure 3.11 displays the apparent viscosity of $CO_2$ foam with phase ratio of 2:1 and total injection flow rate of 6 ml/min. The base in Fig. 3.11 was the injection of $CO_2$ and brine, by which no $CO_2$ foam was expected to generate. When nanosilica was introduced in the system, the apparent viscosity of the mixture increased from 7.23 cP ($CO_2$+brine) to 10.23 cP, 14.18 cP, and 15.55 cP for AS-silica, C-silica, and AW-silica, respectively. The increase in apparent viscosity indicated that nanoparticle-stabilized $CO_2$ foam could improve the $CO_2$ performance in fractured reservoirs.

# 4, Transport behavior of nanoparticle in porous media

The objective of this study is to investigate the fundamental adsorption, transport, and retention properties of nanoparticles at reservoir conditions using actual core materials (Berea sandstone, Indiana limestone, and dolomite). Silica nanoparticles from *AkzoNobel* Corp. were used to investigate nanoparticles adsorption and transportation behavior in different core samples.

## 4.1 Materials and equipment

### *4.1.1 Nanoparticles adsorption onto core samples*

Static experiments were performed to study nanosilica particle adsorption onto three different core samples. Before the experiment, a core sample was cleaned with 2.0% NaCl solution and then dried for 24 hr. Nanosilica dispersion (*AkzoNobel* Corp. ) was diluted to 5,000 ppm with 2.0% NaCl solution. Then 250 ml diluted nanosilica dispersion was delivered into three different flasks. The weighted core samples were poured into the flasks and vigorously agitated for about a minute. After that, the flasks were placed into a mechanical shaker and agitated continuously. A sample was removed from the flask at every designated interval. The collected sample was filtered and silicone concentration in the liquid was determined by inductively coupled plasma–atomic emission spectrometry (ICP-AES). The concentration difference between the stock and the sample were used to evaluate nanoparticle adsorption behavior.

### *4.1.2 Nanoparticles transport in different cores*

Three kinds of cores—Berea sandstone, Indiana limestone, and dolomite—were purchased and used for this study. The purchased core samples were machined on a lathe to reduce the length and diameter to 25.5cm and 5.5cm respectively to fit into the core holder. Once the core was machined to the required dimensions, it was then put into a rubber core sleeve and mounted into the core holder together. After the core was mounted, a confining external overburden pressure of 3,000 psi was set up around the core.

Figure 4.1 shows a schematic illustration of the experimental apparatus used to conduct the laboratory coreflood experiments. The apparatus is located in a temperature-controlled air bath, with a syringe pump and separator system outside the air bath (see Fig. 4.1). The ISCO syringe pumps are used to pump the distilled water into the two accumulators filled with nanosilica dispersion (accumulator 1) and 2.0% NaCl solution (accumulator 2) to push the pistons, which in turn pushes the nanosilica dispersion and NaCl solution through the two back pressure regulators (BPR) which are set at required pressures. The fluid passes through three filters of 7µm, 5µm and 2µm before entering the core. At the outlet of the core holder another BPR is used which maintains the pressure inside the core.

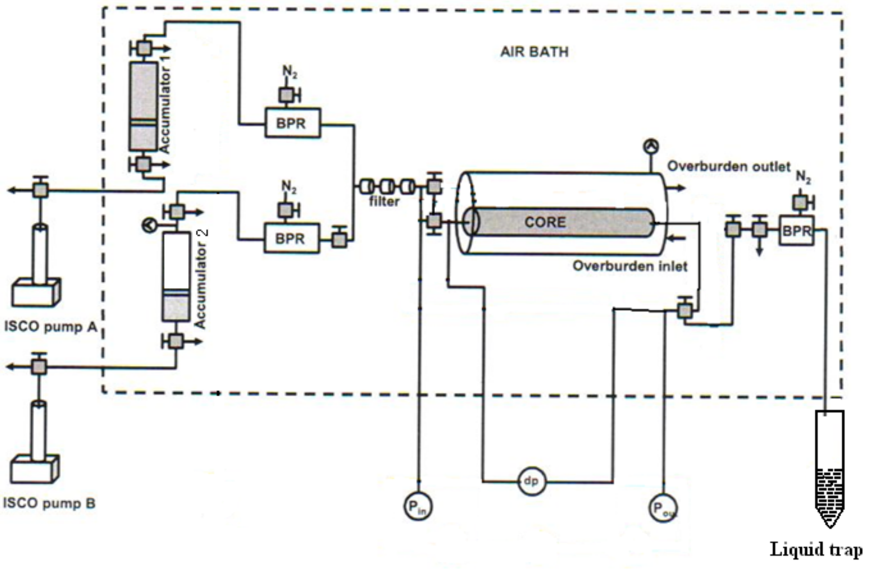

**Fig. 4.1 Schematic diagram of coreflooding apparatus.**

Two digital pressure transmitters are connected at the inlet and outlet of the core holder, which reads the differential pressure. The inlet pressure, outlet pressure, and differential pressure transducers are all interfaced with the data acquisition system which reads and records all the data. The procedure of the coreflood experiments is as follows:

1. Core is assembled into the core holder.
2. Overburden pressure of 3000 psi is applied by distilled water.
3. Backpressure regulators are set at operating pressure by pressuring the BPR dome with nitrogen gas.
4. Nanosilica dispersion and NaCl solution are loaded into accumulator 1 and accumulator 2, respectively.
5. The dry core is vacuumed for 30 minutes once it is installed to remove the air from the pores.
6. The ISCO pumps A& B are loaded with distilled water. Pump B is turned on first to flood the core sample with brine solution. When the core sample is saturated with brine, pump B is stopped and pump A is turned on to start injection of the nanosilica dispersion. The effluent is collected at every 1 pore volume (PV) injection and pressure drop across the core is recorded.
7. After the required volume of nanosilica dispersion is injected, pump A is turned off and pump B is turned on to inject brine to displace the particles retained inside the core.

## 4.2 Results and discussion

### *4.2.1 Nanosilica adsorption onto three core samples*

The nanosilica dispersion, after diluted to 5,000 ppm, has particle size of around 11 nm as measured by DLS and TEM (Figures 4.2 and 4.3). The small particle size allows the particles to smoothly pass through the porous media. TEM images of the nanosilica show the are spherical, which is critical to guarantee their transport in core samples.[20]

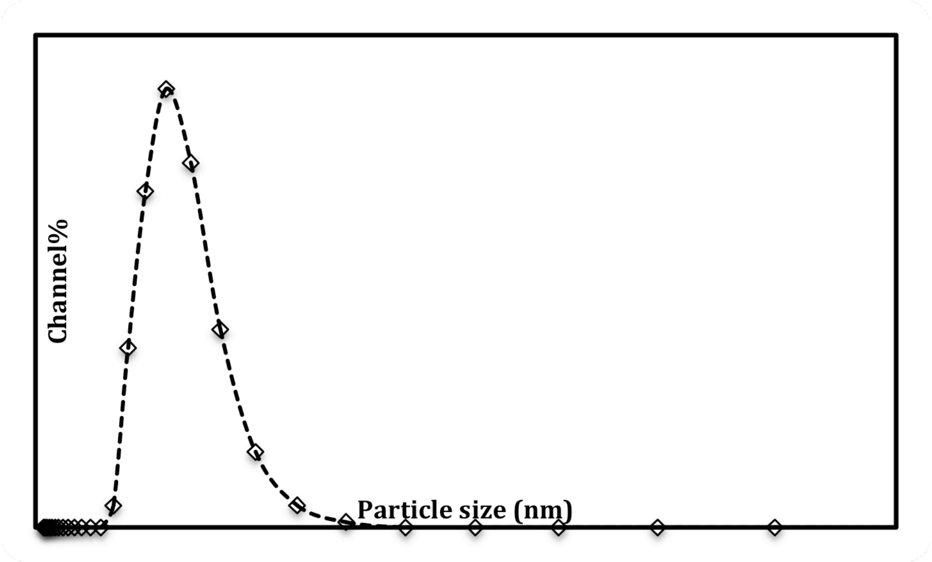

**Fig. 4.2 Nanosilica particle size distribution in 5,000 ppm dispersion.**

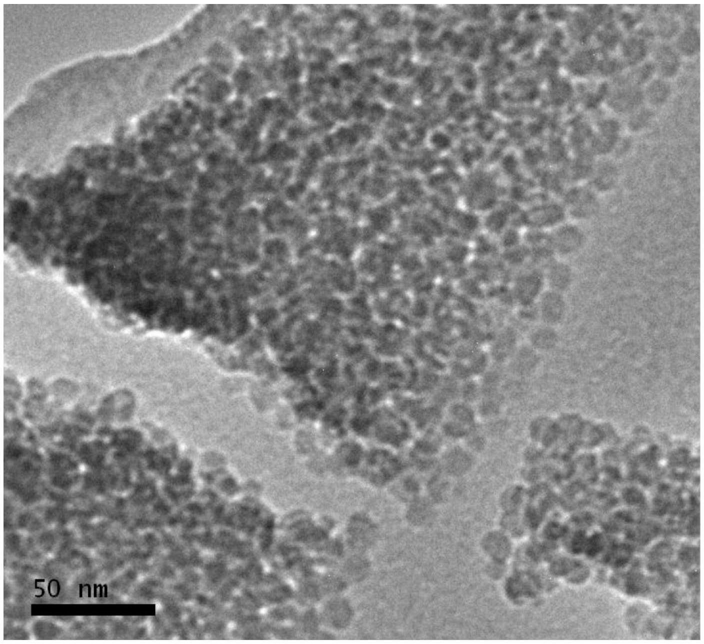

**Fig. 4.3 SEM image of the nanosilica particles.**

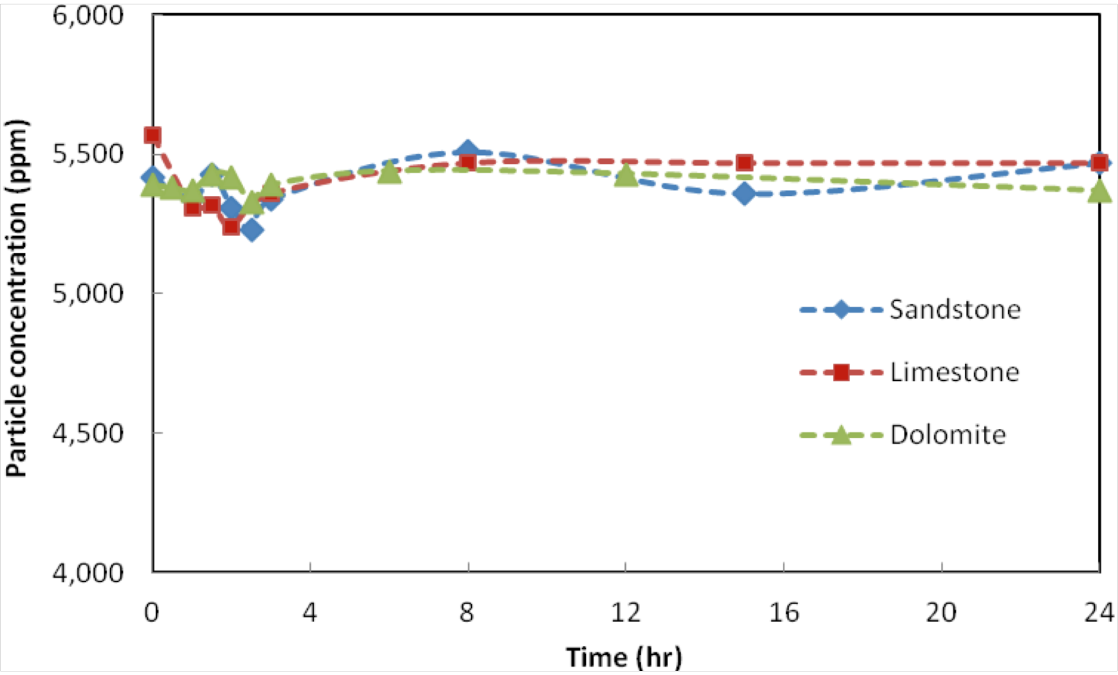

**Fig. 4.4 Nanosilica particles adsorption onto three different rocks.**

Figure 4.4 shows the results of nanosilica adsorption onto three core samples. In the adsorption experiments, 8.677 g sandstone, 8.759 g limestone, and 11.001 g dolomite samples were added to three different flasks. The flasks were placed in a thermostatic shaker bath and samples were collected at a designated interval. The results shown in Fig. 4.4 demonstrate that the silica concentration changed with the adsorption time. Adsorption reached equilibrium; this was observed to be less than 12 hr for all three core samples. The equilibrium adsorptions for sandstone, limestone, and dolomite were estimated as 1.272 mg/g, 5.501 mg/g, and 0 mg/g. It is known that the composition of sandstone is mainly of $SiO_2$, which has the same composition as the nanoparticles, and thus it is assumed an electrostatic repulsion existed between the sandstone and nanosilica particles. The low adsorption of nanosilica particles onto sandstone was probably due to the clay in the sandstone sample.[21] Indiana limestone consists of 98% calcite with minor quantities of dolomite. The higher adsorption density could contribute to the electrostatic force between the silica nanoparticle and limestone surface.[22] Dolomite was observed to have adsorption density of almost 0 mg/g. The experiments for dolomite adsorption were repeated several times and most of the results indicated the equilibrium adsorption was 0 mg/g.

### *4.2.2 Nanosilica particles transport in three core samples*

Berea sandstone, Indiana limestone, and dolomite core samples were polished and cut in a designed size to mount in the core holder. Porosity and permeability were measured for each of the core sample before the nanosilcia dispersion injection. Table 4.1 shows the parameter of each core sample.

**Table 4.1, Core Parameters**

| **Parameters** | Sandstone #1 | Sandstone #2 | Limestone | Dolomite |
|---|---|---|---|---|
| Sample length (cm) | 25.5 | 25.5 | 25.5 | 25.5 |
| Sample diameter (cm) | 5.5 | 5.5 | 5.5 | 5.5 |
| Permeability (md) | 33 | 57.6 | 132 | 5.29 |
| Porosity (%) | 17.5 | 18 | 18.7 | 16.5 |
| Pore volume ($cm^3$) | 86 | 96 | 106 | 92 |

*Berea Sandstone Coreflood #1*

The first flood was performed in a sandstone core with permeability of 33 md. Before injection of nanosilica dispersion, the core was flooded with brine. Then nanoparticle dispersion (5,000 ppm) was injected at a flow rate of 200 ml/hr. Three PV of nanosilica dispersion were injected first. Figure 4.5 shows the changes of nanoparticle concentration in the effluent samples and pressure drop across the core with injection volume. The beginning of breakthrough for the nanoparticles was observed at 1 PV injection. As 3 PV were injected, the particle concentration reached over 3,030 ppm, which was about 60% of the original nanoparticle concentration. Since the core was first saturated with brine, a diffusion exchange between the injected particle dispersion and the captured brine occurred, keeping the particles in the core. After 3 PV of nanoparticle dispersion were injected, the injection was switched to brine. It was observed that as

1.5 PV of brine were injected, the particle concentration in the effluent was almost 0. A mass balance calculated that 23% of the injected particles were recovered. Figure 4.5 also shows the change of pressure drop across the core during the coreflood. A slight pressure drop decrease was observed when the coreflood was switched from nanosilica dispersion to brine. The decrease of the pressure drop is probably due to the viscosity change, which removed some adsorbed particles from the pore surface. However, there was no evidence of alternation of core permeability or core plugging by the nanosilica particles.

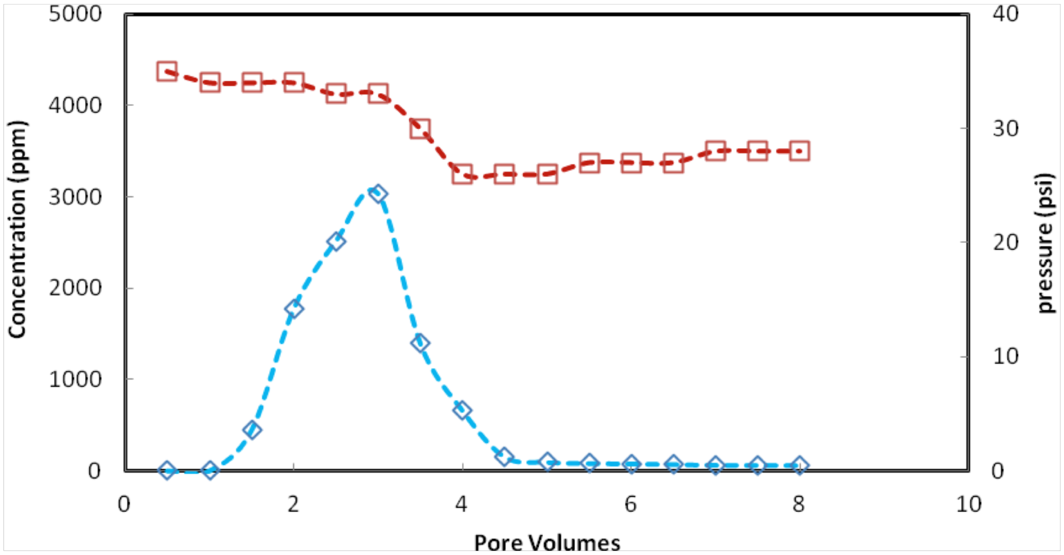

**Fig. 4.5 Effluent concentration and pressure drop change with injected volume (sandstone #1).**

*Berea Sandstone Coreflood #2*

The second coreflood was performed with a new sandstone core, this one having permeability 57.6 mD, at the same experimental conditions as coreflood #1. However, 10 PV of nanosilica dispersion were injected in this experiment, followed by brine injection. Results of particle concentration in effluent and pressure drop across the core are shown in Fig. 4.6. As in coreflood

#1, nanoparticle breakthrough was observed to start after 1 PV was injected. When 5 PV nanosilica dispersion was injected, the particle concentration in the effluent achieved 5,000 ppm, which indicated that the diffusion equilibrium was achieved between the injected nanodispersion and captured brine. After 10 PV particle dispersion was injected, brine was injected to displace the remained particles. The particle concentration in the effluent decreased almost to 0 as 1 PV brine was injected. The total recovery of the injected particle was calculated as 86%. The higher particle recovery compared with coreflood #1 is probably due to the diffusion equilibrium achieved as 5 PV of particle dispersion were injected. The pressure drop across the core (Fig. 4.6) indicated that core plugging did not occur during the coreflooding test and the permeability of the core was not altered.

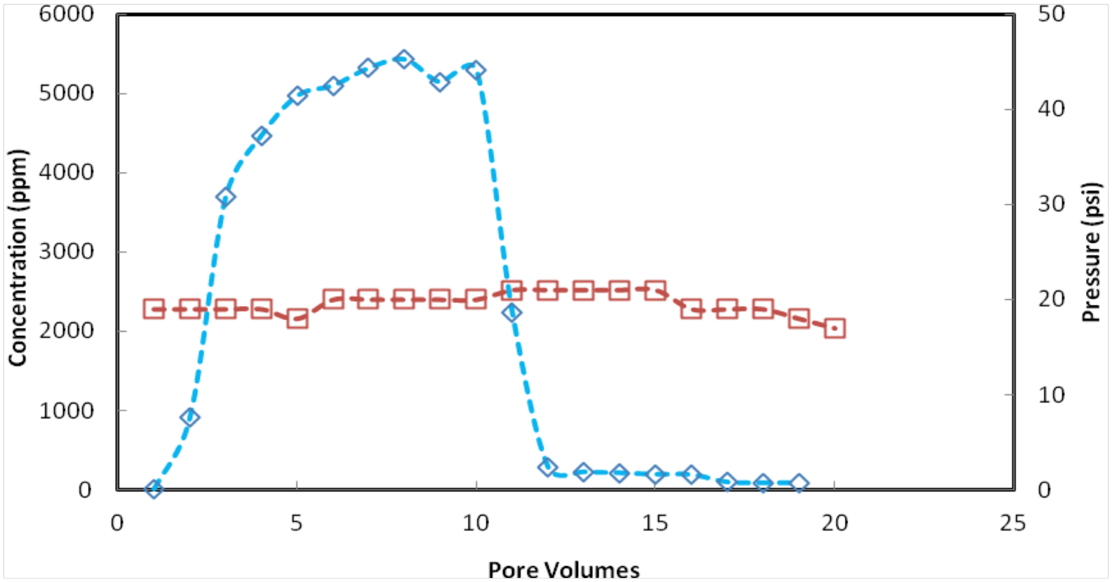

**Fig. 4.6 Effluent concentration and pressure drop change with injected volume (sandstone #2).**

*Indiana Limestone Coreflood #3*

Figure 4.7 shows the results of the concentration and pressure drop change with injection volume for Indiana limestone. The coreflood test in the limestone core was performed with injection of

5.5 PV nanosilica disperaions and then 7.5 PV brine. The results indicated that the particle breakthrough started after 2 PV particle dispersion was injected, which is a little delayed compared with the sandstones in shown in Figs. 4.5–4.6. The lag in the particle breakthrough for limestone is due to the adsorption. As discussed earlier, limestone has a higher adsorption capacity compared to sandstone. After 5.5 PV nanosilica dispersion was injected, the effluent particle concentration was measured as 3,130 ppm, which is 62% of the injected concentration. The total particle recovery after brine injection was estimated as 32.6% for limestone. Pressure drop across the core was observed to change slightly during the coreflood test. Thus, it can be concluded that althrough a few nanoparticles were adsorbed in the core, the permeability of the core was not altered.

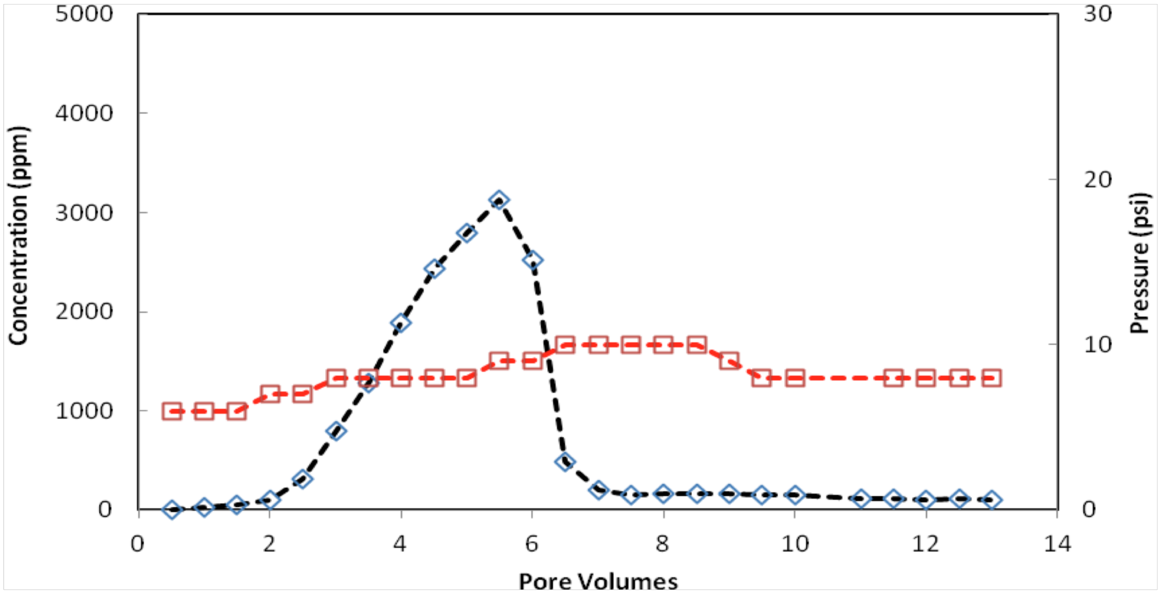

**Fig. 4.7 Effluent concentration and pressure drop change with injected volume (limestone).**

*Dolomite Coreflood #4*

For the dolomite coreflood test, 5.5 PV of nanosilica dispersions were injected at a flow rate of 100 ml/hr. The effluent concentration history, Fig. 4.8, shows that particle breakthrough occurred rapidly. When 2 PV particle dispersion were injected, silica concentration in the effluent reached 4,800 ppm, almost the same as the injection concentration. After injection of 5.5 PV nanosilica dispersion, brine injection was started and effluent concentration immediately decreased. Total particle recovery was calculated as 95.8% after 1.5 PV brine were injected. The high particle recovery is due to the low particle adsorption capacity in dolomite as discussed previously. The pressure drop, shown in Fig. 4.8, was observed to continuously increase during the coreflood test, which means that particle plugging occurred in the core and core permeability was changed. The alteration of the core permeability could contribute to the pore structure in the core. Dolomite has permeability of 5.29 mD. This low permeability could lead to higher interactions between moving particles and pore surfaces that promote pore-surface processes (e.g., deposition) and pore-throat processes (e.g., plugging, screening, and bridging).[23] Figure 4.9 shows the pore size distribution of the three different cores. A small pore size, around 26 nm, was observed for dolomite which could have resulted in the change in core permeability.

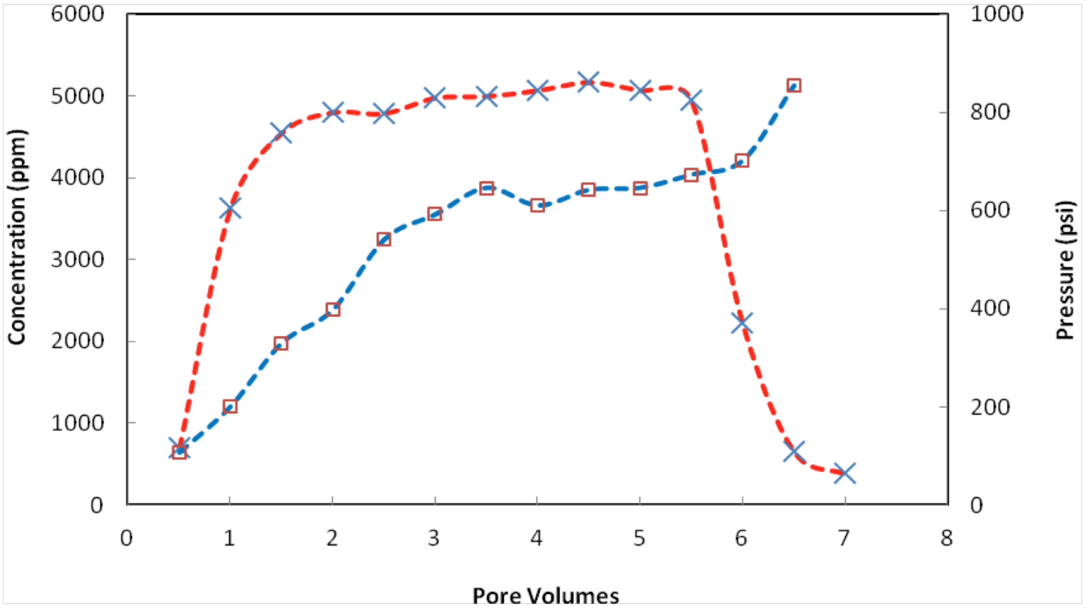

**Fig. 4.8 Effluent concentration and pressure drop change with injected volume (dolomite).**

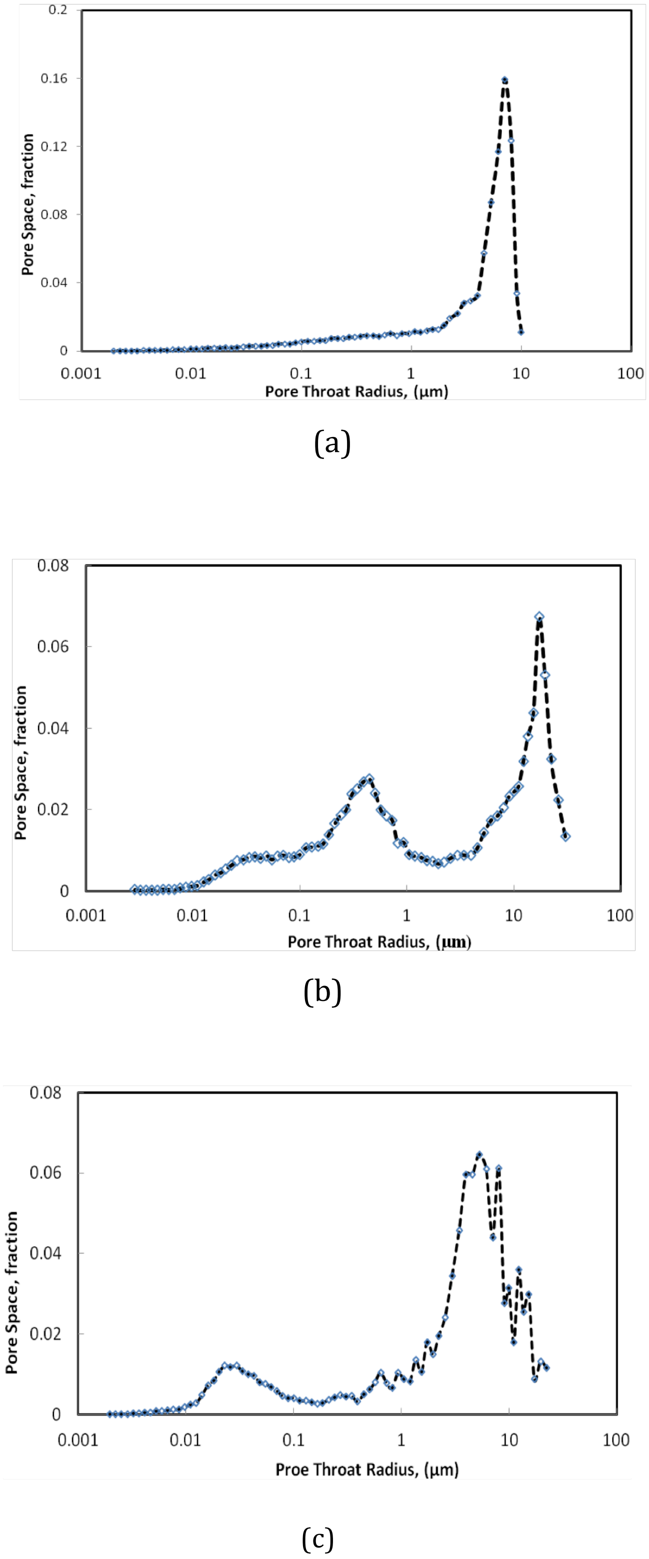

**Fig. 4.9 Pore size distribution of dolomite core; (a) sandstone #1; (b) limestone; (c) dolomite.**

# 5, Nanoparticle-stabilized $CO_2$ foam generation in coreflooding tests

In chapter 4, we observed that silica nanoparticles could freely flow through different core samples (sandstone and limestone). In this chapter, coreflooding tests were performed to investigate $CO_2$ foam generation as $CO_2$ and nanosilica dispersion flowed through a core sample. Foam stability, foam texture, and foam mobility were studied. Factors such as $CO_2$/brine ratio, particle concentration, and injection flow rate on $CO_2$ foam performance are discussed.

## 5.1 Materials and experimental devices

### *5.1.1 Materials*

Silica nanoparticles obtained from AkzoNobel were used for this study. The obtained aqueous dispersion was diluted with 2.0% NaCl to the desired concentration. Berea sandstone core samples were purchased from Cleveland Quarries. The core was cut to diameter of 2.12 in. and length of 10.0 in and polished. Then the core was mounted in a core holder with an overburden pressure of 3,500 psi. Initial brine permeability and the porosity of the core were measured as 33.01 md and 17.36%, respectively.

### *5.1.2 Experimental devices*

The experimental apparatus is shown in Fig. 5.1. Two ISCO syringe pumps (model 260D) were used to inject nanosilica dispersion and liquid $CO_2$ into the core sample. Three floating piston accumulators were used to reserve nanosilica dispersion, liquid $CO_2$ and the mixtures (foam+nanosilica+$CO_2$), respectively. Three TEMCO backpressure regulators (BPR) were used to maintain the required operation pressure. The injected liquid $CO_2$ and nanosilica dispersion were mixed in the core sample, supplying a strong shearing energy and forcing the nanosilica to adsorb to the interface between $CO_2$ and water. A sapphire observation cell was installed behind the core holder to estimate the foam morphology and bubble size. Pressure drop along the core was measured with a Honeywell 3000 differential pressure transducer connected to a Daq56 data acquisition system, which recorded the pressure change with time.

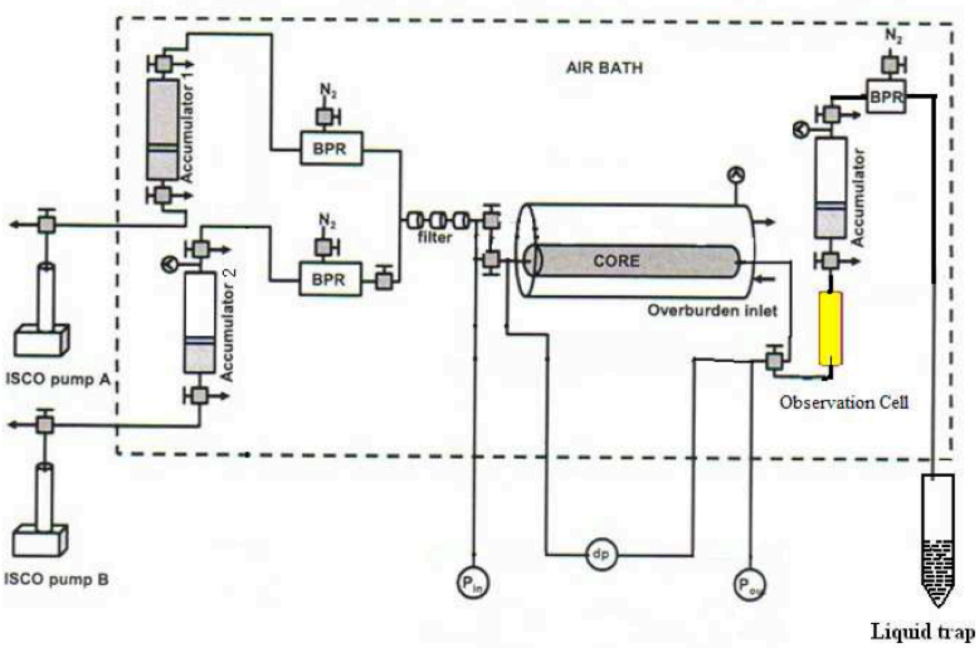

Fig. 5.1 Schematic diagram of the core flooding experiments.

All the coreflooding tests were conducted at 25°C and 1500 psig. In order to evaluate the effect of nanosilica on $CO_2$ foam generation and mobility control, a series of baseline experiments were performed first by simultaneously injecting $CO_2$ and brine, without nanosilica particles, into the core at different volumetric injection ratios. Each baseline experiment lasted until a steady-state pressure drop was achieved.

### *5.1.3 Foam characterization*

#### *Foam mobility*

The foam mobility in this study is defined as the total mobility of $CO_2$/nanosilica dispersion. The mobility can be evaluated from Equation 1:

$$\lambda = \frac{\frac{q}{A}}{\frac{\Delta P}{L}} \ldots\ldots\ldots\ldots\ldots\ldots\ldots\ldots\ldots\ldots (1)$$

where $q$ is the flow rate, $A$ the cross-area of the core, $\Delta p$ is the pressure drop along the core, and $L$ is the length of the core.

*Foam resistance factor*

The foam resistance factor is defined here as the foam mobility (total mobility of $CO_2$/nanosilica dispersion) divided by the total mobility of $CO_2$/brine at the same flow rate and phase ratio. In this study, the same sandstone core was used for all the tests. The calculation of the foam resistance factor is as follows:

$$\gamma = \Delta p_{\mathrm{CO2\text{-}NPs}} / \Delta p_{\mathrm{brine\text{-}CO2}} \ldots\ldots\ldots\ldots\ldots\ldots\ldots (2)$$

where $\Delta p_{CO2\text{-}NPs}$ is pressure drop across the core with $CO_2$/nanoparticle dispersion injection and $\Delta p_{brine\text{-}CO2}$ is the pressure drop during the baseline experiment with brine and $CO_2$ injection.

## 5.2 Results and Discussions

### ***5.2.1 $CO_2$ foam generation in Berea sandstone core***

Figure 5.2 shows the result of pressure drop along the core and $CO_2$ foam image from the observation cell in the presence and absence of nanosilica particles ($CO_2$/brine=3:2). The pressure drop across the core was around 14.2 psi when $CO_2$ and brine had flooded the core. The pressure drop quickly reached equilibrium as 1 PV $CO_2$ and brine were injected into the core. On the other hand, it was observed that, as nanosilica dispersion was added, it took a longer time to reach the steady state. The equilibrium pressure drop was ~238.3 psi after injection of 8–10 PV $CO_2$/nanosilica dispersion. Here, it is necessary to emphasize that the core was flushed with brine after each test, and the core permeability was observed to be almost the same in all the tests, indicating no particle plugging occurred during the tests. Therefore, the pressure drop in the presence of nanosilica can be explained by the $CO_2$ foam generation.

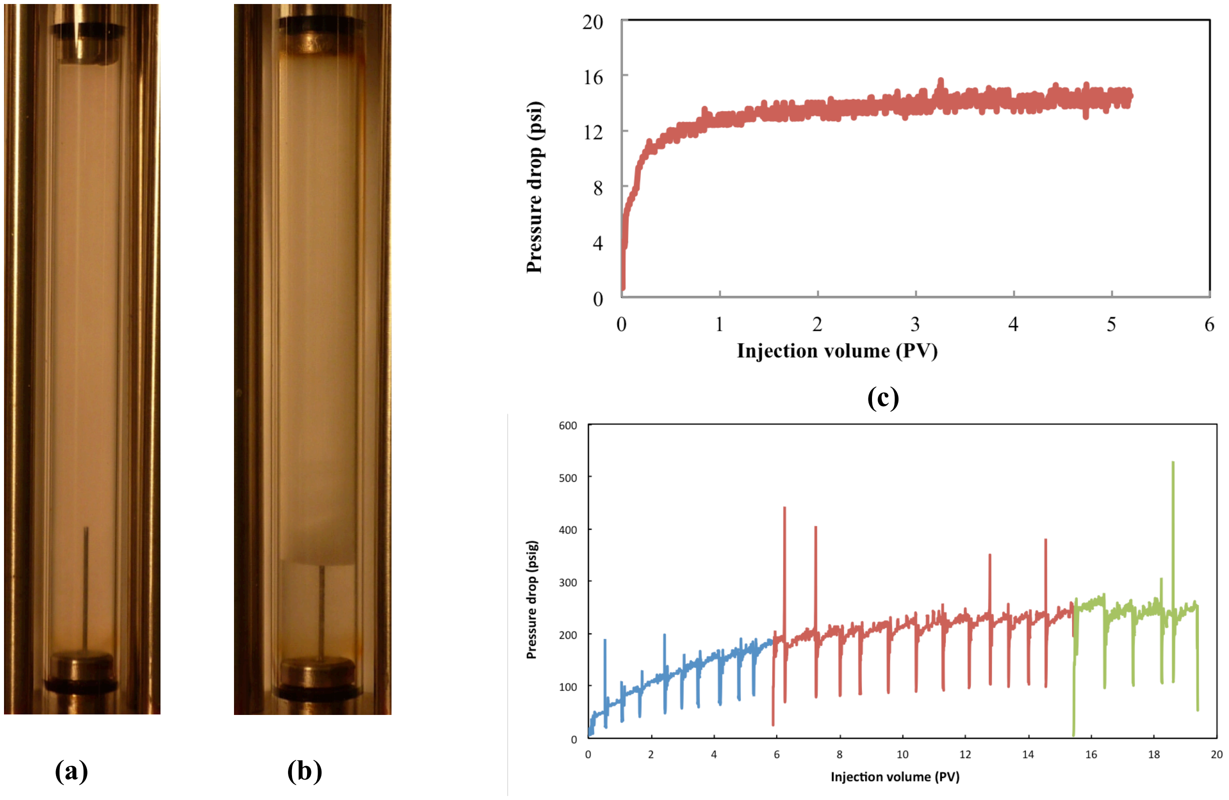

(a) (b) (c) (d)

**Fig. 5.2 Images of $CO_2$ foam with brine and $CO_2$ (a); nanosilica and $CO_2$ (b); and pressure drop in absence of nanosilica particles (c), in the presence of nanosilica particles (d) in the $CO_2$/brine core flood (Total flow rate is 150 ml/hr, and $CO_2$/brine is 3:2).**

Further investigation of the foam stability and texture is shown in Fig. 5.3 that displays images of the $CO_2$ foam at different times after coreflooding. The foam images in Fig. 5.3 correspond to actual core effluent being observed in the observation cell of Fig. 5.1. The results show that the nanosilica-stabilized $CO_2$ foam remained almost unchanged after standing 48 hours. It is known that, when surfactant is used as stabilizer, surfactant molecules, adsorbed at the $CO_2$-water interface, are mobile, whereby adsorption and desorption occur continuously at the interface.[4] Solid particles impart foam stability by adsorbing at the $CO_2$-water interface and forming a rigid barrier that is capable of impeding coalescence. The attachment energy of solid particles adsorbed at the $CO_2$-water interface is one thousand, or several thousands of $kT$ (several $kT$ for surfactant molecules).[7] Figure 5.3 demonstrates that the generated $CO_2$ foam was very stable. The bubble size did not change after 48 hours.

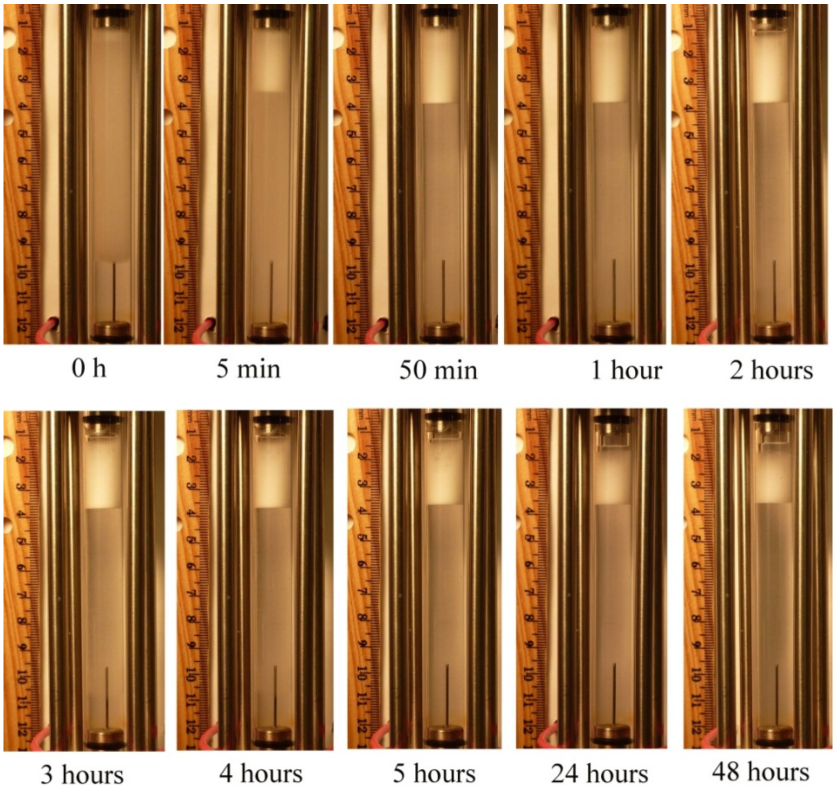
0 h 5 min 50 min 1 hour 2 hours

3 hours 4 hours 5 hours 24 hours 48 hours

**Fig. 5.3 $CO_2$ foam images at different times after coreflooding.**

### *5.2.2 $CO_2$ foam generation with different phase ratios*

Figure 5.4 shows the pressure drop during injection of $CO_2$/nanosilica dispersion with different $CO_2$ fractions (or phase ratio) (nanosilica concentration = 5,000 ppm). The results demonstrated that, at low $CO_2$ fraction, it took a longer time to reach the steady state. For example, as the $CO_2$ fraction was 20%, the steady state was observed after injection of 22–24 PV of $CO_2$/nanosilica dispersion. For the $CO_2$ fraction of 60%, steady state was observed after injection of 8–10 PV $CO_2$/nanosilica dispersion. The requirement of high PV injection to reach steady state had also been observed by other researchers and currently is not well understood.[24,25] The experiments of Ettinger suggest that the slow increases in pressure are due to the propagation of a capillary end effect from the back of the core to the front of the core.[25] However, as the $CO_2$ fraction was increased to 90%, steady state was quickly reached as 0.4–0.6 PV of $CO_2$/nanosilica dispersion was injected. The rapid achievement of steady state at a $CO_2$ fraction of 90%, shown in Fig. 2C, implied that, at high $CO_2$ fraction, the equilibrium of $CO_2$ foam generation and coalescence in the pores was quickly reached. Compared with the conditions of low $CO_2$ fraction, there were sufficient nanoparticles to generate much finer $CO_2$ foams. These foams could enter into those small pores and keep the foam lamellae, which require more $CO_2$/nanosilica dispersion injection volume to move the foam into those pores. However, when $CO_2$ fraction was high, the amount of the nanoparticles was not enough to generate finer foams. Foam coalescence occurred as the $CO_2$ bubble moved from pore throats to pore bodies. The steady state was obtained when a small amount of $CO_2$/nanosilica dispersion was injected. Figure 5.5 displays the images of $CO_2$ foam at different $CO_2$ fractions. The results indicated that, as the $CO_2$ fraction increased, the $CO_2$ foam texture changed from finer small bubbles to coarser big bubbles.

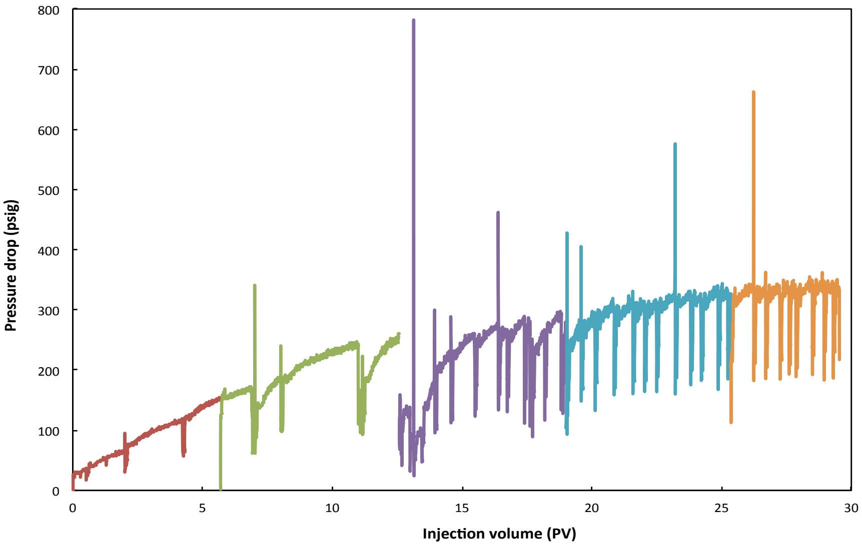

Pressure drop (psig)
800
700
600
500
400
300
200
100
0
0
5
10
15
20
25
30
Injection volume (PV)

(a)

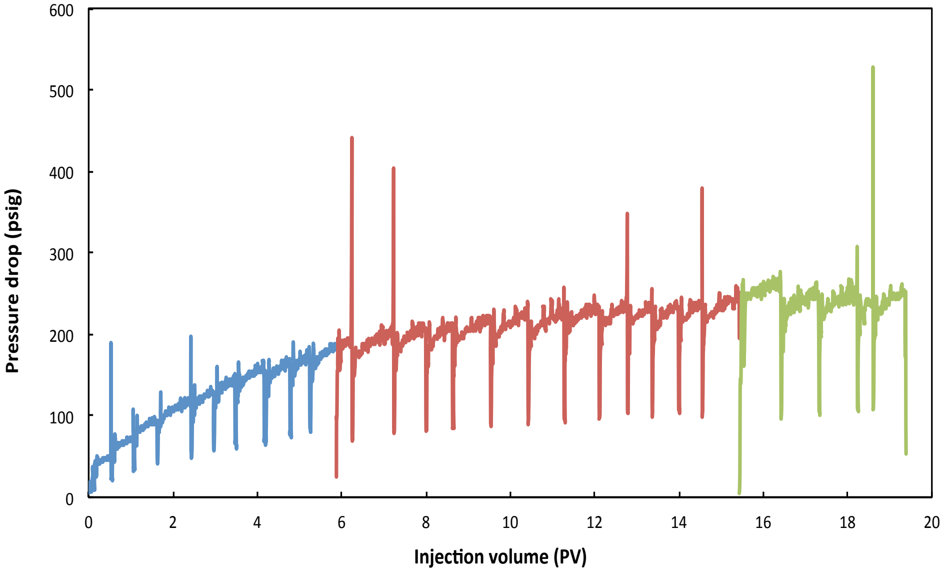

Pressure drop (psig)
600
500
400
300
200
100
0
0
2
4
6
8
10
12
14
16
18
20
Injection volume (PV)

(b)

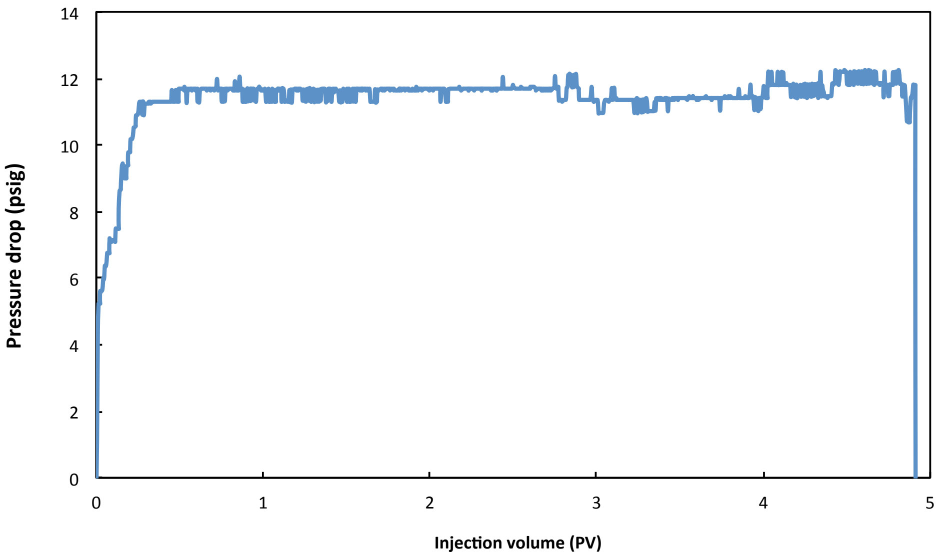

(c)

**Fig. 5.4 Pressure drop along the core versus $CO_2$/nanosilica dispersion injection volume; (a) $CO_2$ fraction 20%; (b) $CO_2$ fraction 60%; (c) $CO_2$ fraction 90%.**

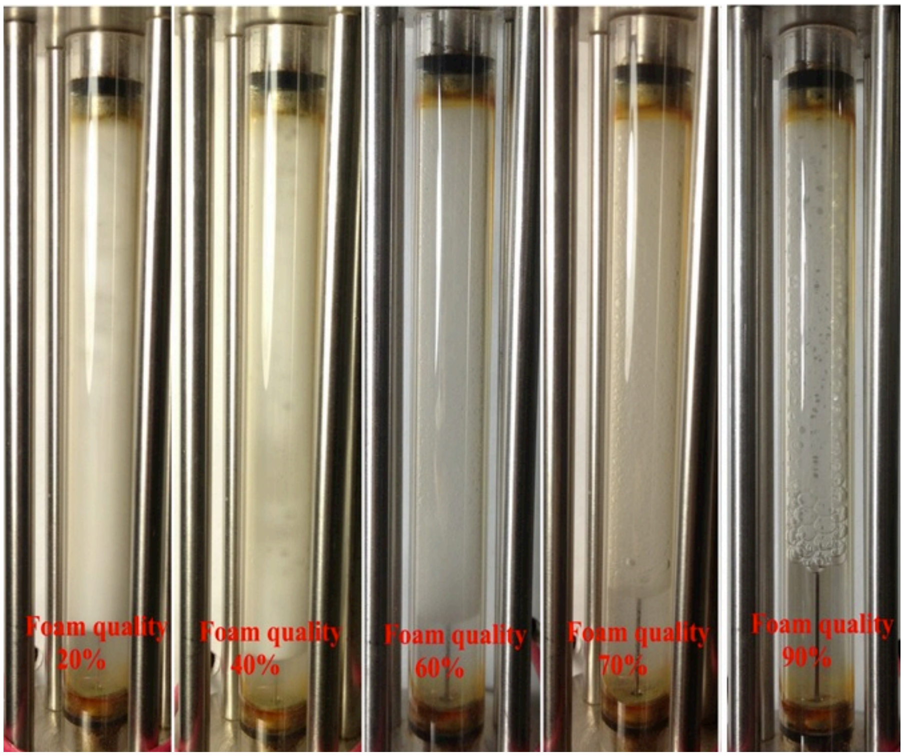

**Fig. 5.5 Images of the $CO_2$ foam at different $CO_2$ fractions.**

Figure 4 shows the foam mobility changing with the foam quality. The results show that foam mobility remain almost same as foam quality increased from 20% to 60% and then increased quickly as foam quality increased from 60% to 95%. The effect of foam quality effect on foam flow behavior has been widely investigated with surfactant being used as a $CO_2$ foam stabilizer. For example, Lee and Heller[26] and Yaghoobi[27] reported that foam mobility increases slightly with increased phase ratio. On the contrary, Khatib[28] and Chang[29] found that, at a given flow rate, foam mobility decreases slightly with increased phase ratio. De Vries and Wit[30] performed a series of tests and concluded that a critical point (break point) for foam mobility existed at an imposed total flow rate; beyond that point foam mobility increases with foam quality.

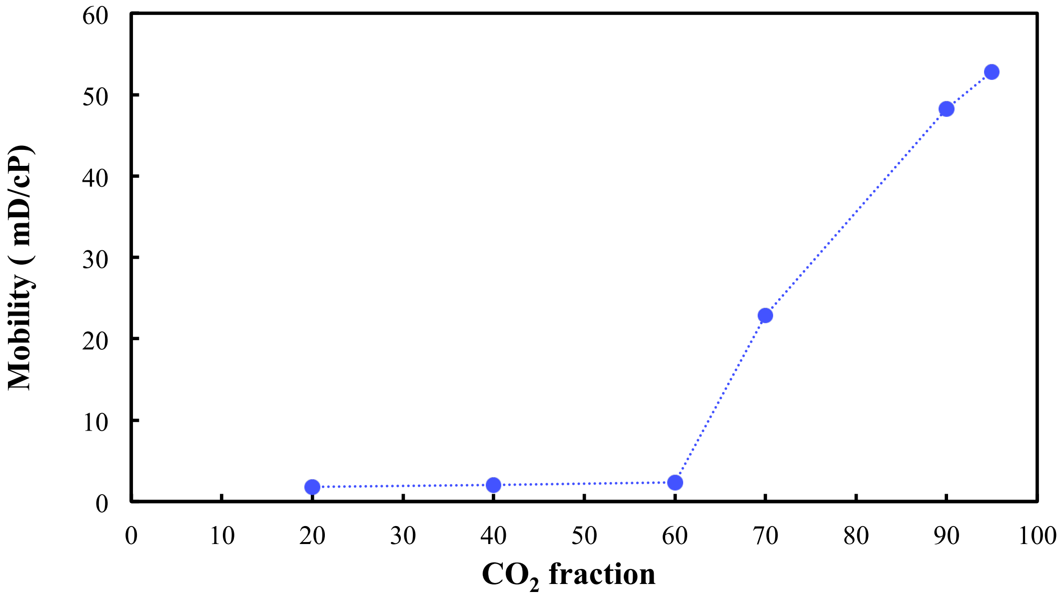

**Fig. 5.6 Foam mobility versus foam quality (flow rate=150 ml/hr; Temperature=25°C; Pressure=1,500 psi).**

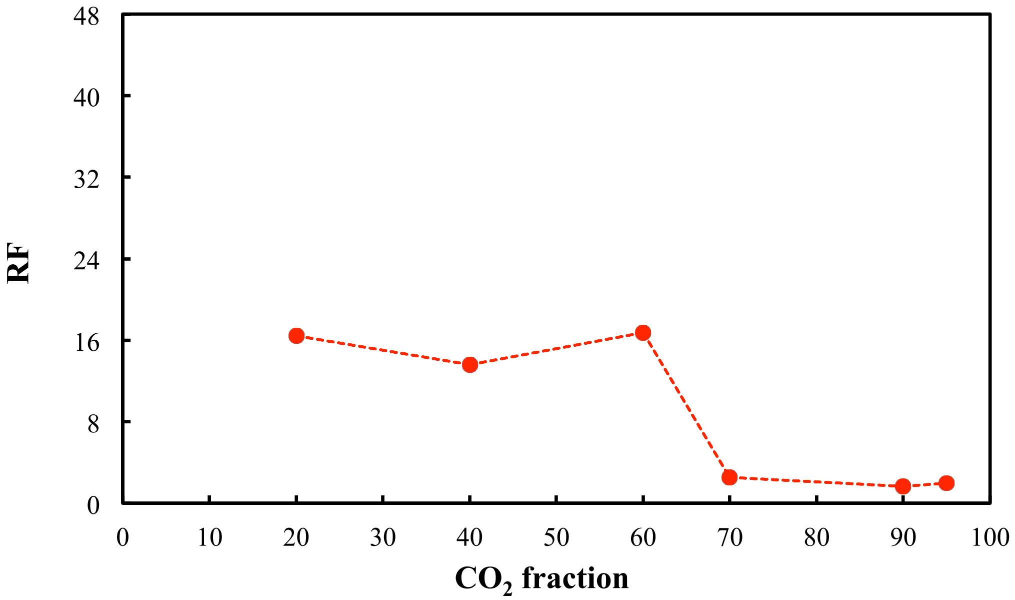

**Fig. 5.7 Foam resistance factor versus foam quality (flow rate=150 ml/hr; Temperature=25°C; Pressure=1,500 psi).**

### *5.2.3 Effect of nanosilica concentration on foam mobility*

The effect of nanosilica concentration on foam flow behavior in sandstone was investigated. Tests for the particle concentration range were from 100 ppm to 5,000 ppm while foam quality was kept at 60% and total flow rate at 150 ml/h. A plot of foam mobility versus nanosilica concentration is shown in Fig. 5.8. The mobility was reduced as the nanosilica concentration increased. The foam mobility decreased sharply from 14.2 md/cp to 3.78 md/cp as the nanosilica concentration increased from 100 ppm to 1,000 ppm, then decreased slowly as the particle concentration increased from 2,500 ppm to 5,000 ppm. This could be because the lamellae formed in the pore spaces between $CO_2$ and brine, becoming more stable as the nanosilica concentration increased. Stability of the lamellae improved the foam resistance to coalescence and allowed more $CO_2$ to flow through the core sample. Foam images in Fig. 5.9 indicated that the foam height increased with the nanosilica concentration being increased from 100 ppm to 5000 ppm, which is well-consistent with the results of foam mobility. In addition, the foam texture was observed to be finer as the nanosilica concentration increased, indicating more stable foam generated at high concentration of nanosilica dispersion. Figure 5.9 also shows that the foam texture was almost same for the nanosilica concentration of 2,500 ppm and 5,000 ppm, which was consisted with similar foam mobilities in Fig. 5.8. The dependence of the foam resistance factor on particle concentration is plotted in Fig. 5.10. The resistance factor was 2.9 for particle concentration as low as 100 ppm. As the nanosilica concentration was increased from 100 ppm to 1000 ppm, the resistance factor increased to 10.7 and then slowly increased to 17.9 as the nanosilica concentration increased to 5,000 ppm.

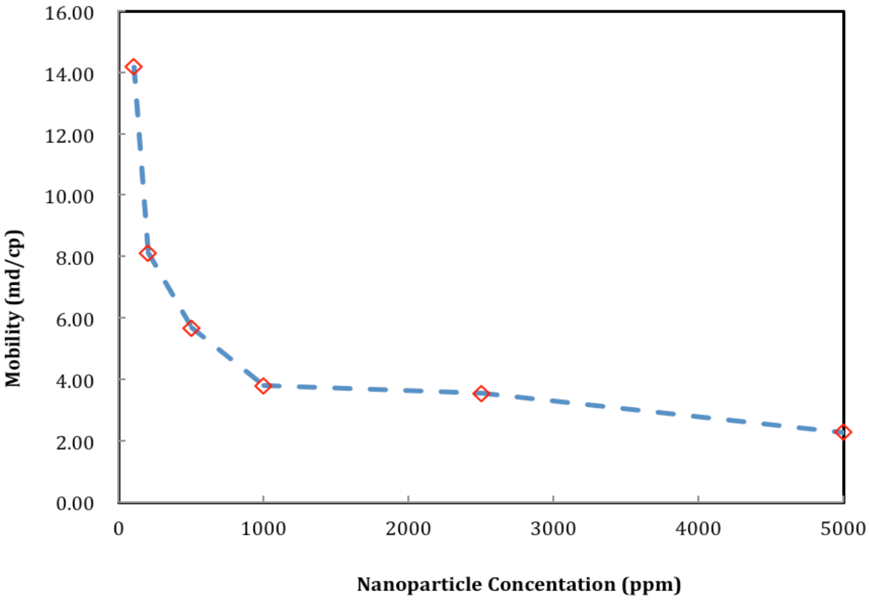

**Fig. 5.8 Foam mobility versus particle concentration at flow rate of 150ml/h, foam quality of 60%, temperature of 25$^o$C, and pressure of 1,500 psi.**

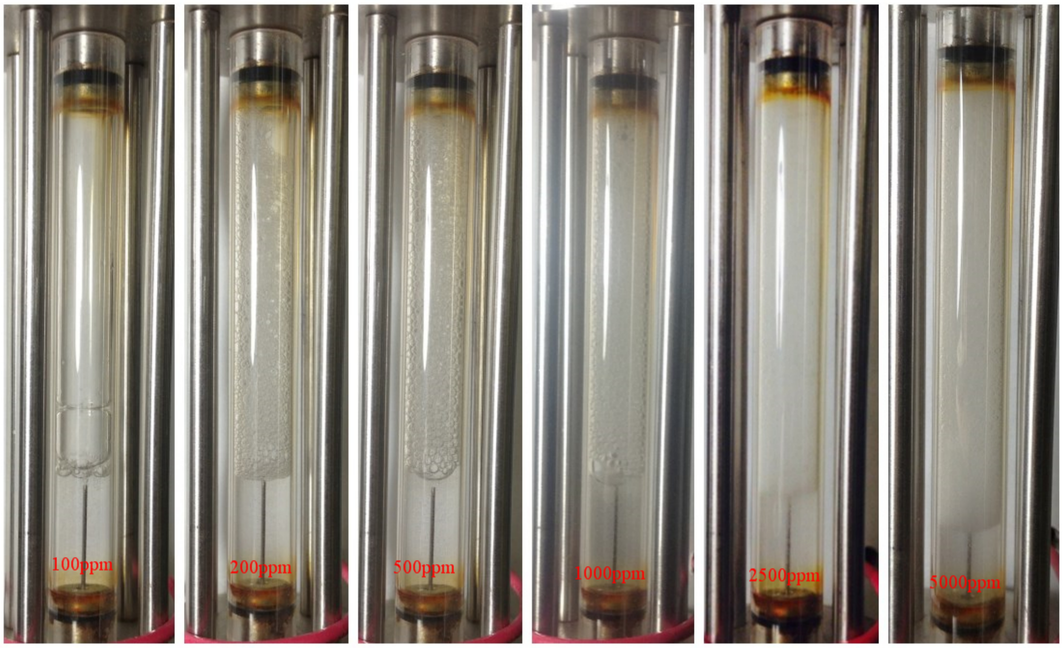

**Fig. 5.9 Images of the $CO_2$ foam generation at different nanosilica concentrations with flow rate of 150 ml/h and 60% foam quality.**

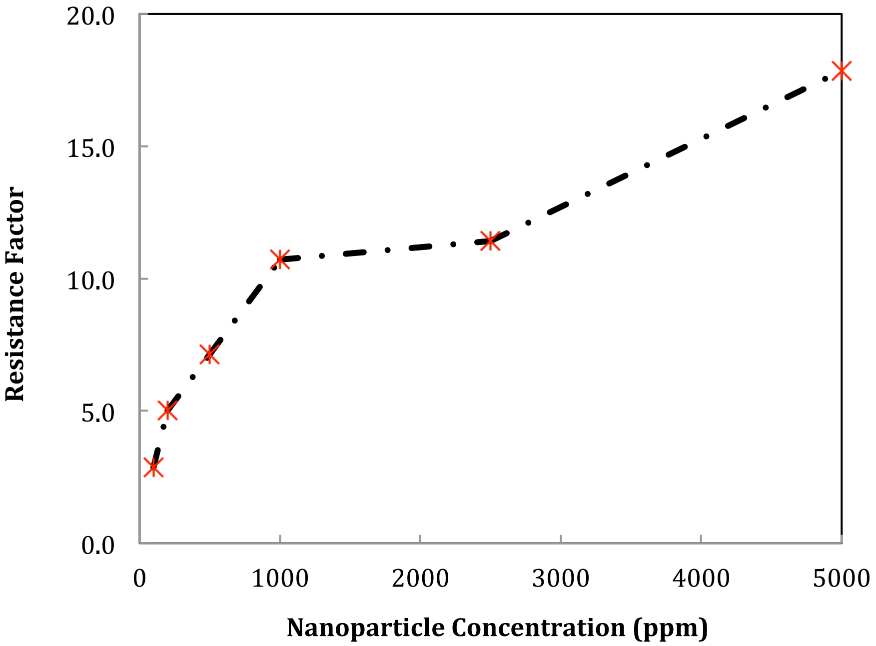

**Fig. 5.10 Foam resistance factor versus particle concentration at flow rate of 150ml/h, foam quality of 60%, temperature of 25°C, and pressure of 1,500 psi.**

### *5.2.4 Effect of flow rate on foam mobility*

A plot of foam mobility vs. flow rate at particle concentration of 5,000 ppm and foam quality of 60% is shown in Fig. 5.11. It can be seen that the total foam mobility was reduced from 9.55 md/cp to 2.3 md/cp as the flow rate increased from 20 ml/h to 60 ml/h. The significant mobility reduction can be explained by the shear rate increase due to the flow rate increase, which in turn promotes silica nanoparticle attachment at the water-$CO_2$ interface, resulting in more stable $CO_2$ foam generation. Further increase of the flow rate from 60 ml/h to 150 ml/h did not result in obvious mobility change, indicating stable $CO_2$ foam was obtained as the flow rate was 60 ml/h. Figure 5.12 shows images of foam generation at different injection rates with foam quality of 60% and nanosilica concentration of 5,000 ppm. It is obvious that finer $CO_2$ foams were obtained as the flow rates were 60, 90, and 150 ml/h.

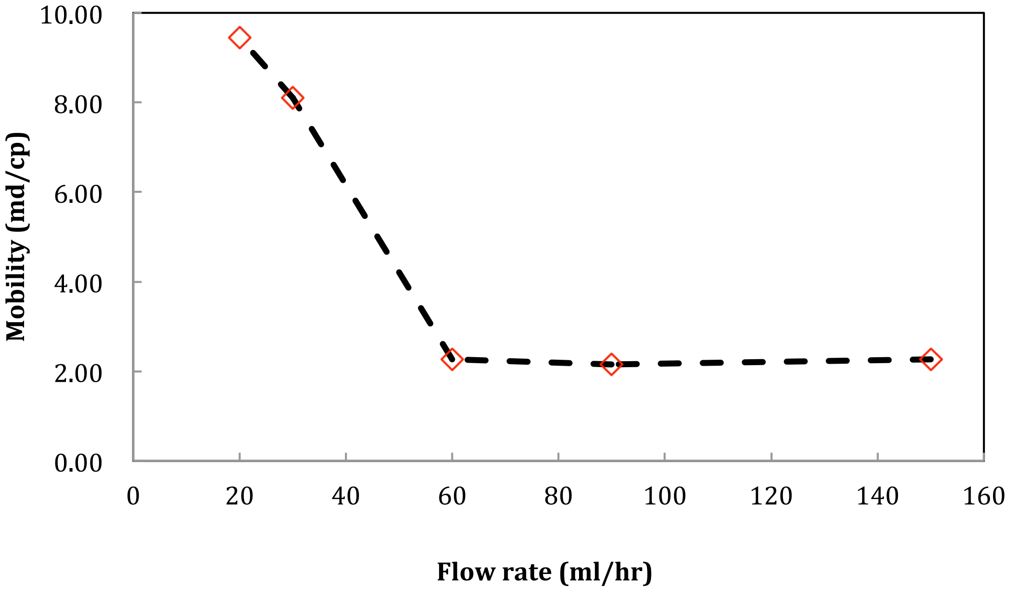

**Fig. 5.11 Foam mobility versus flow rate with particle concentration = 5,000 ppm, foam quality = 60%, temperature = 25$^o$C, and pressure = 1,500 psi.**

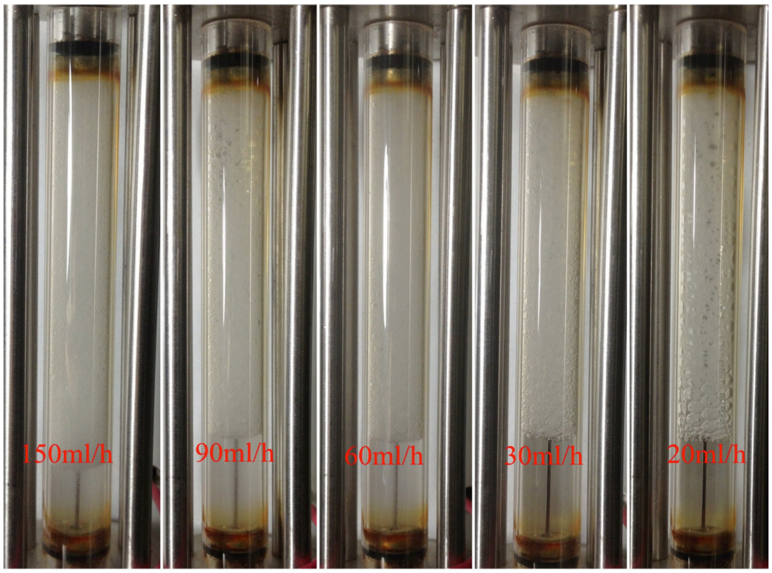

**Fig. 5.12 Images of $CO_2$ foam generated at different flow rates.**

A similar result emerged from the relationship between the foam resistance factor and the flow rate, as shown in Fig. 5.13. The resistance factor slightly increased from 3.2 to 3.3 as the flow rate increased from 20 ml/h to 30 ml/h, and then dramatically jumped to 14.3 as the flow rate further increased to 60 ml/h. Then the resistance factor slowly increased from 14.3 to 17.9 as the flow rate increased from 60 ml/h to 150 ml/h. It is well-known that foam propagation in porous media is a process of breaking and reforming the lamellae of the foam.[31] The more stable the lamellae, the higher is the resistance factor of the foam. Our results indicate that stable lamellae start to form when the flow rate is around 60 ml/h.

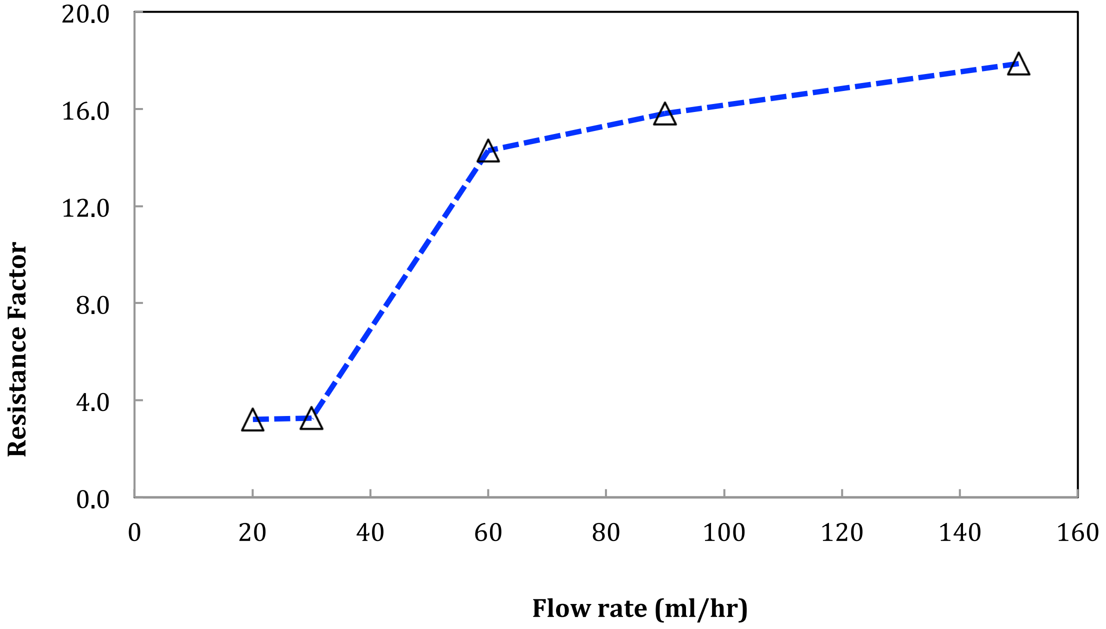

**Fig. 5.13 Foam resistance factor versus flow rate the particle concentration = 5,000 ppm, foam quality = 60%, temperature = 25$^{o}$C, and pressure = 1,500 psi.**

# 6, Effects Of Surfactants On Nanoparticle stabilized $CO_2$ Foam Generation And Foam Stabilization

Since surfactants are widely used in oil industry to recovery residual oil, the effect of surfactants on nanoparticle performance in $CO_2$ foam generation will be investigated in this chapter. Surfactant molecular is expected to adsorb onto the nanoparticle surface and activate the surface performance for $CO_2$ foam generation. Hence, one objective of this chapter is to find a way that introduces a small amount of surfactant can decrease the particle concentration for $CO_2$ foam generation.

## 6.1 Materials and equipment

### *6.1.1 Materials*

Silica nanoparticles obtained from *AkzoNobel* were used for this study. The obtained aqueous dispersion was diluted with 2.0% NaCl to the desired concentration. Berea sandstone core samples from Cleveland Quarries were used for this study. The core was cut to diameter of 2.12 in. and length of 10.0 in. and polished. Surfactants (cationic, anionic, and non-ionic surfactants) were supplied by Huntsman, Chaser International, Inc. and Stepan.

### *6.1.2 Nanosilica dispersion stability test*

The stability of nanosilica dispersion at different temperature and ions/surfactant was investigated. To test the effects of temperature on particle stability, the prepared nanosilica dispersion placed in a closed cylinder and put in the oven under different temperature for 24 hours. After that, the samples were cooled at room temperature and particle size was measured with a Microtrac Zetatrac (Model NPA152-31A), a dynamic light scattering (DLS) analyzer. The nanosilica dispersion was also tested by adding different ions and surfactants and observed the particle size change.

### *6.1.3 $CO_2$ foam generated with nanosilica particle and surfactant*

The experimental apparatus for this study is similar to that used in previous study (Fig. 5.1). Two ISCO syringe pumps (model 260D) were used to inject nanosilica dispersion/nanosilica dispersion + surfactant and liquid $CO_2$ into the core sample. Two floating piston accumulators were used to reserve nanosilica dispersion/nanosilica dispersion + surfactant and supercritical $CO_2$, respectively. Three TEMCO backpressure regulators (BPR) were used to maintain the required operation pressure. Pressure drop along the core was measured with a Honeywell 3000 differential pressure transducer connected to a Daq56 data acquisition system, which recorded the pressure change with time. A sapphire tube, located behind the core, was used to observe the texture of the generated $CO_2$ foam and foam stability.

## 6.2 Results and discussions

### *6.2.1 Factors effect on the nanosilica dispersion stability*

#### *6.2.1.1Temperature effect on the nanosilica dispersion stability*

Figure 6.1 displays the results of nanosilica particle size change with different temperatures. Nanosilica concentration in the diluted dispersion was 5,000 ppm in the tests. The particle size was 18.1 nm at 25°C and 18.2 nm at 85°C. A slight change in particle size under different temperatures implied that no particle aggregation occurred even when the temperature reached 85°C. That indicates that the nanosilica dispersion can stand temperature changes in different reservoirs and no particle plugging is expected to occur due to reservoir temperature change.

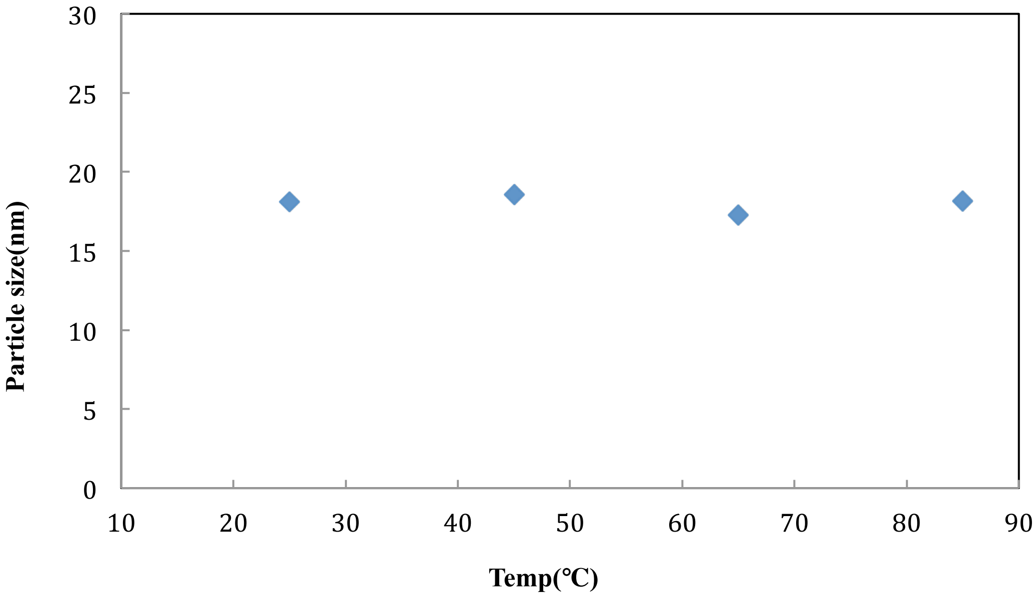

**Fig. 6.1 Nanosilica particle size change with temperature (particle concentration: 5,000 ppm).**

#### *6.2.1.2 Effect of different ions on nanosilica stability*

The effects of different ions such as $Na^+$, $Ca^{2+}$, $Mg^{2+}$ and $SO_4^{2-}$ on nanosilica stability were investigated in case all these ions existed in produced water. The tests were performed by adding different amounts of NaCl, $CaCl_2$, $MgCl_2$, and $Na_2SO_4$ into the diluted nanosilica dispersion, respectively. Then particle size was measured with the ion concentration change in the dispersion. Figure 6.2 displays the results of nanosilica particle size change with the concentration of NaCl. The nanosilica concentration in the dispersion was 5,000 ppm; different amounts of NaCl were then added into the solution. The results indicated that, when NaCl concentration remained below 50,000 ppm, nanosilica particle size was observed not to change with NaCl concentration. The particle size was measured as ~16.2 nm when NaCl concentration increased from 5,000 ppm to 50,000 ppm. A slight particle size change was observed as NaCl concentration increased to 100,000 ppm, in which the particle size increased to 18.1 nm. As NaCl concentration increased to 230,000 ppm, some particle aggregration occured because the particle size increased to 27.8

nm. Upon further increasing NaCl concentration to 255,000 ppm, particle precipitation appreared and some larger particle clusters were oberved as described in Fig. 2; 2.77% of particles were observed to increase in size to 336.0 nm.

Figure 6.3 shows nanosilica particle size change with $CaCl_2$ concentration. The effect of $Ca^{2+}$ on nanosilica particle size change was observed more obviously, compared with $Na^+$ ions. The results indicated that, as $CaCl_2$ concentration increased to 5,000 ppm, nanosilica particle size was measured as ~16.5 nm and no particle aggregation was expected. When $CaCl_2$ concentration increased to 6,000 ppm, slight particle aggregation was oberved and particle size increased to 21.2 nm. A further increase of $CaCl_2$ concentration, up to 7,000 ppm, caused particle precipitation to begin to appear and particle size increased to 24.2 nm, with 2.0% of silica particles increasing to 141.0 nm.

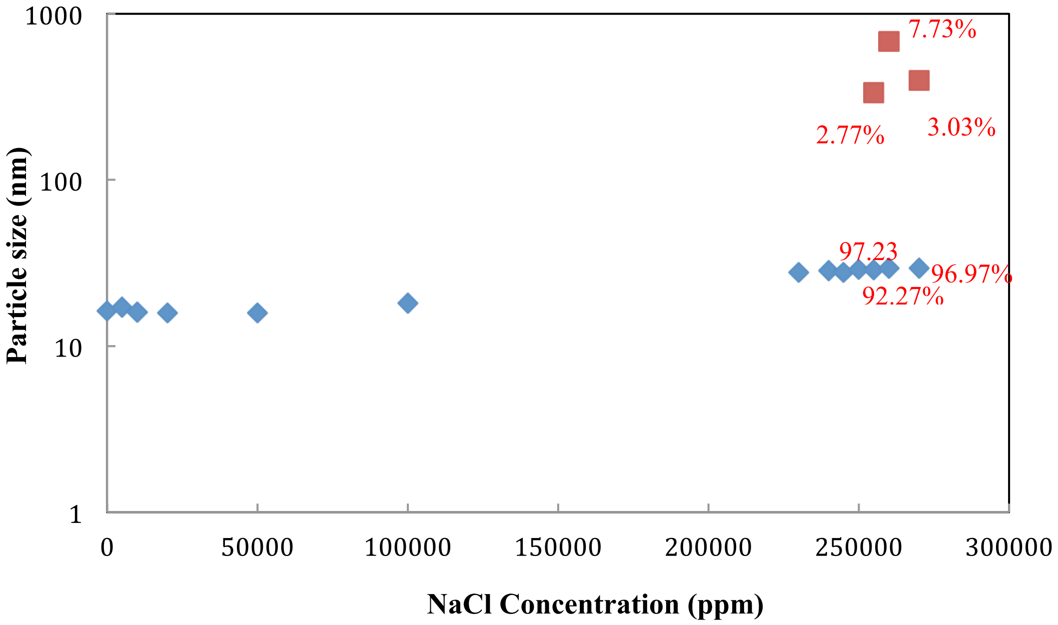

**Fig. 6.2 Nanosilica particle size change with NaCl concentraiton (particle concentration: 5,000ppm).**

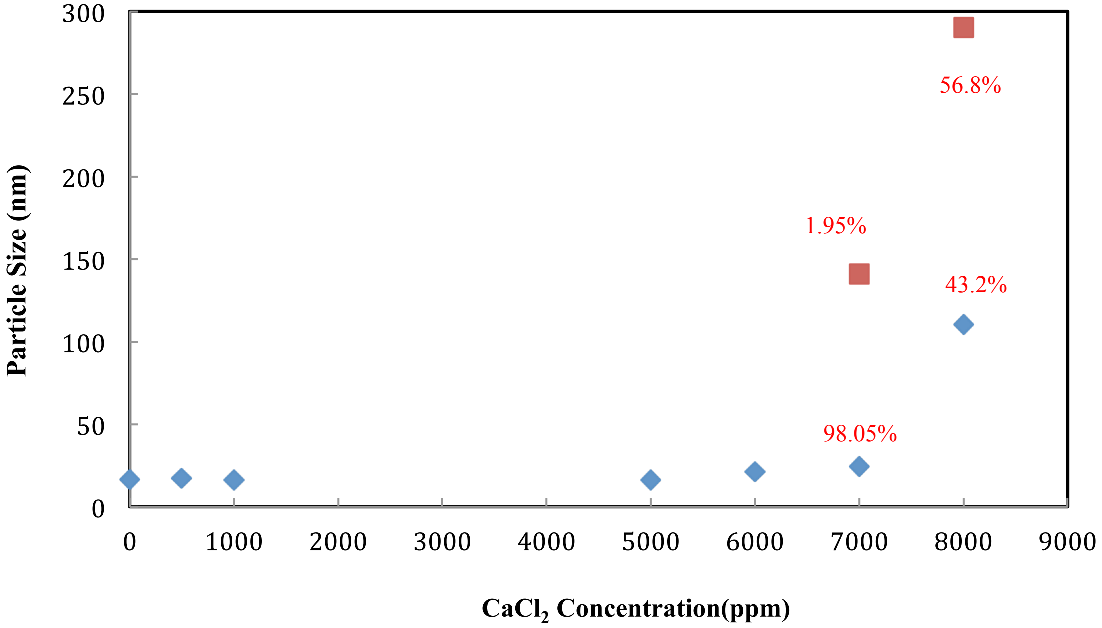

Fig. 6.3 Nanosilica particle size change with $CaCl_2$ concentration (particle concentration: 5,000ppm).

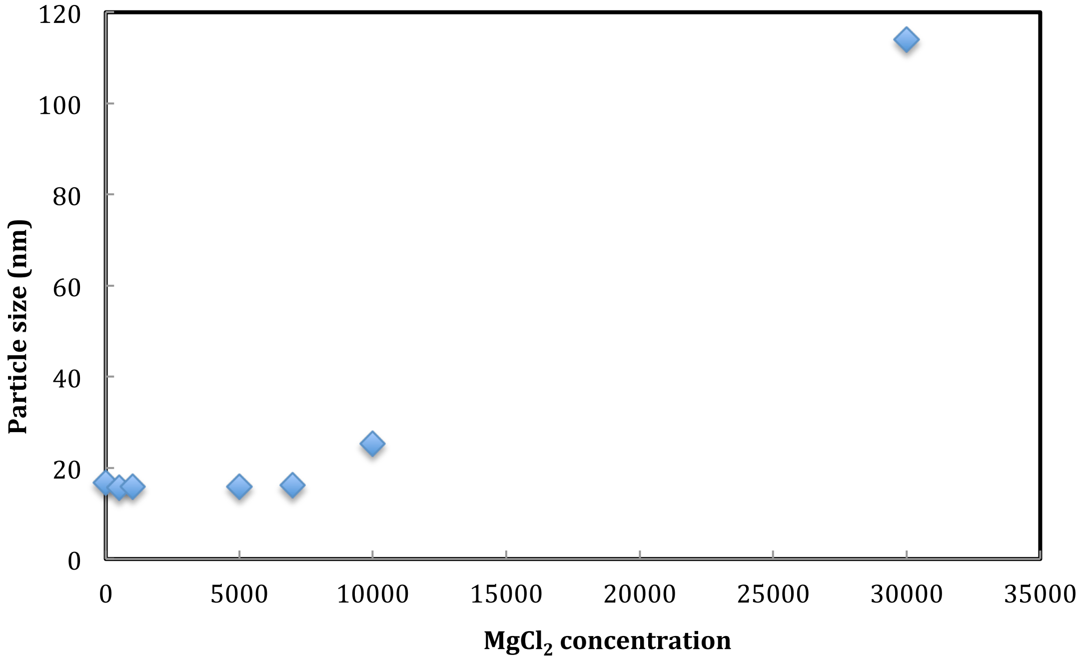

Fig. 6.4 Nanosilica particle size change with $MgCl_2$ concentration (particle concentration: 5,000 ppm).

Figure 6.4 displays the effect of $Mg^{2+}$ concentration on nanosilica particle size change. The results of $Mg^{2+}$ concentration effect on silica particle size change are similar to concentration of $Ca^{2+}$. That is, when $Mg^{2+}$ concentration was lower than 7,000 ppm, no particle aggregation was observed and particle size in the dispersion was around 16.1 nm. When $Mg^{2+}$ concentration increased to 10,000 ppm, particle size increased to 25.3 nm and silica particle aggregation began. With further increase of $Mg^{2+}$ concentration to 30,000 ppm, particle size increased to 114.0 nm and the dispersion became cloudy, indicating silica particle precipitation occurred.

Figure 6.5 shows the effect of $SO_4^{2-}$ on nanosilica particle size change. The effect of $SO_4^{2-}$ on silica particle size is less than that of $Ca^{2+}$ and $Mg^{2+}$. The particle size was 16.4 nm when $SO_4^{2-}$ concentration increased to 10,000 ppm. No particle aggregation was observed when $SO_4^{2-}$ was added to the nanosilica dispersion.

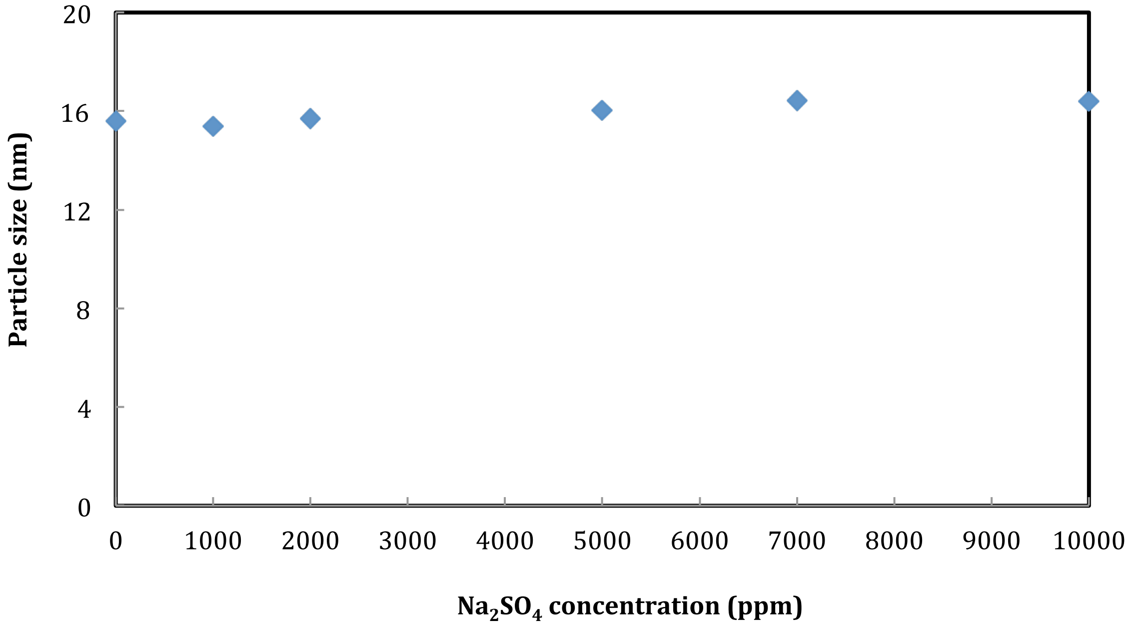

**Fig. 6.5 Nanosilica particle size change with $Na_2SO_4$ concentration (particle concentration: 5,000 ppm).**

### *6.2.1.3 Effect of produced water on nanosilica dispersion stability*

The effect of produced water on the stability of nanosilica dispersion was studied for the case where nanosilica and produced water are co-injected in $CO_2$ EOR. Two compositions of produced waters, one with low Total Dissolved Solids (TDS) value and one high, were prepared. These TDS values were 180,013 ppm and 3,321 ppm. The compositions of these produced waters are shown in Table 6.1. Figures 6.6 and 6.7 show the results of nanosilica particle size change in the two types of synthetic produced waters over seven days. Particle size in low TDS water was around 15.2 nm and showed no change in a week. In the high TDS produced water, the particle size was around 21.1 nm. That implied that some particle aggregation might be occurring in the high TDS produced water. In addition, Figure 6.7 also indicates that, although particle aggregation occurred in high TDS produced water, the particle size showed no change in seven days and no further particle aggregation occurred.

**Table 6.1 The Compositions of Permian Basin Produced Waters[32]**

| mg/L | | $Na^+$ | $Ca^{2+}$ | $Mg^{2+}$ | $K^+$ | $Cl^-$ | $SO_4^{2-}$ | $HCO_3^-$ | TDS |
|---|---|---|---|---|---|---|---|---|---|
| Permian Basin | 1 | 61842 | 3486 | 3524 | 180 | 108486 | 2017 | 134 | 180013 |
| | 2 | 788 | 304 | 13 | 42 | 1040 | 1000 | 134 | 3321 |

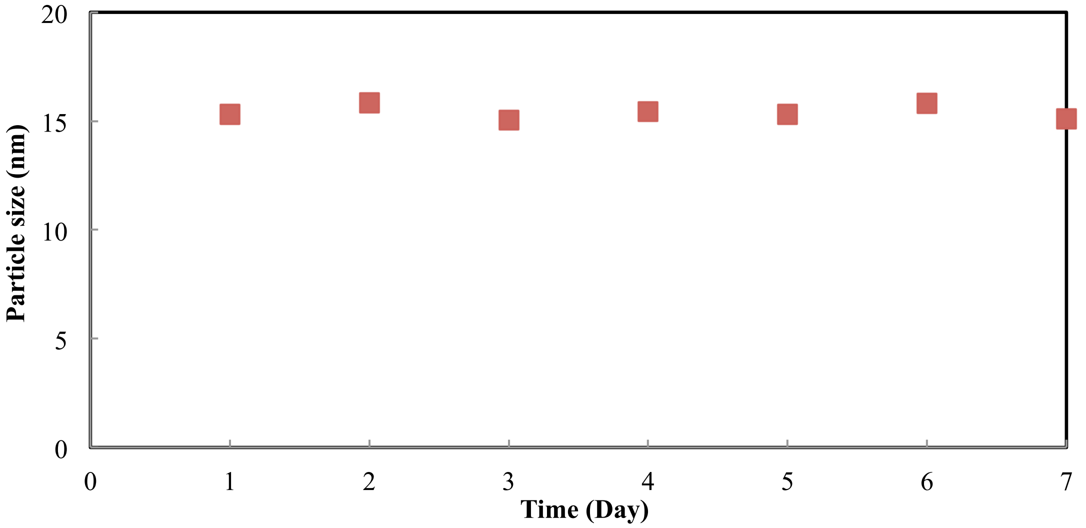

Fig. 6.6 Nanosilica particle size change in low TDS produced water (particle concentration: 5,000 ppm).

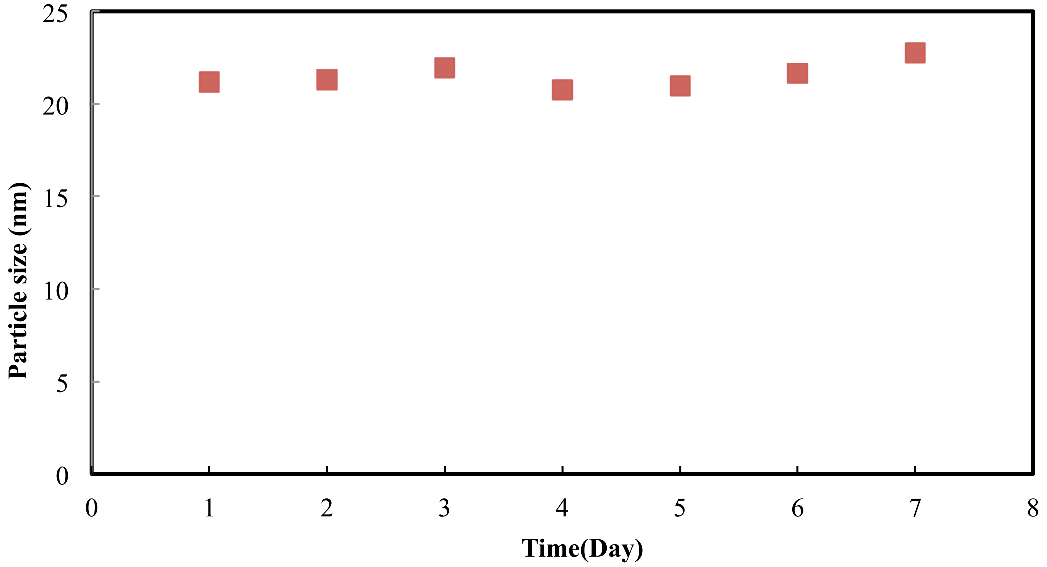

Fig. 6.7 Nanosilica particle size change in high TDS produced water (particle concentration: 5,000 ppm).

#### *6.2.1.4, Effects of surfactants on nanosilica dispersion stabilty*

It was reported that surfactant could adsorb onto a nanoparticle surface and change its surface properties.[33,34] The use of nanoparticle and surfactant mixtures is probably an alternative way to generate $CO_2$ foam, and at the same time, to decrease particle concentration and cost. Hence, the effects of surfactants on nanosilica stability were studied. Three different types of surfactants, cationic, anionic, and non-ionic surfactants, were used for this study. The cationic surfactant, XOF 215, is an alkylamidopropyl betaine. The anionic surfactant, XOF 700S/70, is an alcohol ether sulfate and the non-ionic surfactant, Surfonic N-120, is a nonyphenol. Figure 6.8 shows the results of the cationic surfactant's (XOF 215) effect on silica particle size change. The particle size was measured when surfactant was added in the dispersion and then measured again after 24 hours standing. The results demonstrated that no particle aggregation occurred when the surfactant concentration increased to 100 ppm. The particle size was around 16.9 nm and showed no change after 24 hours standing as a surfactant, XOF 215, was added to the dispersion.

Figure 6.9 shows the results of the effect of anionic surfactant XOF 700s/70 on silica particle size change. No particle aggregation was observed as the XOF 700s/70 concentration increased to 500 ppm. The particle size was around 16.5 nm and showed no change for 24 hours. Figure 6.10 displays the effect of non-ionic surfactant, Surfonic N-120 on silica particle size change. The particle size was around 16.4 nm and stayed constant as the surfactant concentration increased to 200 ppm. No particle aggregation was observed after three days of standing as Surfonic N-120 was added in the dispersion.

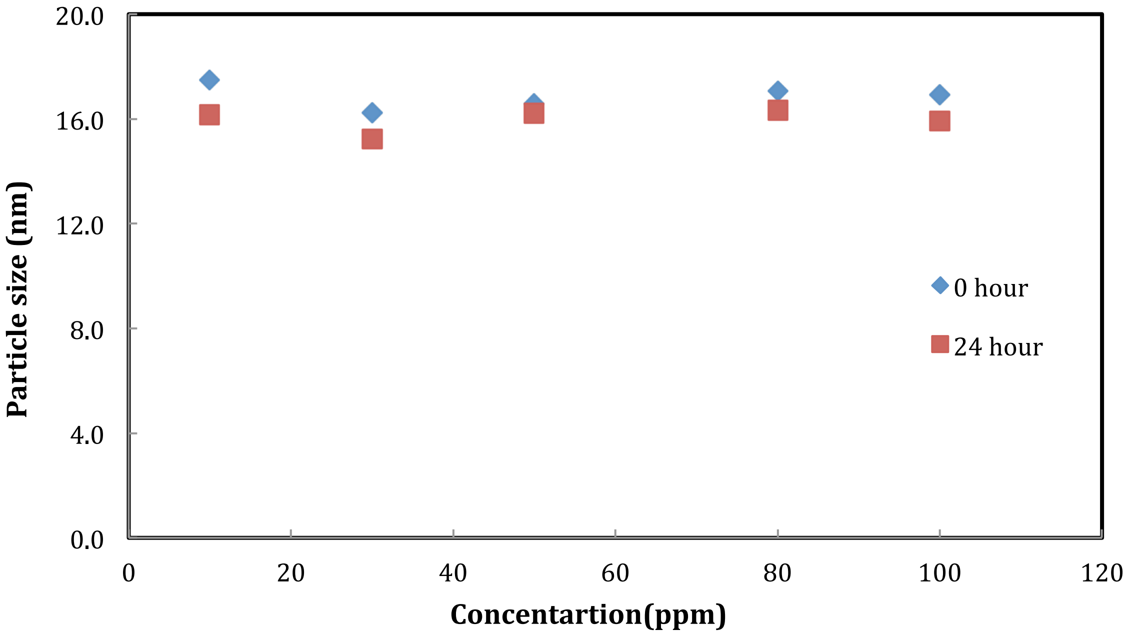

Fig. 6.8 Nanosilica particle size change with cationic surfactant XOF 215 (particle concentration: 5,000 ppm).

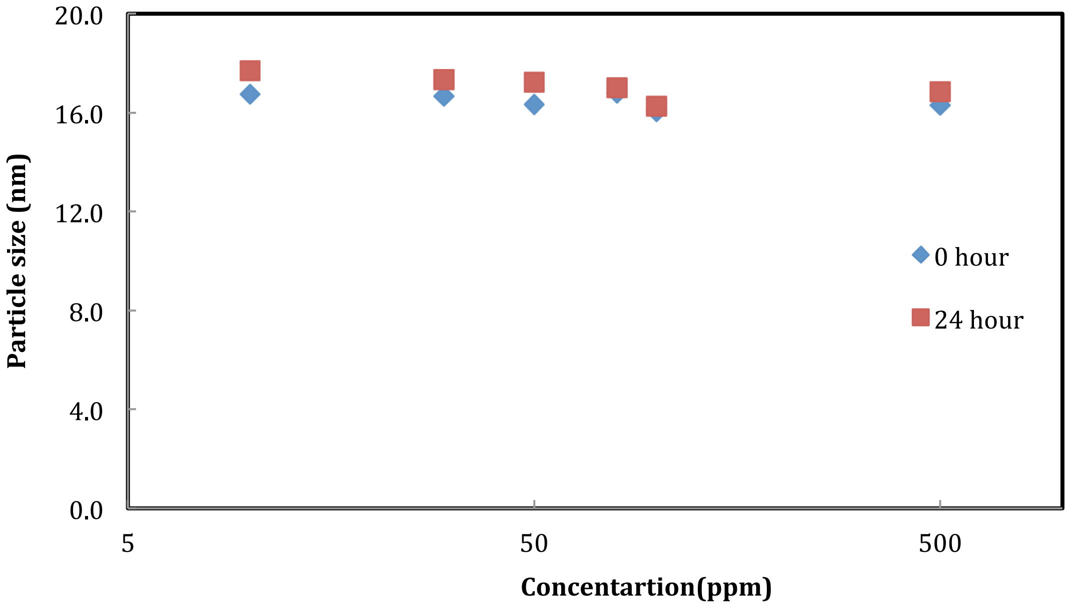

Fig. 6.9 Nanosilica particle size change with anionic surfactant XOF 700s/70 (particle concentration: 5,000 ppm).

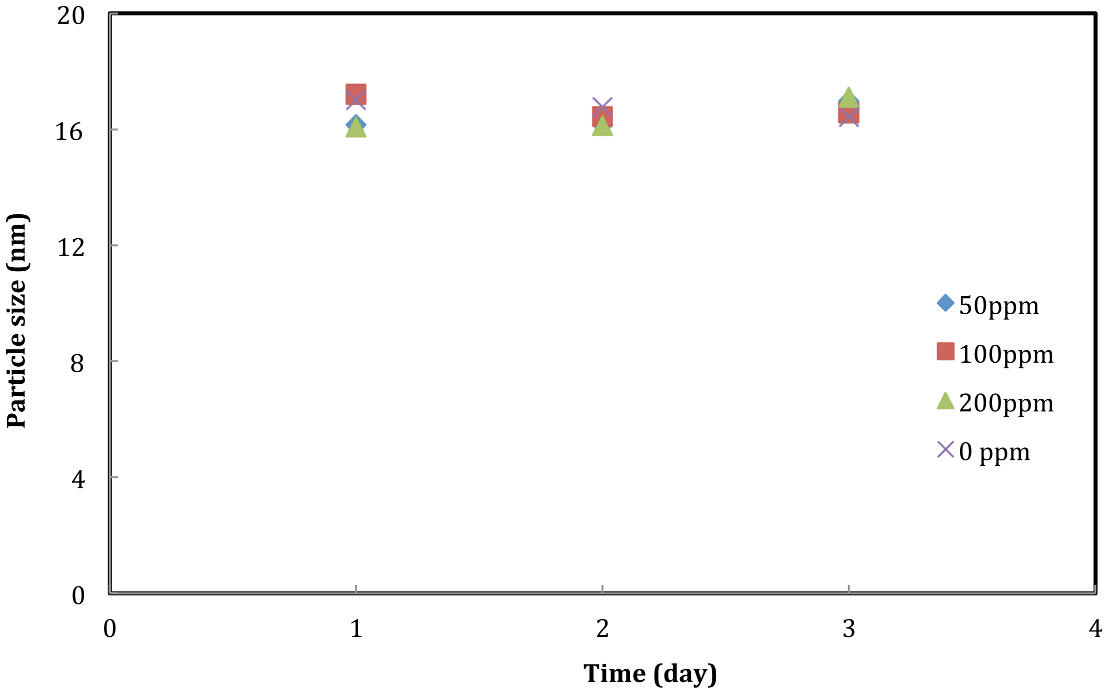

**Fig. 6.10 Nanosilica particle size change with non-ionic surfactant N-120 (particle concentration: 5,000 ppm).**

### *6.2.2 Surfactants effects on the nanosilica-stabilized $CO_2$ foam generation and foam stability*

#### *6.2.2.1 $CO_2$ foam generated with nanosilica particle and $CO_2$*

Before the study of the effects of surfactant on nanosilica-stabilized $CO_2$ foam generation, a control test was perfomed to collect data without adding the surfactant. The test was carried out by injection of 500 ppm nanosilica dispersion (dispersed in 2.0% brine) and $CO_2$ into the core with phase ratio of $CO_2$:nanosilica dispersion = 3:2 and total flow rate = 150 ml/hr. Figure 6.11 displays the pressure drop along the core during the test. At the beginning of the test, 2.0% brine was injected into the core to measure core permeability. After injection of 2.3 pore volume (PV) of brine, $CO_2$/nanosilica dispersion injection into the core was initiated. The pressure drop along the core increased with the injected $CO_2$/nanosilica dispersion volume until 15 PV of $CO_2$/nanosilica dispersion were injected, which was around 142 psi as displayed in Fig. 6.11. Figure 6.12 shows the image of the $CO_2$ foam from the observation cell. The foam fully filled the cell with the height of 7.5 cm at the beginning. However, it started to collapse as soon as it was generated. For example, the foam height decreased to 6.2 cm after 3 hours. After 15 hours standing at the room temperature, the foam height decreased to 4.3 cm.

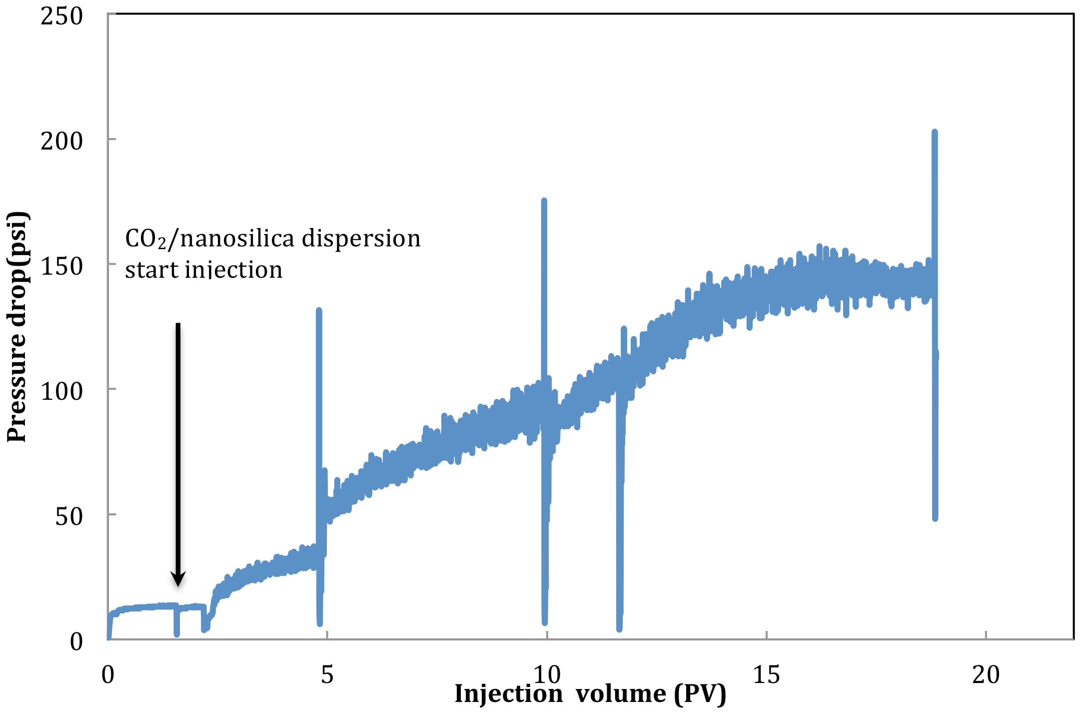

**Fig. 6.11 Pressure drop along the core when 500 ppm nanosilica and $CO_2$ flowed through the core.**

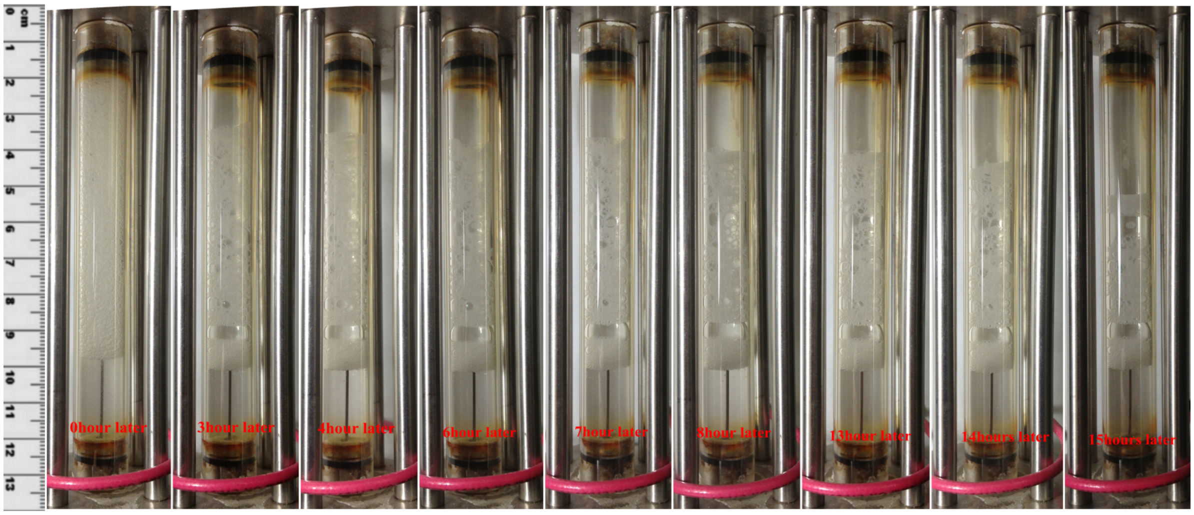

**Fig. 6.12 The height of the $CO_2$ foam changed with time ($CO_2$ foam generated with 500 ppm nanosilica dispersion and $CO_2$).**

#### *6.2.2.2 Effect of Anionic surfactants on nanosilica-stabilized $CO_2$ foam generation*

After the control test, anionic surfactant (XOF 700S/70 from Huntsman) was added to the nanosilica dispersion to investigate its effect on $CO_2$ foam generation. The experiemntal procedure was the same as that for the control test, except XOF 700S/70 + nanosilica dispersion mixture was injected into the core together with $CO_2$. The concenration of XOF 700S/70 in the nanosilica dispersion was 30 ppm. Figure 6.13 shows the pressure drop along the core during the test. The pressure drop increased to more than 400 psi when XOF 700S/70 was added into the nanosilica dispersion. However, it was observed that the core permeability decreased to less than 10 md after the test, which means that the higher pressure drop might contribute to the core plugging. Further studies of the $CO_2$ foam image (Fig. 6.14) indicated that little or no foam was generated when $CO_2$/ nanosilica dispersion + XOF 700S/70 was co-injected into the core. The results implied that the higher pressure drop in Fig. 6.13 could be due to the core adsorption and core plugging.

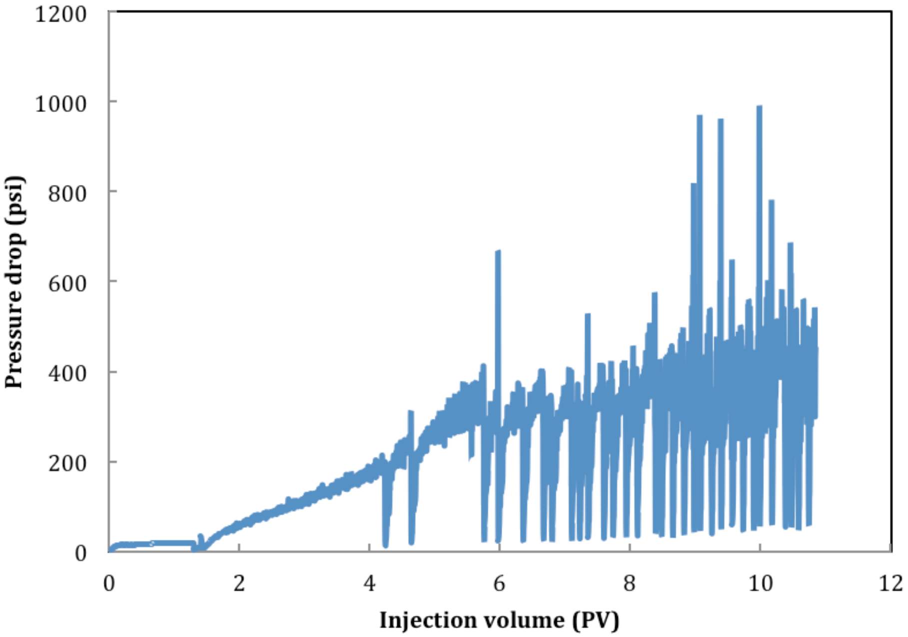

**Fig. 6.13 Pressure drop along the core when 500 ppm nanosilica+30 ppm XOF 700S/70 and $CO_2$ was flowed through the core.**

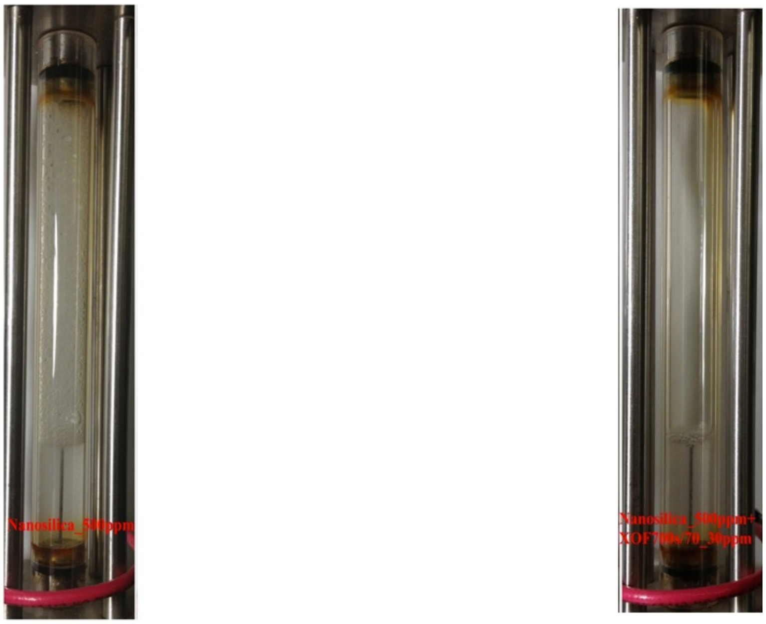

(a) (b)

**Fig. 6.14 Images of the $CO_2$ foam at (a) 500 ppm nanosilica dispersion / $CO_2$; (b) 500 ppm nanosilica dispersion + 30 ppm XOF 700S/70 /$CO_2$.**

Another anionic surfactant, CD1045TM (Chaser International Inc.), was also selected and tested to study its effect on the $CO_2$ foam generation and foam mobility. CD1045TM, identified as one of the best foaming agents in several other studies[35,36], has a different molecular structure from XOF 700S/70. Figure 6.15 shows the pressure drop along the core during the $CO_2$/nanosilica dispersion + CD1045TM injection. The pressure drop at the steady state was around 265 psi, which is higher than the pressure drop at the control test. A higher pressure drop indicated that the mobility of $CO_2$ decreased when surfactant CD1045TM was introduced. However, the foam image from the observation cell (Fig. 6.16) shows that little $CO_2$ foam was generated when surfactant CD1045TM was added. The life-time of the foam was observed to be very short, ~10 minutes when standing at room temperature. The short life-time of the generated $CO_2$ foam and higher pressure drop along the core when surfactant CD1045TM was added probably can be explained by: (1) the $CO_2$ foam was more easily generated in the porous media as surfactant

CD1045TM was added; (2) the generated $CO_2$ foam (when surfactant CD1045TM was added) was not as stable as the $CO_2$ foam generated with $CO_2$/nanosilica dispersion.

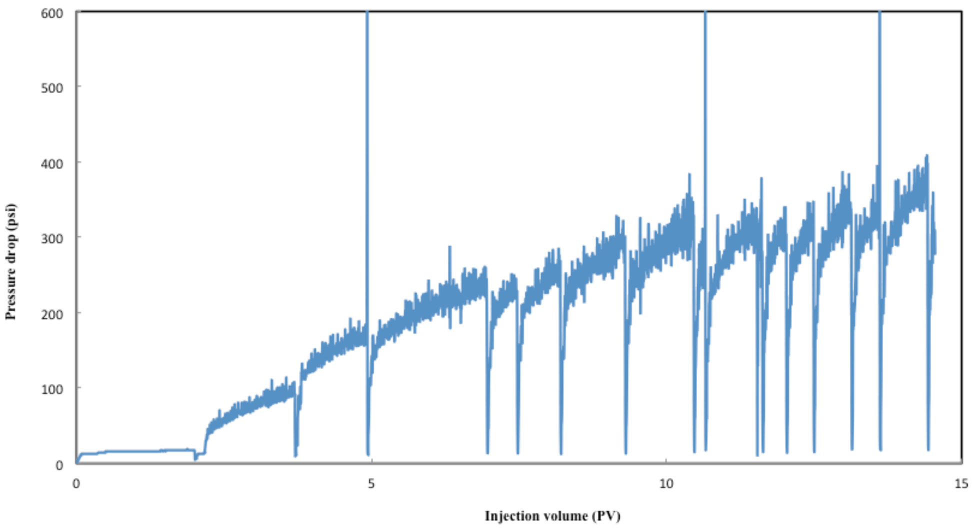

**Fig. 6.15 Pressure drop along the core when 500 ppm nanosilica + 50 ppm CD1045 and $CO_2$ flowed through the core.**

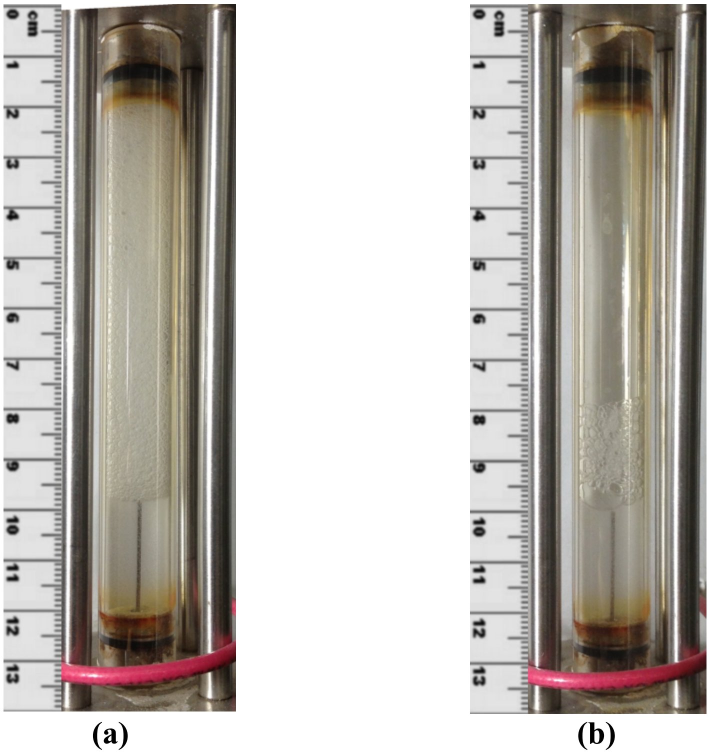

**(a)** **(b)**

**Fig. 6.16 Images of the $CO_2$ foam at (a) 500 ppm nanosilica dispersion / $CO_2$; (b) 500 ppm nanosilica dispersion + 50 ppm CD1045$^{TM}$ /$CO_2$.**

#### *6.2.2.3 Effect of cationic surfactant on $CO_2$ foam generation*

Figure 6.17 show the pressure drop along the core when 100 ppm cationic surfactant XOF-214 was added into nanosilica dispersion. Pressure drop along the core was 117 psi when surfactant concentrations in the nanosilica dispersion was 100 ppm. Compared with the pressure drop in the control test, the lower pressure drop as surfactant XOF-214 was added indicated that adding the cationic surfactant XOF-214 into 500 ppm nanosilica dispersion inhibited $CO_2$ foam generation. Figure 6.18 displays the foam images from the observation cell when 100 ppm XOF-214 was used. The volume of the generated $CO_2$ foam was much less than that seen in the control test. Furthermore, the lifetime of the foam was observed to be very short. All the foam collapsed after standing at room temperature for several minutes.

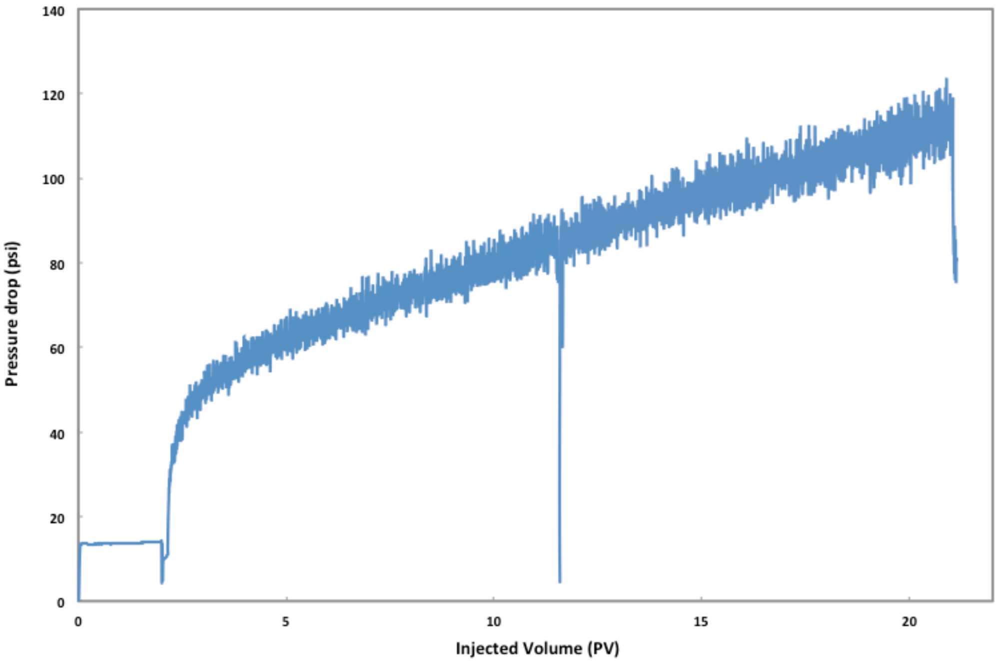

**Fig. 6.17 Pressure drop along the core when $CO_2$/ nanosilica dispersion (500 ppm in 2% brine) + 100 ppm XOF-214 was flowed through the core.**

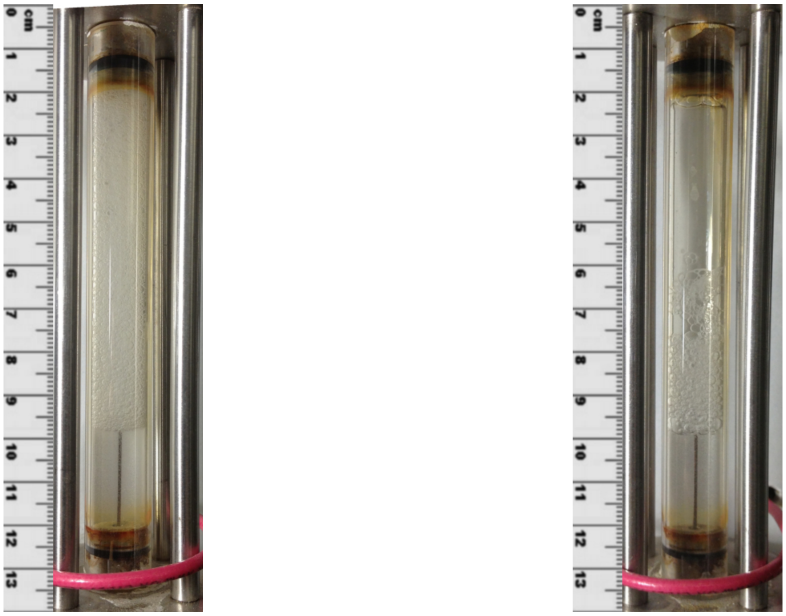
(a) (b)

**Fig. 6.18 Images of the $CO_2$ foam at (a) 500 ppm nanosilica dispersion / $CO_2$; (b) 500 ppm nanosilica dispersion + 100 ppm XOF-214/$CO_2$.**

### *6.2.2.4 Effect of non-ionic surfactant on $CO_2$ foam generation*

Figure 6.19 shows the pressure drop along the core when 100 ppm amphosol CS-50 was added into 500 ppm nanosilica dispersion. Pressure drop along the core was 365 psi when surfactant + nanosilica dispersion/$CO_2$ were flowed through the core. Compared with the pressure drop in the control test, the higher pressure drop as surfactant amphosol was added indicated that adding the surfactant amphosol CS-50 into the nanosilica dispersion probably promoted $CO_2$ foam generation. The image of the $CO_2$ foam was displayed in Fig. 6.20 when 100 ppm amphosol CS-50 + 500 ppm nanosilica dispersion/$CO_2$ flowed through the core. The volume of the generated $CO_2$ foam as 100 ppm amphosol CS-50 was added into the nanosilica dispersion almost filled the cell, which furthemore indicated that surfactant samphosol CS-50 improved $CO_2$ foam generation. Similar results were also reported by Andrew Worthen, where bare colloidal silica and surfactant (caprylamidopropay betaine) were mixed to generate $CO_2$ foam. Synergistic interactions at the interface of nanosilica particles and surfacatant were observed to result in stable $CO_2$-in-water foams. The stability of nanosilica/amphosol CS-50–stabilized $CO_2$ foam was also investigated. Figure 5 also displays the $CO_2$ foam height change with standing time. Unlike the $CO_2$ foam generated with anionic and cationic surfactants, the $CO_2$ foams generated with amphosol CS-50 and nanosilica particles are very sable. The height of the $CO_2$ foam decreased from 7.5 cm to 1.2 cm after standing at room temperature for 20 hours (Fig. 6.20).

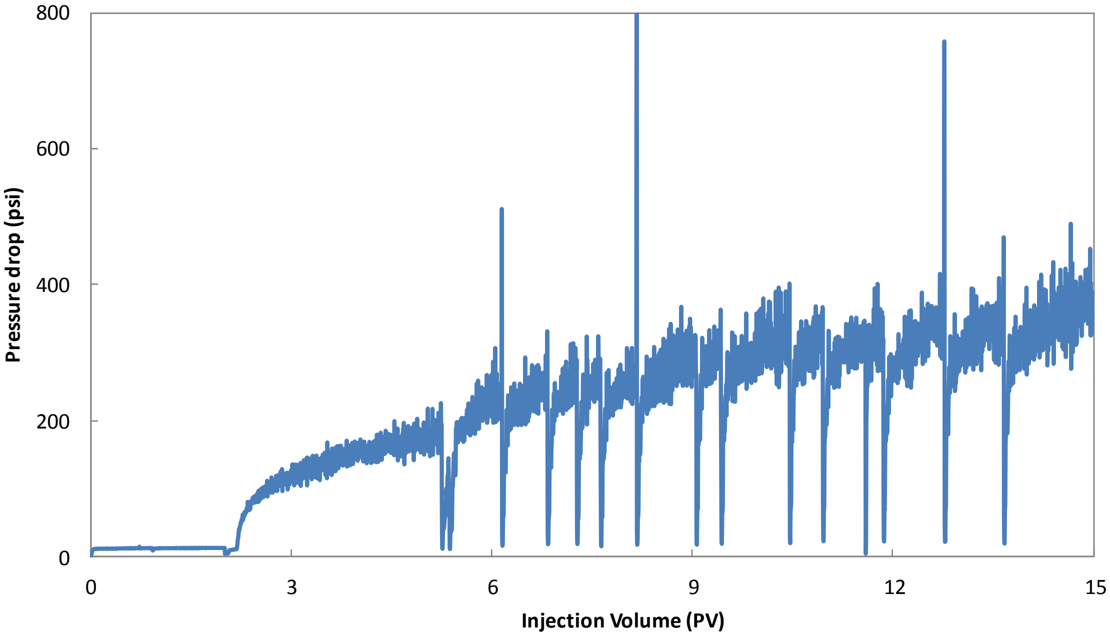

**Fig. 6.19 Pressure drop along the core when 500 ppm nanosilica + 100 ppm amphosol CS-50 and $CO_2$ were flowed through the core.**

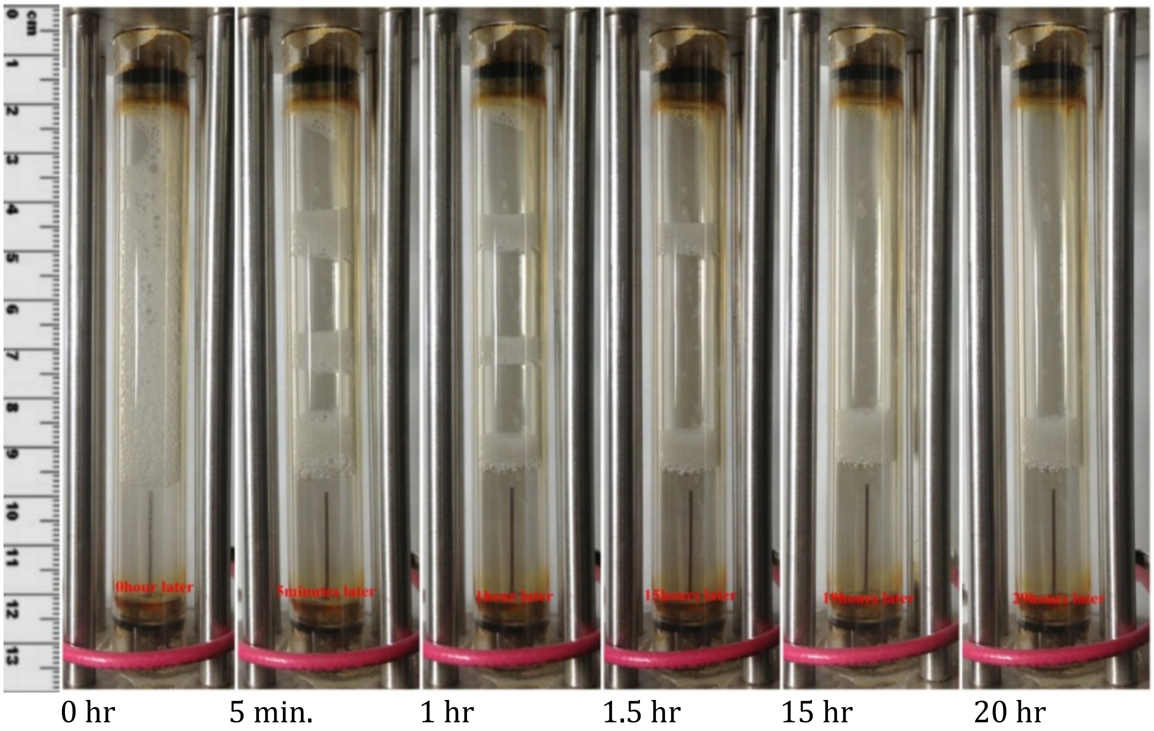

**Fig. 6.20 The height of the $CO_2$ foam changed with time ($CO_2$ foam generated with 500 ppm nanosilica dispersion + 100ppm 7-Amphosol CS-50 and $CO_2$).**

*6.2.2.5 $CO_2$ foam generation with different surfactants*

To further understand the synergistic interaction between surfactant and nanosilica, a series of tests of $CO_2$ foam generation with different surfactants were conducted. The test procedure and conditions were same as above. Figures 6.21–6.22 show the pressure drop along the core during the tests. The pressure drop along the core was around 376 psi when 100 ppm surfactant CD1045 and $CO_2$ were flowed through the core, which is almost same as that of nanosilica + CD1045/$CO_2$. The foam picture (Fig. 6.23a) also indicated that, after being mixed with nanosilica dispersion, there was no significant synergistic interaction between nanosilica particles and surfactant CD1045 for $CO_2$ foam generation. It seemed that, after being mixed with nanosilica disperion, $CO_2$ foam generation and foam flow behavior were dominated by surfactant CD1045 and nanosilica particles had no effect in the process. Figures 6.22 and 6.23b show the pressure drop along the core and the image of the $CO_2$ foam when surfactant Amphosol CS-50 was used. The pressure drop was around 142 psi and much lower than that of Amphosol CS-50/nanosilica dispersion (365 psi in Fig. 6.19). The foam images of Figs. 6.20 and 6.23b clearly indicate a strong synergistic interaction for the $CO_2$ foam generation that occurred when Amphosol CS-50/nanosilica dispersion was injected into the core. In addition, the viscosity of different surfactants with nanosilica dispersion was measured and displayed in Table 6.2, which revealed that the mixture viscosity was almost the same and the pressure drop along the core were not from the viscosity difference.

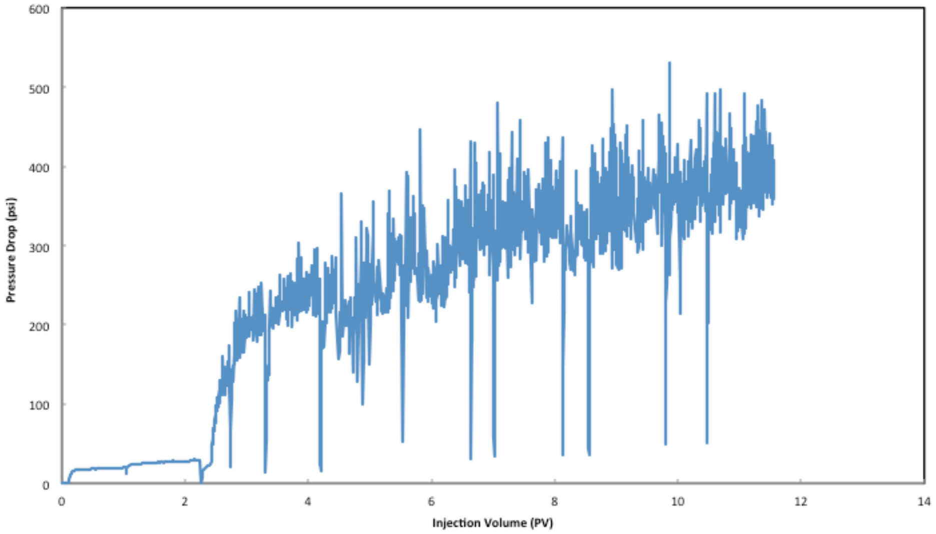

**Fig. 6.21 Pressure drop along the core when $CO_2$ and 100 ppm CD1045 were flowed through the core.**

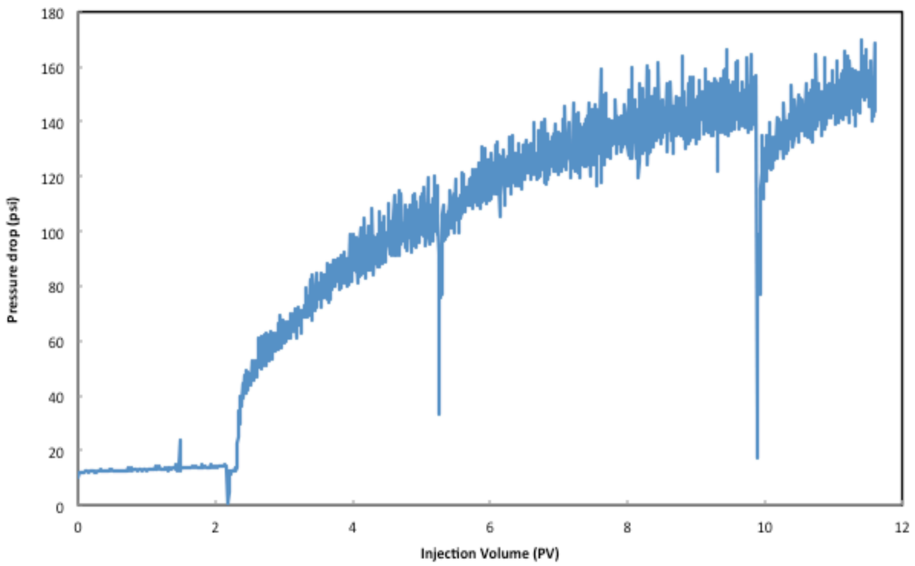

**Fig. 6.22 Pressure drop along the core when $CO_2$ and 100 ppm 7-Amphosol CS-50 were flowed through the core.**

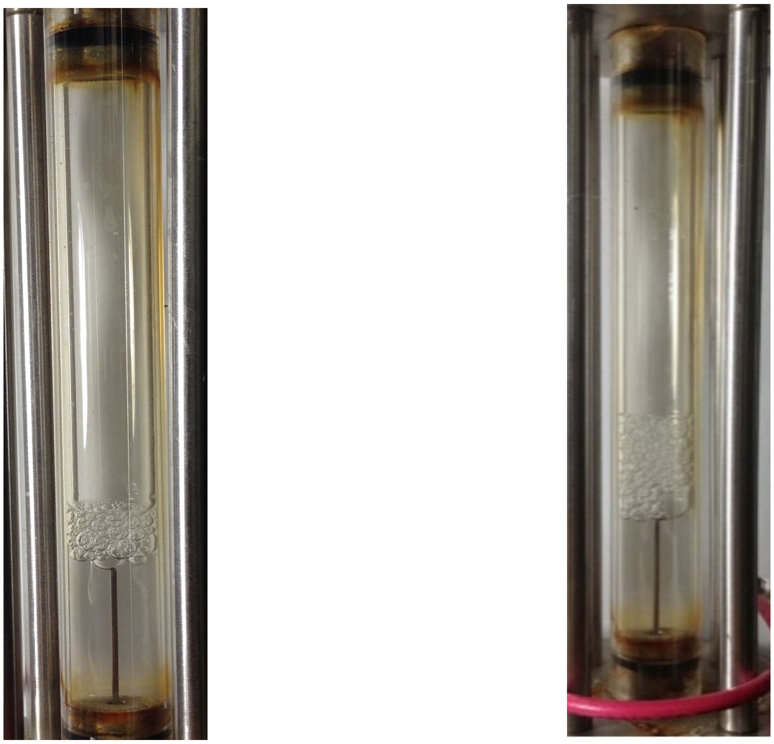
**(a)** **(b)**

**Fig. 6.23 Images of the $CO_2$ foam generated at (a) 100 ppm CD1045; (b) 100 ppm Surfonic™ N-120; (c) 100 ppm 7-Amphosol CS-50.**

**Table 6.2. Viscosity of Nanosilica Dispersion + Surfactant**

| Name | Viscosity (cp) |
|---|---|
| 500ppm Nanosilica dispersion | 0.90255 |
| 100ppm CD 1045 + 500ppm Nanosilica dispersion in 2% brine | 0.902567 |
| 100ppm 7-Amphosol CS-50 + 500ppm Nanosilica dispersion in 2% brine | 0.903186 |

# 7, Nanoparticle-stabilized $CO_2$ Foam for residual oil recovery

The previous studies indicated that $CO_2$ foam was generated as liquid $CO_2$ and nanosilica were flowed through core samples. In this chapter, nanosilica-stabilized $CO_2$ foam for residual oil recovery was investigated.

## 7.1 Experimental Descriptions

### *7.1.1 Materials*

Silica nanoparticles were obtained from *AkzoNobel Corp.* as an aqueous dispersion and diluted with 2.0% NaCl to the desired concentration. Berea sandstone core samples were purchased from Cleveland Quarries. Limestone and dolomite were purchased from Kocurek Industries. Table 7.1 shows the parameters of the core samples.

**Table 7.1 Core Properties**

| Core | | Length (cm) | Diameter (cm) | Porosity | Initial Brine Permeability (md) | Pore volume (ml) |
|---|---|---|---|---|---|---|
| Sandstone | A | 25.4 | 5.4 | 20.5% | 270 | 115 |
| | B | 25.4 | 5.4 | 17.4% | 31 | 100 |
| Limestone | | 25.4 | 5.4 | 18.4% | 106 | 96.7 |
| Dolomite | | 25.4 | 5.4 | 18.5% | 295 | 99.0 |

### *7.1.2 Experimental Devices*

The apparatus used to perform oil recovery experiments is shown in Fig. 7.1. The procedure of the test was similar as in chapter 5 with these differences: (1) a burette with a plug on the top fixed on a frame, used as an oil-gas separator, replaced the liquid trap shown in Fig. 1; (2) the observation cell was removed from the system. For each test, degassed brine was injected into the evacuated core to determine the pore volume at a pore pressure of 1,200 psi. Then the core was flushed with 2–3 pore volumes (PV) of brine to further saturate the core and the initial brine volume in the core was recorded. Finally, 2 PV crude oil were injected into the core followed by a 72 hr soak period at room temperature. The properties of the crude oil sample are listed in Table 7.2. After that, another 2 PV crude oil were injected into the core until no additional brine was being produced. To obtain the residual oil saturation, the core sample with initial oil saturation was flooded with brine. The residual oil saturation was calculated after 5 PV brine were injected into the core. Then the core sample was flooded with $CO_2$ and nanosilica dispersion (particle concentration is 5,000 ppm in 2.0% brine) with the phase ratio of 1:1. After it was injected with 5 PV $CO_2$ and nanosilica dispersion, the core was cleaned with tetrahydrofuran (THF) and dried in preparation for the next study.

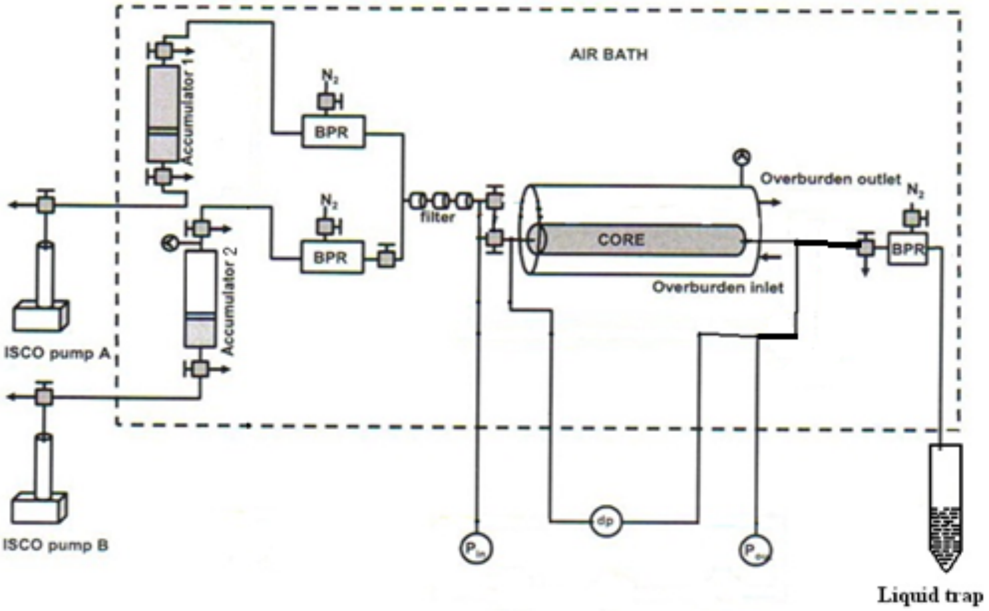

**Fig. 7.1. Schematic diagram of the coreflooding experiments.**

**Table 7.2 Properties of the Crude Oil**

| Oil sample | Temperature (°C) | Density (kg/m$^3$) | Viscosity (cP) | Total acid number (mg KOH/g oil) | Total base number (mg KOH/g oil) |
|---|---|---|---|---|---|
| 1 | 25 | $0.8324\times10^3$ | 5.14 | 0.16 | 0.62 |

## 7.2 Results and discussion

### *7.2.1 Nanosilica-stabilized $CO_2$ foam for oil recovery in Berea Sandstone*

To determine the performance of nanoparticle-stabilized $CO_2$ foam in oil recovery, several coreflooding experiments were implemented using Berea sandstone. Figure 7.2 shows the cumulative oil recovery change versus the injection volume in the Berea sandstone, with permeability of 31 md. Waterfloods in Fig. 7.2 are in the range of 0–5 PV and $CO_2$/nanoparticle dispersion floods are in the 5–10 PV range. When 0.5 PV brine was injected, the total oil recovery from the core was 30.6%. After 1.0 PV brine was injected, recovery increased to 33.1%. Then it increased slowly and reached to 34.7% as 5 PV brine were injected. Following the waterfloods, $CO_2$ and nanosilica dispersion were injected into the core. The cumulative oil recovery increased from 34.7% to 39.7% as 0.5 PV $CO_2$/nanosilica dispersion was injected. Then it increased to 60.5% after 1 PV $CO_2$/nanosilica dispersion was injected. When 5 PV $CO_2$/nanosilica dispersion were injected, the cumulative oil recovery reached 83.4%, where the oil saturation in the core was calculated as 9.95%. The total oil recovery by $CO_2$/nanosilica,

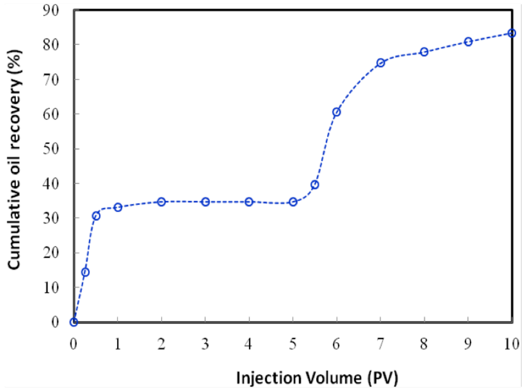

**Fig. 7.2 Cumulative oil recovery change with injection volume (in presence of nanosilica).**

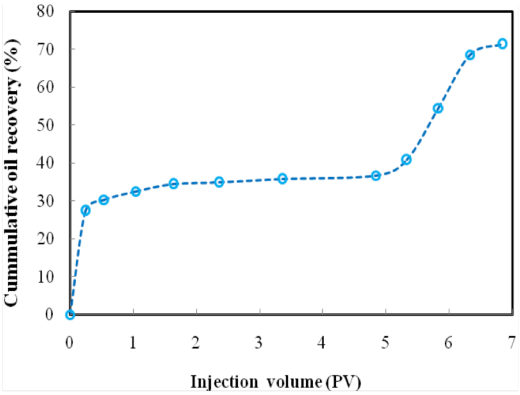

**Fig. 7.3 Cumulative oil recovery change with injection volume (without nanosilica).**

based on the results shown in Fig. 7.2, was calculated as 48.7%. Figure 7.3 shows the cumulative oil recovery change with the injection volume in the absence of nanoparticles with the same core sample. The residual oil saturation was 38.7% when 5 PV of brine was injected. Then $CO_2$/brine was injected into the core. The cumulative oil recovery increased to 54.5% when 1 PV of $CO_2$/brine was injected and 71.28% as 1.85 PV of $CO_2$/brine was injected. Compared with oil recovery of 60.4% and 74.7% when 1 PV and 2 PV $CO_2$/nanosilica dispersion were injected, $CO_2$ foam induced by nanosilica particles could improve an additional of 3–6% of residual oil.[37]

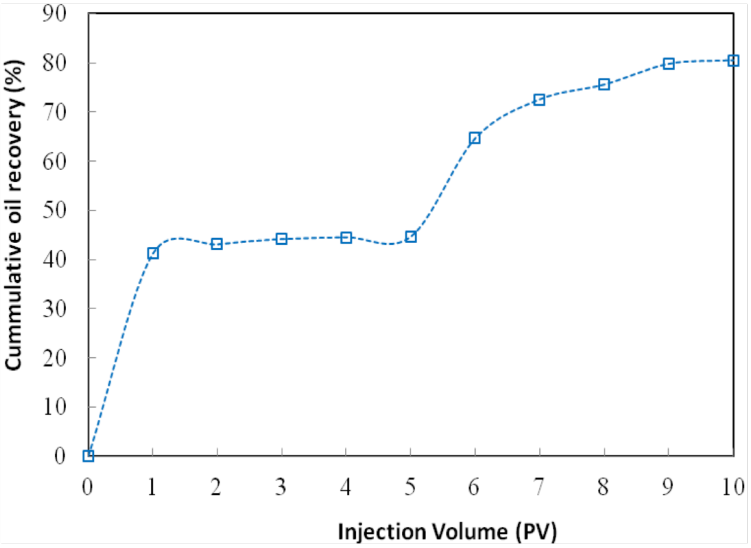

**Fig. 7.4 Cumulative oil recovery change with injection volume (core permeability=270 md).**

Figure 7.4 shows the cumulative oil recovery change with injection volume in the core sample of 270 md. When 1.0 PV brine was injected, 41.2% of the oil was produced from the core. Then it increased to 43.1% as 2.0 PV brine were injected. The cumulative oil recovery stabilized at 44.7% when the injection volume increased from 3.0 PV to 5 PV. When $CO_2$/nanosilica dispersion injection into the core began, the cumulative oil recovery increased from 64.7% to

80.5% when the injection volume of $CO_2$ and nanosilica dispersion increased from 1 PV to 5 PV. The oil saturation in the core was calculated as 13.97% after 5 PV of $CO_2$/nanosilica dispersion were injected. Total oil recovery by $CO_2$/nanosilica, based on the results shown in Fig. 7.4, was calculated as 35.8%.

The oil recovery results revealed that, in low permeability core of 31 md, nanoparticle-stabilized $CO_2$ foam had higher oil recovery efficiency compared with that in the high permeability core (270 md).

### *7.2.2 Pressure effect on the performance of nanoparticle-stabilized $CO_2$ foam for residual oil recovery*

The effect of operation pressure on nanoparticle-stabilized $CO_2$ foam for residual oil recovery was studied. Table 7.3 summarizes the results of nanosilica-stabilized $CO_2$ foam for residual oil recovery under different pressures. Table 7.3 shows the core permeability before crude oil injection in each test. The permeability of the core sample was almost the same in each test, indicating that no particles were plugging the core during the tests. This indicates that, even in contact with the crude oil, the silica nanoparticle dispersion was stable and no particle aggregation or core plugging occurred. The results in Table 7.3 on cumulative oil recovery displayed that the cumulative oil recovery increased with an increase in operation pressure from 1,200 psi to 2,500 psi. For example, the cumulative oil recovery was 80.5% under 1,200 psi and 87.3% under 2,500 psi. This can be atttributed to: (1) the increase in $CO_2$ foam stability with an increase in pressure;[35,38] and (2) the increase in solubility of $CO_2$ in crude oil with an increase in pressure. Normally, the overall displacement efficiency of any oil recovery displacement process can be considered as the product of microscopic and macroscopic displacement efficiencies.[39] As the pressure increases, the interfacial tension between $CO_2$ and brine decreases, resulting in a more stable $CO_2$ foam. This stable $CO_2$ foam could prevent $CO_2$ fingering and result in higher sweep efficiency, which increases the macroscopic displacement efficiency. At the same time, as more $CO_2$ dissolves in oil, the oil will expand and the viscosity will decrease, which in turn decreases the residual oil saturation and improves the microscopic displacement.

Figure 7.5 shows the residual oil recovery (percent of waterflooded residual oil) with operation pressure. Here the residual oil recovery was calculated as $(S_{orw}-S_{orf})/S_{orw}$, where $S_{orw}$ is the oil saturation after waterflooding and $S_{orf}$ is the oil saturation after nanoparticle-$CO_2$ foam flooding. The residual oil recovery increased from 64.9% to 75.8% as the operation pressure increased from 1,200 psi to 2,500 psi. The slow increase of residual oil recovery with pressure increase indicated that all tests of particle-stabilized $CO_2$ foam for residual oil recovery were under, near, or above the minimum miscibility pressure (MMP).[40]] Grigg and Gregory observed that the residual oil recovery decreased dramatically as the operation pressure fell below the MMP in both slim-tube tests and coreflooding tests. However, as the pressure rose above the MMP, the oil recovery increased or slowly increased with the pressure increase.

**Table 7.3 Summary of the Test Results of Nanosilica-Stabilized $CO_2$ Foam for Residual Oil Recovery at Different Pressures (Temp.=25°C)**

| Pressure (psi) | Core permeability (md) | Initial oil saturation (%) | Waterflooded residual oil saturation (%) | Cumulative oil recovery (%) |
|---|---|---|---|---|
| 1200 | 276 | 71.7 | 39.8 | 80.5 |
| 1500 | 270 | 72.2 | 39.7 | 82.1 |
| 2000 | 277 | 69.6 | 36.0 | 85.6 |
| 2500 | 270 | 68.7 | 36.1 | 87.3 |

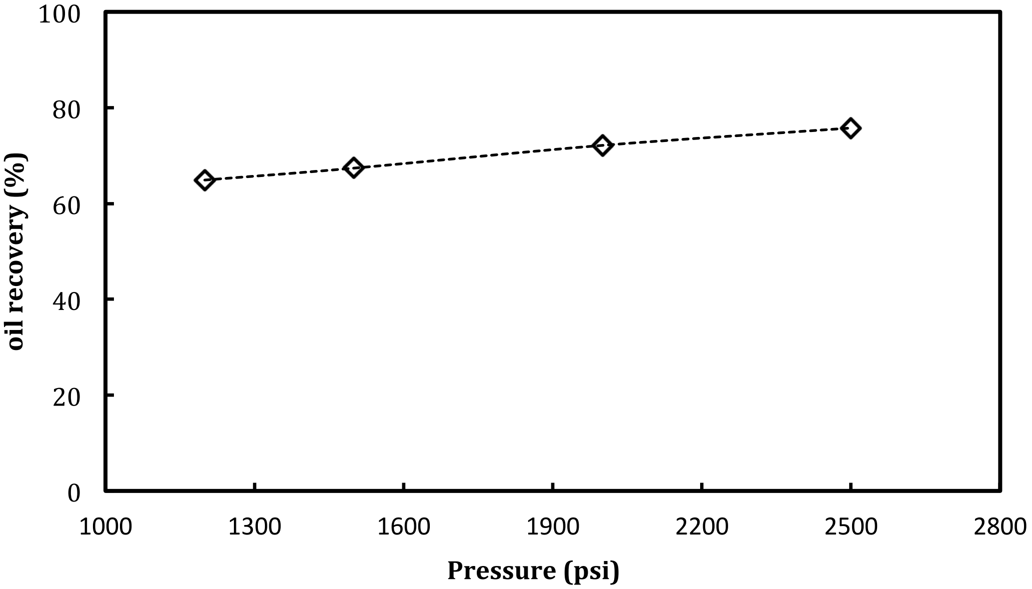

**Fig. 7.5 Residual oil recovery at different pressures (Temp.=25°C).**

### *7.2.3 Temperature effect on the performance of nanoparticle-stabilized $CO_2$ foam for residual oil recovery*

The effect of temperature on nanoparticle-stabilized $CO_2$ foam for residual oil recovery is summarized in Table 7.4. The results displayed in Table 7.4 for cumulative oil recovery show that the cumulative oil recovery by waterflooding increased with temperature from 25°C to 45°C, with no change as temperature increased from 45°C to 60°C. It is known that oil viscosity decreases with temperature increase; thus, the mobility ratio between brine and crude oil decreases with temperature increase, resulting in an increase in oil recovery. The viscosity of the crude oil change with temperature was measured as displayed in Fig. 7.6. The viscosity of the crude oil was 11.3 cp at 25ºC, 6.1 cp at 45ºC, and 5.0 cp at 60ºC. As temperature increased from 25ºC to 45ºC, the oil viscosity decreased from 11.3 cp to 6.1 cp, resulting in an increase in waterflooding oil recovery from 36.7% to 40.0%. However, when the temperature increased from 45ºC to 60ºC, only a slight decrease in oil viscosity was observed (from 6.1 cp to 5.0 cp). This slight decrease in oil viscosity was not observed to substantially improve the waterflooding oil recovery. Table 7.4 also shows that the oil recovery by $CO_2$/nanosilica dispersion decreased with temperature increase from 25ºC to 60ºC. For example, oil recovery was 39.6% at 25ºC, 35.4% at 45ºC, and 31.2% at 60ºC. This decrease can be explained by the stability of particle-stabilized $CO_2$ foam decreasing with an increase in temperature. As the temperature increases, the nanoparticle-stabilized $CO_2$ foam becomes less stable and the $CO_2$ foam sweep efficiency decreases.[35,38]

**Table 7.4. Summary of the Test Results of Nanosilica-Stabilized $CO_2$ Foam for Residual Oil Recovery at Different Temperatures (Pressure=2,000 psi)**

| Temperature (ºC) | Core permeability (md) | Initial oil saturation (%) | Oil recovery by waterflooding (%) | Oil recovery by $CO_2$/nanosilica dispersion (%) | Cumulative oil recovery (%) |
|---|---|---|---|---|---|
| 25 | 176 | 71.3 | 36.7 | 39.6 | 76.3 |
| 45 | 170 | 67.8 | 40.0 | 35.4 | 75.4 |
| 60 | 173 | 66.1 | 40.0 | 31.2 | 71.2 |

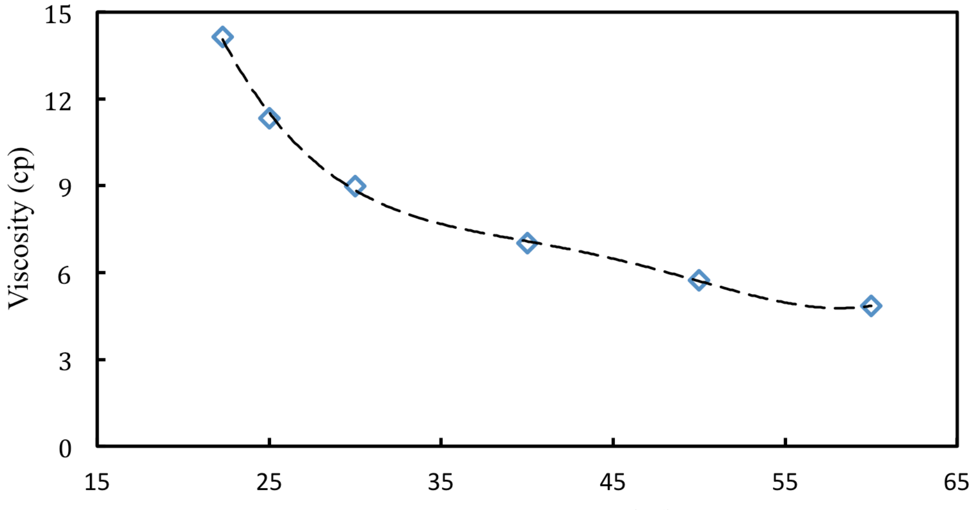

Fig. 7.6 Crude oil viscosity change with temperature.

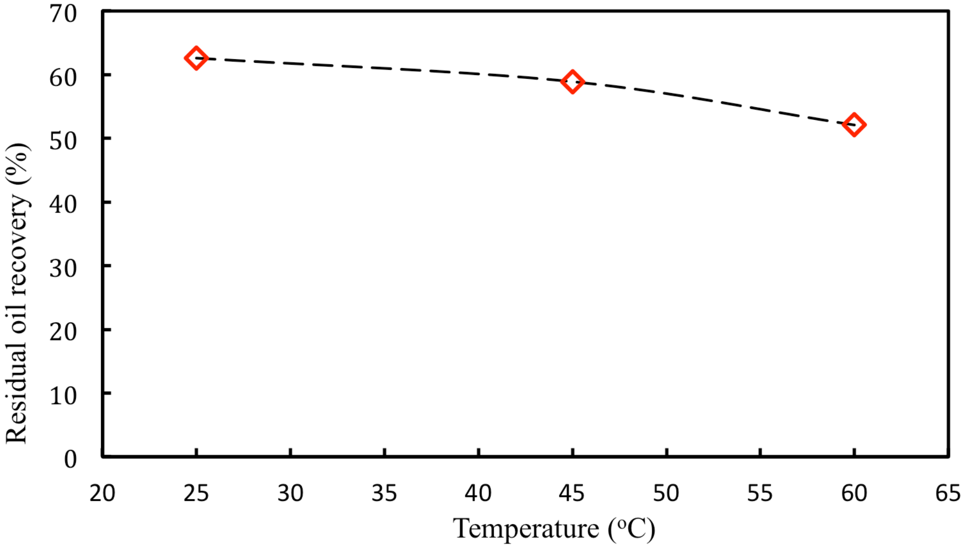

**Fig. 7.7 Residual oil recovery at different temperatures (Pressure=2,000 psi).**

The total oil recovery (by both waterflooding and $CO_2$/nanosilica flooding) also decreased with temperature increasing from 25°C to 60°C. Although the waterflooding efficiency increased with increasing temperature, the decrease of the $CO_2$ foam sweep efficiency with temperature may have had more effect on the total oil recovery. As a result, Figure 7.7 shows the residual oil recovery (percent of waterflooded residual oil) changing with temperature. The results indicated that the efficiencies of residual oil recovery decreased from 62.6% to 52.1% as the temperature increased from 25°C to 60°C.

### *7.2.4 Nanoparticle-stabilized $CO_2$ foam for residual oil recovery from different rock samples*

Table 7.5 summarized the silica particle-stabilized $CO_2$ foam for residual oil recovery from different rock samples, sandstone, limestone, and dolomite. The results indicated that the performance of particle-stabilized $CO_2$ foam for residual oil recovery was 39.6%, 33.2%, and 26.5% from sandstone, limestone, and dolomite, respectively. In addition, we also observed that the core sample permeability of dolomite reduced from 295 md to 110 md after the core was cleaned with THF, which was probably due to the particles plugging in the core.[41]

**Table 7.5 Summary of the Test Results of Nanosilica-Stabilized $CO_2$ Foam for Residual Oil Recovery from Different Rock Samples (Pressure=2,000psi)**

| Core sample | Core permeability (md) | Initial oil saturation (%) | Oil recovery by waterflooding (%) | Oil recovery by CO2/nanosilica dispersion (%) | Cumulative oil recovery (%) |
|---|---|---|---|---|---|
| Sandstone | 176 | 71.3 | 36.7 | 39.6 | 76.3 |
| Limestone | 110 (60) | 50.0 | 33.0 | 33.2 | 66.2 |
| Dolomite | 295 (110) | 64.6 | 69.7 | 26.5 | 96.2 |

# 8, The performance of nanoparticle-stabilized $CO_2$ foam for residual oil recovery in long-term and short-term coreflooding tests

In this chapter, the performance of nanosilica-stabilized $CO_2$ foam for residual oil recovery in long-term and short-term coreflooding tests will be investigated. Residual oil recovery, particle retention, and core permeability change will be measured. In addition, a brief evaluation of this technique will be performed.

## 8.1 Materials and equipment

Silica nanoparticles were obtained from AkzoNobel Corp. as an aqueous dispersion and diluted with 2.0% NaCl to the desired concentration. Berea sandstone core samples were purchased from Cleveland Quarries. The core was cut and polished with the diameter of 2.12 in. and length of 10.0 in. Then the core was mounted in a core holder with an overburden pressure of 4,000 psi. Initial brine permeability and the porosity of the core were measured as 255 md and 18.9%, respectively. For the coreflooding test, the core was first flushed with 2–3 pore volumes (PV) of brine to saturate the core. Then 2 PV crude oil were injected into the core followed by a 72 hr soak period at room temperature. After that, another 1 PV crude oil was injected into the core until no additional brine was being produced. To obtain the residual oil saturation, the core sample with initial oil saturation was flooded with brine. The residual oil saturation was calculated after 5 PV brine were injected into the core. Then the core sample was flooded with $CO_2$ and nanosilica dispersion (particle concentration is 5,000 ppm in 2.0% brine) with the phase ratio of 1:1. After it was injected with 20 PV $CO_2$ and nanosilica dispersion, the core was cleaned with tetrahydrofuran (THF). The cleaned core was dried in the oven for future study. To confirm the calculated results of cumulative oil recovery and residual oil saturation after $CO_2$/nanosilica dispersion flooding, the cleaned effluent (including THF, crude oil, and brine) was collected and distilled. After the THF was distilled from the mixture, the remained solution (crude oil and brine) was transferred and settled in a burette with a plug on the top. By measuring the amount of crude oil in the burette, residual oil saturation after $CO_2$/nanosilica dispersion flooding and the cumulative oil recovery were calculated.

## 8.2 Results and discussions

### *8.2.1 The first time long-term coreflooding test of nanoparticle-stabilized $CO_2$ foam for residual oil recovery*

Figure 8.1 shows the cumulative oil recovery with injection volume from the sandstone at 25ºC and 2,000 psi pressure. The operation temperature was also recorded during the coreflooding test (Refer to Fig. 8.2). The temperature was observed almost not to change during the test (25±1°C), which indicated that the effect of temperature on the oil recovery could be neglected. Before the waterflooding, the initial oil saturation in the core was 75.5%. After 5 PV of brine were injected, total oil recovery was calculated as 49.0% and the residual oil saturation to waterflood was 38.5%. Then $CO_2$/nanosilica dispersion flooding was initiated. The total injection volume of $CO_2$/nanosilica dispersion was 20 PV. The cumulative oil recovery increased to 83.0% when 6 PV of $CO_2$/nanosilica dispersion were injected. After that, the cumulative oil recovery increased slowly, reaching 83.2% when 10 PV of $CO_2$/nanosilica dispersion were injected. Little oil was recovered when the injection volume of $CO_2$/nanosilica dispersion increased from 10 PV to 20 PV. The cumulative oil recovery was 83.2% as 20 PV of $CO_2$/nanosilica dispersion were injected, in which the residual oil saturation to $CO_2$/nanosilica dispersion flooding was 12.7%. The measured residual oil saturation, obtained by distilling the cleaned effluent solution, was 13.8%, in which the cumulative oil recovery was 81.7%. The result is consistent with the former result of cumulative oil recovery of 83.2%, indicating the former calculation is reasonable. The total oil recovery by $CO_2$ and nanosilica was estimated as 34.2%.

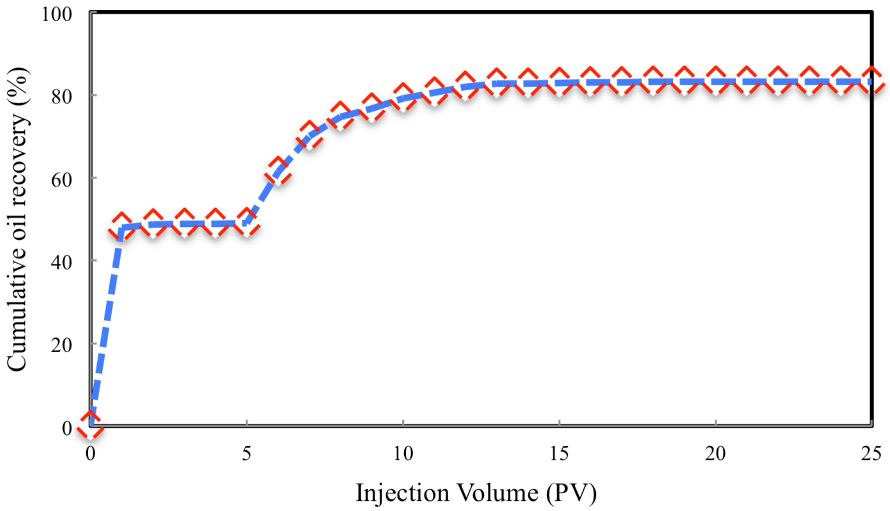

**Fig. 8.1 Cumulative oil recovery change with injection volume (Temp.=25ºC, core permeability=255 md; pressure=2,000 psi).**

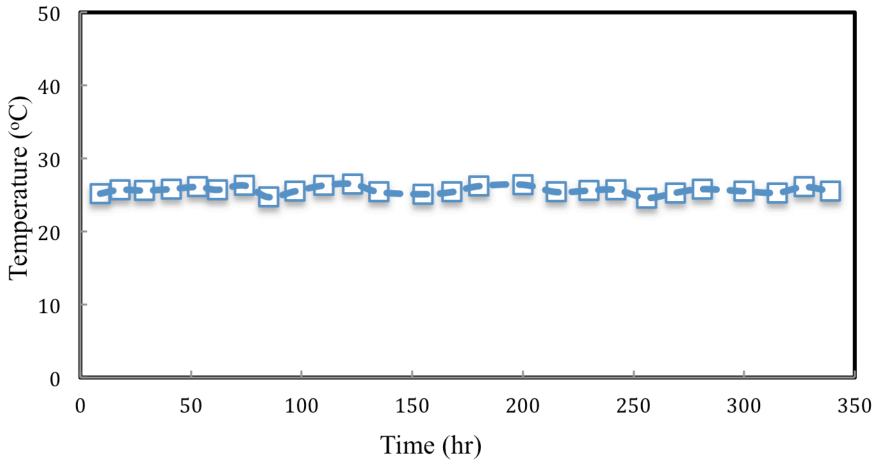

**Fig. 8.2 Temperature change during the long-term coreflooding test.**

Figures 8.3 and 8.4 show the pressure drop across the core during waterflooding and $CO_2$/nanosilica flooding in the long-term test. The pressure drop in the waterflood quickly increased to 12.0 psi and then decreased to 10.8 psi when 0.54 PV of brine were injected into the core. The pressure drop across the core was slowly decreased to 9.6 psi when 5 PV of brine were injected. After the core was brineflooded, it was injected with $CO_2$/nanosilica dispersion. Figure 8.4 shows the pressure drop across the core during the $CO_2$/nanosilica dispersion injection. Because 20 PV of $CO_2$/nanosilica dispersion were injected, 5 PV of $CO_2$/nanosilica dispersion were injected four times. The pressure drop across the core each time increased from ~10 psi and leveled at ~26.5 psi.

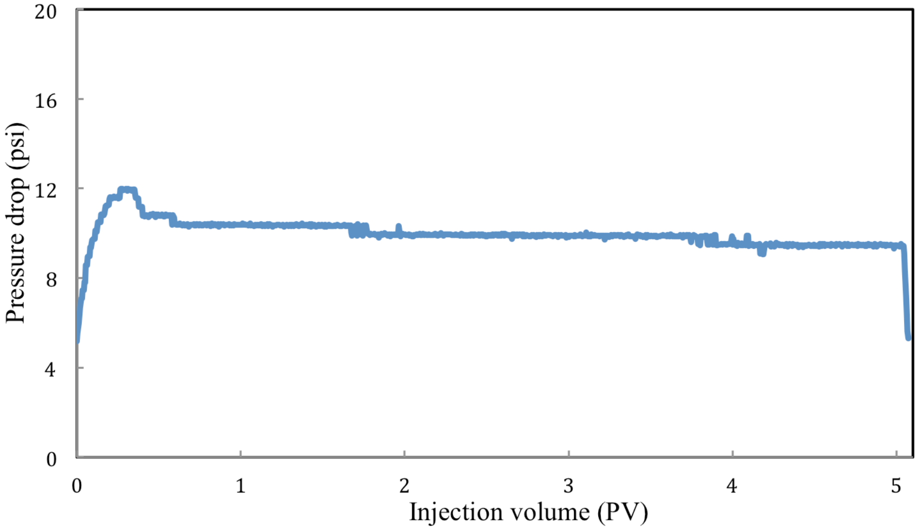

**Fig. 8.3 Pressure drop across the core in waterflood (Temp.=25ºC, pressure=2,000 psi, core permeability=255 md).**

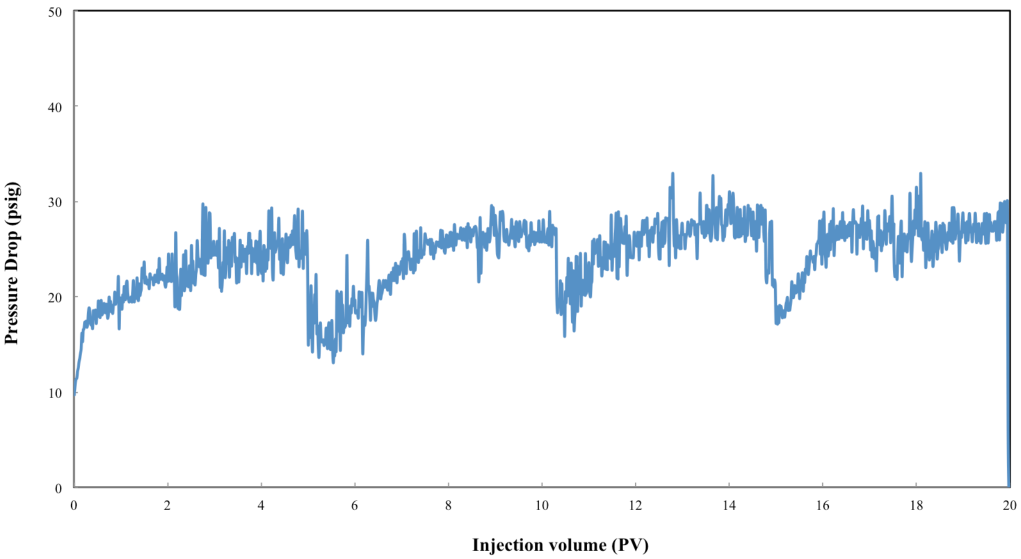

**Fig. 8.4 Pressure drop across the core in $CO_2$/nanosilica dispersion flood (Temp.=25°C, pressure=2,000 psi, core permeability=255 md).**

The effluent water samples were collected at every 5 PV of $CO_2$/nanosilica dispersion injection. Nanosilica concentrations in the effluent water samples were analyzed by ICP-MS to determine the particle recovery during the test. Figure 8.5 displays the nanosilica concentration change in the effluent during $CO_2$/nanosilica dispersion injection. The nanosilica concentration at 0 PV injection volume is the silica concentration in the prepared nanosilica injection dispersion. Figure 8.5 demonstrates that nanosilica concentration in the effluent water solution was almost the same as the injection solution in the second 5 PV of $CO_2$/nanosilica dispersion injection. Based on the results from Fig. 8.5, the total nanosilica recovery was calculated as 96.3% when 20 PV of $CO_2$/nanosilica dispersion were injected. The permeability of the core, after being cleaned with THF, was measured as 184 md. The decrease of the permeability could be attributed to residual oil adsorbed in the core.

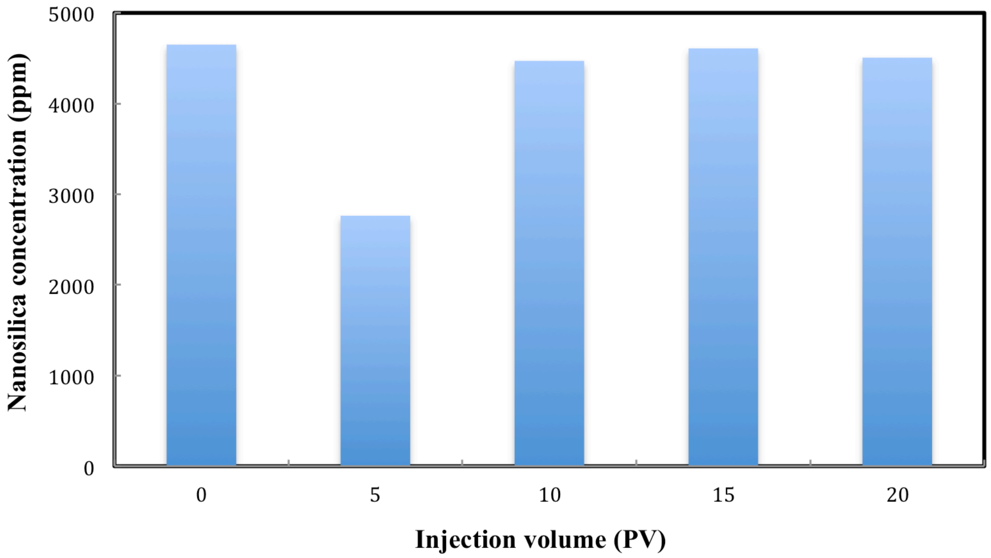

**Fig. 8.5 Nanosilica concentration in the effluent vs. injection volume.**

### *8.2.2, The second long-term core flooding test of nanoparticle-stabilized $CO_2$ foam for residual oil recovery*

After finishing the first long-term coreflooding test of nanoparticle-stabilized $CO_2$ foam for residual oil recovery, we started to perform the second long-term coreflooding test. A new sandstone core sample was polished and cut for the study. Initial brine permeability of the core was measured as 172 mD. Porosity and pore volume of the core were measured as 20.4% and 104 ml, respectively. The initial oil saturation in the core was calculated as 67.3%. Waterflooding residual oil saturation was calculated as 35.4%.

Figure 8.6 shows the cumulative oil recovery with injection volume from the sandstone at 25ºC and 2,000 psi pressure. The operation temperature was $25\pm1^{o}C$ during the test. After 5 PV of brine were injected, total oil recovery was calculated as 47.4% and the residual oil saturation after waterflooding was 35.4%. Then $CO_2$/nanosilica dispersion flooding was initiated. The total injection volume of $CO_2$/nanosilica dispersion was 20 PV. The cumulative oil recovery increased to 82.7% when 10 PV of $CO_2$/nanosilica dispersion were injected. After that, the cumulative oil recovery increased slowly, reaching 83.5% when 14 PV of $CO_2$/nanosilica dispersion were injected. Little oil was recovered when the injection volume of $CO_2$/nanosilica dispersion increased from 14 PV to 20 PV. The cumulative oil recovery was 83.7% as 20 PV of $CO_2$/nanosilica dispersion were injected, in which residual oil saturation to $CO_2$/nanosilica dispersion flooding was 11.0%.

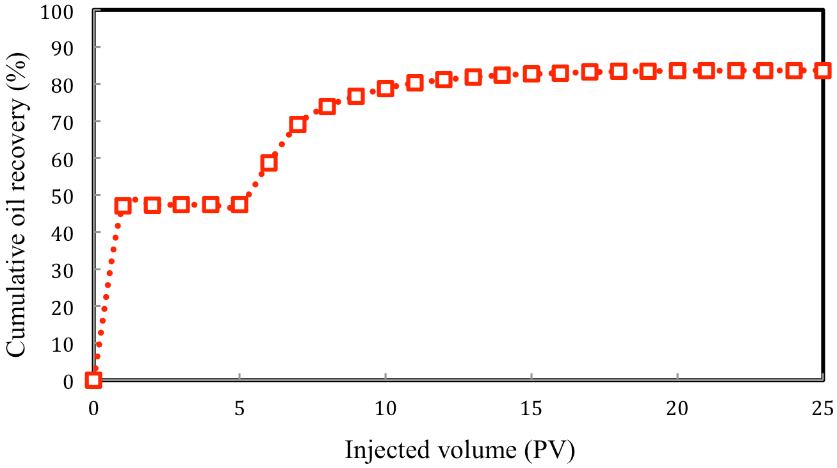

**Fig. 8.6 Cumulative oil recovery change with injection volume (Temp = 25°C, core permeability = 172 md; pressure = 2,000 psi).**

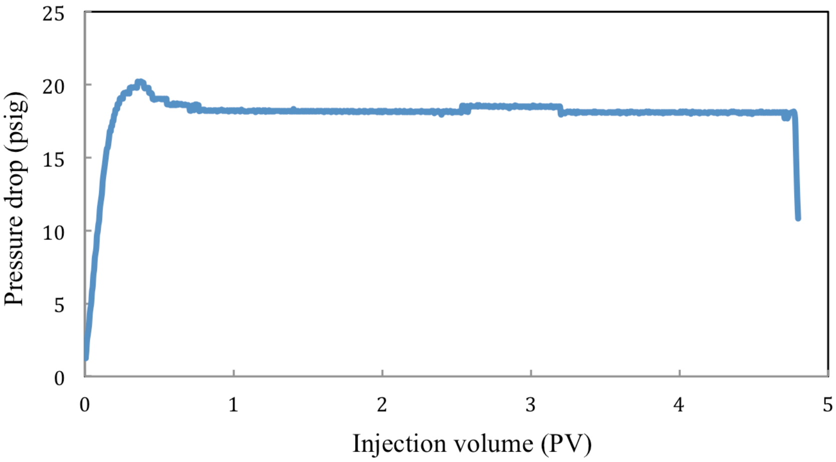

**Fig. 8.7 Pressure drop across the core in waterflood (Temp = 25°C, pressure = 2,000 psi, core permeability = 172 md).**

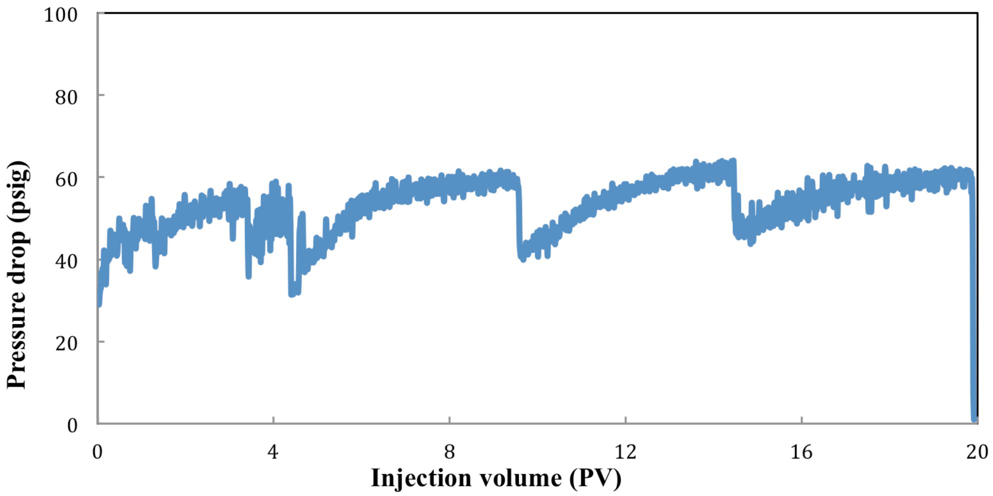

**Fig. 8.8 Pressure drop across the core in $CO_2$/nanosilica dispersion flood (Temp = 25ºC, pressure = 2,000 psi, core permeability = 172 md).**

Figures 8.7 and 8.8 show the pressure drop across the core during waterflooding and $CO_2$/nanosilica flooding. The pressure drop in the waterflood first increased to 19.8 psi and then decreased to 18.3 psi when 0.71 PV of brine were injected into the core. Then the pressure drop leveled at 18.1 psi when 5 PV of brine were injected. After the core was brineflooded, it was injected with $CO_2$/nanosilica dispersion. Figure 8.8 shows the pressure drop across the core during the $CO_2$/nanosilica dispersion injection. The pressure drop across the core increased from ~33 psi and leveled at ~59.2 psi at every 5 PV $CO_2$/nanosilica dispersion injection.

The effluent water samples were collected at each $CO_2$/nanosilica dispersion PV injection to analyze the nanosilica recovery during the test. Figure 8.9 displays the nanosilica concentration change in the effluent during $CO_2$/nanosilica dispersion injection. The nanosilica concentration at 0 PV injection volume is the silica concentration in the prepared nanosilica injection dispersion. The results indicated that nanosilica concentration in the effluent water solution was almost the same as the injection solution in the 6 PV of $CO_2$/nanosilica dispersion injected. Based on the results shown in Fig. 8.9, the total nanosilica recovery was calculated as 93.3% when 20 PV of $CO_2$/nanosilica dispersion were injected. The permeability of the core, after being cleaned with THF, was measured as 110 md.

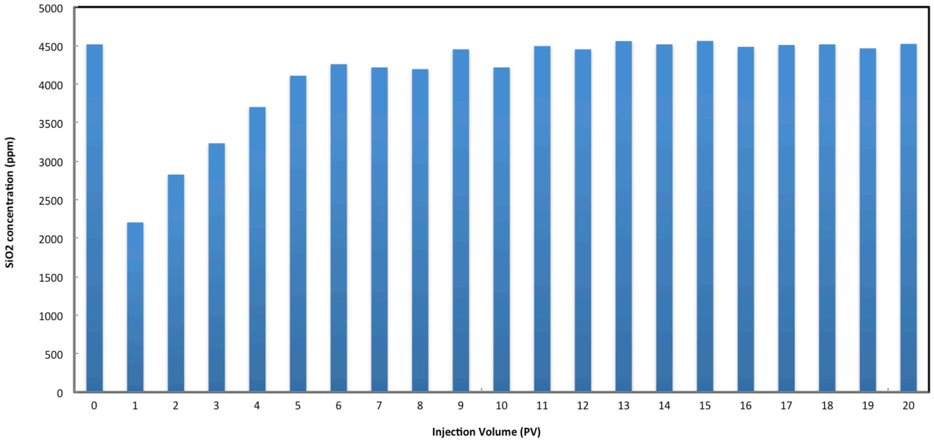

**Fig. 8.9 Nanosilica concentration in the effluent vs. injection volume.**

### *8.2.3 Small volume $CO_2$/nanosilica dispersion coreflooding test for residual oil recovery*

A small-volume $CO_2$/nanosilica dispersion coreflooding was performed to understand the performance of nanosilica-stabilized $CO_2$ foam for residual oil recovery. A sandstone core was prepared and used for this study. The properties of the core are listed in Table 8.1.

**Table 8.1 Core Parameters**

| | |
|---|---|
| Length (inch) | 8.5 |
| Diameter (inch) | 2.1 |
| Porosity (%) | 19.8 |
| Pore volume ($cm^3$) | 95.3 |
| Initial brine permeability (md) | 226 |

Figure 8.10 shows the cumulative oil recovery with injection volume for the second small-volume $CO_2$/nanosilica dispersion coreflooding test. The initial oil saturation in the core was 69.2%. After 5 PV of brine were injected, total oil recovery was calculated as 43.5% and the residual oil saturation to waterflood was 39.2%. Then $CO_2$/nanosilica dispersion flooding was initiated. The cumulative oil recovery increased to 72.3% when 1 PV of $CO_2$/nanosilica dispersion was injected. After that, another 5 PV brine were injected into the core and the cumulative oil recovery increased to 74.5% when 1 PV brine flooded the core. Recovery slowly increased to 75.3% when 5 PV brine were injected into the core. The total nanosilica recovery was calculated as 12.6% when 5 PV of brine were injected. The permeability of the core, after being cleaned with THF, was measured as 182 md.

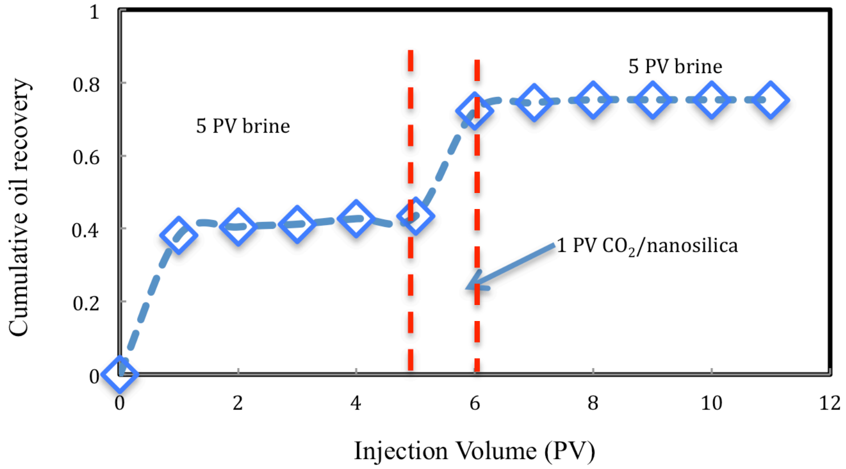

**Fig. 8.10 Cumulative oil recovery vs. brine and NPs/$CO_2$ injection pore volume.**

Figures 8.11–8.13 show the pressure drop across the core during waterflooding, $CO_2$/nanosilica flooding, and the waterflooding after $CO_2$/nanosilica flooding. The pressure drop in the waterflood was first increased to 183.2 psi as 0.18 PV brine were injected into the core. Then the pressure drop decreased to 93.2 psi when 1.0 PV of brine flooded the core and stayed constant during waterflooding. The pressure drop in the $CO_2$/nanosilica flood first increased to 138.3 psi as 0.34 PV of $CO_2$/nanosilica were injected into the core, then slowly decreased to 112.3 psi as 1 PV of $CO_2$/nanosilica flooded the core. Figure 8.13 displays the pressure drop across the core during the waterflooding after the $CO_2$/nanosilica flooding. The pressure drop decreased from 89.2 psi to 23.4 psi when 2 PV of brine flooded the core. Then the pressure drop stayed almost constant until 5 PV of brine were injected into the core.

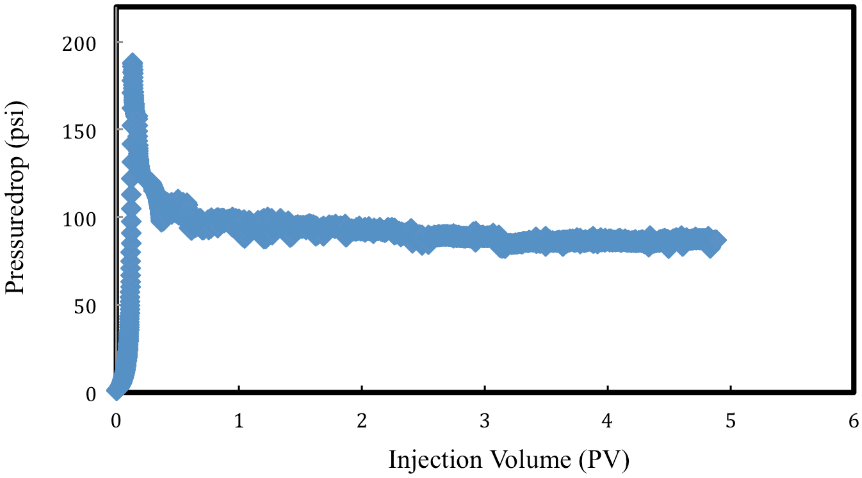

**Fig. 8.11 Pressure drop during waterflooding.**

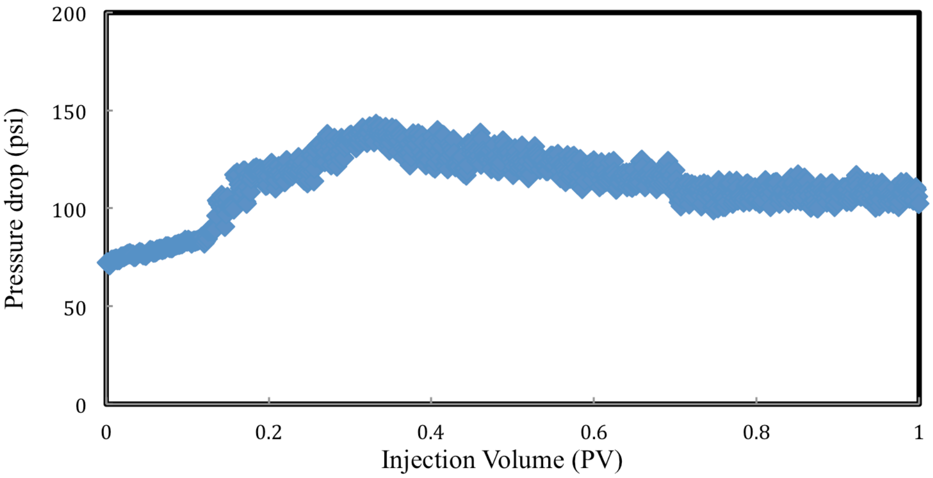

**Fig. 8.12 Pressure drop across the core in $CO_2$/nanosilica flooding.**

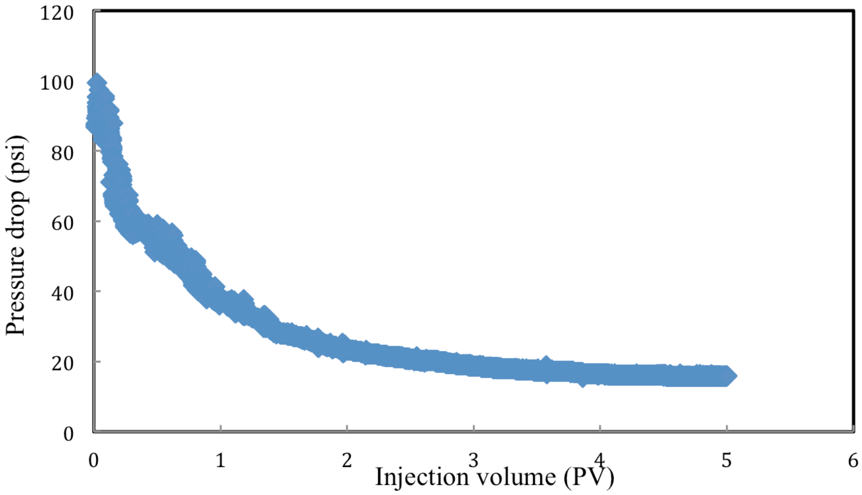

**Fig. 8.13 Pressure drop across the core in the second waterflood.**

### 8.3 Summary of this technique and economic evaluation

Currently, nanotechnology is still a new method in oil industry for improving oil and gas production. Our laboratory results indicated that stable $CO_2$ foams were generated at reservoir conditions as liquid $CO_2$ and nanosilica dispersion flowed through a porous media. The generated $CO_2$ foam could decrease the $CO_2$ mobility and improve the $CO_2$ sweep efficiency. In addition, out results also indicated that the silica nanoparticles could easily pass through core samples without changing the core permeability. The nanoparticle-stabilized $CO_2$ foam demonstrated recovery of more than 30% residual oil after waterflooding, both in long-term and short-term coreflooding tests. However, there is field demonstration with nanoparticles for oil industry application. To comprehensively evaluate this technique, a comparison between this technique with surfactants is listed as following:

1, Particle or surfactant concentration during $CO_2$ foam generation. When surfactant is used to generate $CO_2$ foam, the surfactant concentration is normally higher than its critical micelle concentration (CMC), in which it is expected that stable $CO_2$ foam is formed. There has been some research investigating $CO_2$ foam generated with different surfactants.[42-44] For example, Guo et al. reported that stable $CO_2$ foam was generated with the surfactant ISO2024 (from Stepan) at a concentration of 0.5 wt% or blended surfactant concentration of 0.37 wt% ISO2024 and 0.14 wt% ISO1518 (from Shell).[43] Liu et al. also reported that the CMC for surfactant CD1045$^{TM}$ (from Chaser International Corp.) was around 0.7 wt%.[35,44] When nanoparticles are used to generate $CO_2$ foam, based on our results, it was observed that $CO_2$ form was generated when the nanosilica concentration was 0.02 wt%. Stable $CO_2$ foam was generated as the particle concentration increased to 0.05 wt%.

2, Stability of the $CO_2$ foam generated by nanoparticles and surfactants. $CO_2$ foam stability is a critical parameter for $CO_2$ mobility control in $CO_2$ EOR. A weak $CO_2$ foam is easy to lost its function during the $CO_2$ flooding and results in low $CO_2$ sweep efficiency. The stability of $CO_2$ foam by nanoparticles, as discussed in Chapter 1, displayed excellent long-term stability. The results based on this project indicated that the $CO_2$ foam generated with 0.5 wt% nanosilica dispersion could stand for 3 days with little foam collapse. More recently, the results on nanosilica-stabilized $CO_2$ foam demonstrated that the $CO_2$ foam displayed excellent stability; for example, the height of the $CO_2$ foam did not change after 7 days. In addition, the use of nanoparticles to stabilize aqueous foams was reported. For example, Martinez et al. observed nanosilica-stabilized N2 foam could stand for 9 months.[45] Worthen et al.[33] and Binks et al.[3] also reported long-term stable $CO_2$/air foam generated by nanoparticles. However, $CO_2$ foam generated with surfactant displayed different stability, for example, 60 min. to 2 hours. Commonly, flocculation of water droplets is a common problem for surfactant-stabilized W/C emulsions as a consequence of poor solvation of the surfactant tail groups by $CO_2$. By comparing the $CO_2$ foam generated with nanosilica and surfactants, Adkins et al.[4] observed that no coalescence of water drops occurred over many hours even days when silica nanoparticles were used. However, coalescence of water drops has been observed for surfactant stabilized $CO_2$ foam within 3-4 hours at 15 MPa stabilized by 1 wt% PDMS-b-PAA with 50% $CO_2$ by weight.

3, Particle and surfactant adsorption on rock surface. Surfactants were widely reported to be adsorbed on rock surface. The loss due to rock adsorption leads to surfactant losing its function during oil recovery, but also increases the operation cost. To minimize adsorption loss, Grigg and Bai[46,47] designed a strategy to use a cheap sacrificial surfactant Lignosite® 100 (calcium lignosulfonate) to prevent surfactant CD1045™ adsorption. On the other hand, rock adsorption on nanoparticles is negligible. Our results on this project indicated that almost 98% of the nanosilica flowed out from the core after the long-term coreflooding tests for residual oil recovery.

4, The performance of nanosilica- and surfactant-stabilized $CO_2$ foam. Both nanoparticle-and surfactant-stabilized $CO_2$ foam were observed to decrease $CO_2$ mobility in porous media. In the presence of nanoparticle or surfactant, the total mobility (mobility of $CO_2$ and brine) clearly decreased, compared with the mobility in the absence of nanoparticle or surfactant. It was also observed that the mobility of $CO_2$ and brine increased with the phase ratio of $CO_2$/brine increase from 0.7 to 0.9. $CO_2$ foam, stabilized by nanoparticles or surfactants, could improve residual oil recovery. Nanosilica-stabilized $CO_2$ foam could recovery ~30% residual oil after the waterflooding. Yin et al.[37] reported that more than 20% residual oil was recoveried when surfactant CD1045$^{TM}$ and $CO_2$ flooded the core.

5, Cost of nanoparticle and surfactant. There are quite a few surfactants available on the market. The costs for different surfacants are different, range from \$0.20/lbm to several dollar/lbm.

However, there are not many commercial nanoparticle products available at present. The nanosilica dispersion used for this project is from AkzoNobel Corp. which has price of \$2.25/lbm. The cost will be lower if larger volumes of nanosilica dispersion are purchased.

Since nanotechnology is a new method in oil and gas industy, our evaluation is limited to the laboratory results. Considering the complicated conditions of the reservoir, more research results and field test data on this technology will give us more information to evaluation this technology.

# 9. Technology Transfer

A considerable number of papers and presentations were generated in the pursuit of this research project. These include:

Munawar Khalil, Robert Lee, Ning Liu “Hematite nanoparticles in aquathermolysis: A desulfurization study of thiophene”, *Fuel* 145 (**2015**) 214-220.

Jianjia Yu, Munawar Khalil, Ning Liu, Robert Lee “Effect of particle hydrophobicity on $CO_2$ foam generation and the foam flow behavior in porous media”, *Fuel* 126 (**2014**) 104-108.

Munawar Khalil, Jianjia Yu, Ning Liu, Robert Lee “Non-aqueous hydrophobicity modification of synthesized hematite nanoparticles with Oleic acid*”, Colloids and Surfaces A: Physicochemical and Engineering Aspects* 453 (**2014**) 7-12.

Munawar Khalil, Jianjia Yu, Ning Liu, Robert Lee “Hydrothermal synthesis, characterization and growth mechanism of hematite nanoparticles”, *Journal of Nanoparticles Research* 16 (**2014**) 2362-2371.

Jianjia Yu, Sai Wang, Ning Liu, Robert Lee “Effect of particle hydrophobicity on the flow behavior of nanoparticle-stabilized $co_2$ foam in porous media,” paper SPE 169047 presented at the SPE Improved Oil Recovery Symposium to be held in Tulsa, Oklahoma, USA, 12-16 April, **2014**.

Jianjia Yu, Bao Jia, Ning Liu, Robert Lee “Nanoparticle-stabilized $CO_2$ foam for oil recovery at different pressure, temperature, and rock samples” paper SPE 169110 presented at the SPE Improved Oil Recovery Symposium to be held in Tulsa, Oklahoma, USA, 12-16 April, **2014**.

Jiajia Yu, Di Mo, Ning Liu, Robert Lee "The application of nanoparticle-stabilized $CO_2$ foam for oil recovery", paper SPE 164074 presented at the SPE International Symposium on Oilfield Chemistry held in Woodlands, Texas, USA, 8-10 April, **2013**.

Di Mo, Jianjia Yu, Ning Liu, Robert Lee, "Study of the effect of different factors on nanoparticle-stabilized $CO_2$ foam for mobility control," paper SPE 159282 presented at the SPE Annual Technical Conference and Exhibition held in San Antonio, Texas, USA, 8-10 October, **2012**.

Jianjia Yu, Cheng An, Ning Liu, Robert Lee, "Foam Mobility Control for Nanoparticle-Stabilized Supercritical $CO_2$ Foam", paper SPE 153336 presented at the SPE Symposium on Improved Oil Recovery to be held in Tulsa, USA, April 14-18, **2012**.

Jianjia Yu, Cheng An, Di Mo, Ning Liu, Robert Lee, "Study of adsorption and transportation behavior of nanoparticles in three different porous media", paper SPE 153337 presented at the SPE Symposium on Improved Oil Recovery to be held in Tulsa, USA, April 14-18, **2012**.

Jianjia Yu, Ning Liu, Liangxiong Li, Robert Lee, "Generation of nanoparticle-stabilized supercritical $CO_2$ foams," Paper CMTC 150849 presented at the Carbon Management Technology Conference to be held in Orlando, Florida, USA, February 7-9, **2012**.

# 10, Conclusions

The following conclusions are drawn based on the work performed:

1) Nanosilica particle dispersion such as Bindzil CC301 from AkzoNobel Chemicals Inc displayed excellent ion and temperature resistivity. No particle aggregation or precipitation was observed as the dispersion was as high in TDS as 180,013ppm brine or as high temperatures as 85°C. This implies that nanosilica dispersion can work in oil reservoir without particle aggregation.

2) Silica nanoparticles could easily pass through the sandstone core without changing the core permeability. Little adsorption was observed as nanosilica particles flooded the limestone core, but the core permeability was not changed. Core plugging occurred and core permeability was changed as the particles flowed through dolomite core.

3) Stable $CO_2$-foams were generated at reservoir conditions as liquid $CO_2$ and nanosilica mixture flowed through a porous media. $CO_2$ foam could be generated with the nanosilica concentration as low as 500 ppm. With the increase of nanosilica concentration, foam mobility decreased and the foam resistance factor increased. The $CO_2$ foam mobility remained almost constant as the foam quality increased from 20% to 60% and then increased when further increased the foam quality.

4) A synergistic interaction between the surfactant and nanosilica particles was observed as $CO_2$/nanosilica dispersion + surfactant flowed through a porous media for $CO_2$ foam generation. This result indicates that low concentration nanoparticle and surfactant mixture can be used in the future for $CO_2$ mobility control.

5) Nanoparticle-stabilized $CO_2$ foam was observed to improve the residual oil recovery. The residual oil recovery (percent of waterflooded residual oil) by $CO_2$/nanosilica flooding increased when the pressure was increased from 1,200 psi to 2,500 psi and decreased when the temperature increased from 25°C to 60°C. Nanoparticle-stabilized

$CO_2$ foam also improved residual oil recovery from limestone and dolomite after waterflooding. Core permeability was observed to decrease for dolomite after the test.

6) Long-term coreflooding test of nanoparticle-stabilized $CO_2$ foam for residual oil recovery indicated that after 20 PV of $CO_2$/nanosilica dispersion were injected into the core, total nanoparticles recovery during $CO_2$/nanosilica dispersion flooding was ~95.3%. No significant core permeability change was observed, indicating no particle plugging occurred during the long-term coreflooding.

7) Small volume $CO_2$/nanosilica dispersion coreflooding tests displayed that ~32% oil was recovered as 1 PV $CO_2$/nanosilica dispersion was flooded the core.

# References:

1. Martin F.; Taber J. "Carbon dioxide flooding", *Journal of Petroleum Technology* 44 (**1992)** 396-400.
2. Espinosa, D.; Caldelas, F.; Johnston, K.; Bryant, L.; Huh, C. "Nanoparticle-stabilized supercritical CO2 foams for potential mobility control applications", paper SPE 129925 presented at the SPE Improved Oil Recovery Symposium held in Tulsa, Oklahoma, U. S. A., 24-28 April **2010**.
3. Brinks, B.; Horozov, T. "Aqueous foams stabilized solely by silica nanoparticles", *Angew. Chem. Int. Ed.* 44 (**2005**) 3722-3725.
4. Adkins, S.; Gohil, D.; Dickson, J.; Webber, S.; Johnston, K. "Water-in-carbon dioxide emulsions stabilized with hydrophobic silica particles", *Physical Chemistry Chemical Physics* 9 (**2007**) 6333-6343.
5. Gonzenbach, U.; Studart, A.; Tervoort, E.; Gauckler, J. "Tailoring the microstructure of particle-stabilized wet foams", *Langmuir* 23 (**2007**) 1025-1032.
6. Dickson, J.; Binks, B.; Johnston, K. "Stabilization of carbon dioxide-in-water emulsions with silica nanoparticles", *Langmuir* 20 (**2004**) 7976-7983.
7. Binks, B. "particles as surfactants-similarities and differences", *Current Opinion in Colloid & Interface Science* 7 (**2002**) 21-41.
8. Zhang, T.; Roberts, M.; Bryant, S.; Huh, C. "Foams and emulsions stabilized with nanoparticles for potential conformance control applications", paper SPE 121744 present at the SPE International Symposium on Oilfield Chemistry held in Woodlands, Texas, USA, 20-22 April **2009**.
9. Rodriguez, E.; Roberts, M.; Yu, H.; Huh, C.; Bryant, S. "Enhanced migration of surface-treated nanoparticles in sedimentary rocks", paper SPE 124418 present at the SPE Technical Conference and Exhibition held in New Orleans, Louisiana, USA, 4-7 October **2009**.
10. Bernard P. Binks; John Philip; and Jhonny A. Rodrigues "Inversion of silica-stabilized emulsions induced by particle concentration", *Langmuir* 21 (**2005**) 3296-3302.
11. Tommy S. Horozov; Robert Aveyard; John H. Clint; and Bernard P. Binks "Order-disorder transition in monolayers of modified monodisperse silica particles at the Octane-water interface", *Langmuir* 19 (**2003**) 2822-2829.

12. A. Stocco; E. Rio; B.P. Binks; and D. Langevin "Aqueous foams stabilized solely by particles", *Soft Matter* 7 (**2011**) 1260-1267.
13. Kostakis T, Ettelaie R, Murray BS "Effect of high salt concentration on the stabilization of bubbles by silica particles", *Langmuir* 22 (**2006**) 1273-1280.
14. Dickinson E, Ettelaie R, Kostakis T, Murray BS "Factors controlling the formation and stability of air bubbles stabilized by particle hudrophobic silica nanoparticles", *Langmuir* 20 (**2004**) 8517-8525.
15. Liu N, Ghorpade S, Harris L, Li L, Grigg R, Lee R, "The Effect of Pressure and Temperature on Brine-$CO_2$ Relative Permeability and IFT at Reservoir Conditions", SPE 139029 presented at the SPE Eastern Regional Meeting held in Morgantown, West Virginia, USA, 12–14 October **2010**.
16. Li L, Dong J, Nenoff TM. "Transport of water and alkali metal ions through MFI zeolite membranes during reverse osmosis", *Sep Purif Technol* 53 (**2007**) 42–48.
17. Sanders AW, Johnston KP, Nguyen Q, Adkins S, Chen X, Rightor EG. Dispersion compositions with nonionic surfactant for use in petroleum recovery, U.S. Patent US 2012/0103635 A1, May 3, **2012**.
18. Farajzadeh R, Andrianov A, Bruining H, Zitha PLJ. "Comparative study of $CO_2$ and $N_2$ foams in porous media at low and high pressure–temperatures", *Ind Eng Chem Res* 48 (**2009**) 4542–4552.
19. Khalil F, Asghari K. "Application of $CO_2$-foam as a means of reducing carbon dioxide mobility", *J Can Pet Technol* 45 (**2006**) 37–42.
20. Mohammed Alaskar, Morgan Ames, Steve Connor, Chong Liu, Yi Cui, Kewen Li, Roland Horne "Nanoparticle and microparticle flow in porous and fractured midia: An experimental study", paper SPE 146752 presented at the SPE Annual Technical Conference and Exhibition held in Denver, Colorado, USA, 30 October-2 November **2011**.
21. Federico Caldelas, Michael J. Murphy, Chun Huh, Steven L. Bryant "Factors governing distance of nanoparticle propagation in porous media", paper SPE 142305 presented at the SPE Production and Operation Symposium held in Oklahoma City, Oklahoma, USA, 27-29 March **2011**.

22. P. Moulin, H. Roques “Zeta potential measurement of calcium carbonate”, *Journal of Colloid and Interface Science* 261 (**2003**) 115-126.
23. Q.P. Nguyen, Peter K. Currie, P.S.R. Bouzanga “The effect of gas on the injectivity of particles in sandstone”, *SPE Journal* 16 (**2011**) 95-103.
24. Ettinger, R.A. "Foram flow resistance in Berea sandstone", M.S. Thesis, University of California, Berkeley, CA, **1989**.
25. Aronson, A.S., Bergeron, V., Fagan, M.E., Radke, C.J. "The influence of disjoining pressure on foam stability and flow in porous media", *Colloids and Surf. A* 83 (**1994**) 109.
26. Lee, H.O. and Heller, J.P. "Laboratory measurements of $CO_2$-foam mobility", *SPE Reservoir Engineering*, 5 (**1990**): 193-197.
27. Yaghoobi, H. "Laboratory investigation of parameters affecting $CO_2$-foam mobility in sandstone at reservoir conditions", Paper SPE 29168 presented at the SPE Eastern Regional Meeting held in Charleston, West Virginia, USA, 8-10 November, **1994**.
28. Khatib, Z.I. and Hirasaki, G.J. "Effects of capillary pressure on coalescence and phase mobilities in foams flowing through porous media", *SPE Reservoir Engineering*, 3 (**1998**) 919-926.
29. Chang, S.H. and Grigg, R.B "Effects of foam quality and flow rate on $CO_2$-foam behavior at reservoir temperature and pressure", *SPE Reservoir Evaluation & Engineering*, 2 (**1999**) 248-254.
30. De Vries, A.S., and Wit, K. "Rheology of gas/water foam in the quality range relevant to steam foam", *SPE Reservoir Engineering*, 5 (**1990**) 185-192.
31. P.A. Gauglitz, F. Friedmann, S.I. Kam, W.R. Rossen “Foam generation in porous media”, Paper SPE 75177 presented at the SPE/DOE Improved Oil Recovery Symposium held in Tulsa, Oklahoma, USA, 13-17 April **2002**.
32. Breit, G.N. “Produced water database” United States Geological Survey **2003**.
33. Worthen, A.J.; Bryant, S.L.; Huh, C.; Johnston, K.P. “Carbon dioxide-in-water foams stabilized with nanoparticles and surfactant acting in synergy” *AIChE Journal* 59 (**2013**) 3490-3500.
34. Cui, Z.G.; Cui, Y.Z.; Cui, C.F.; Chen Z.; Binks, B.P. “Aqueous foams stabilized by in situ surface activation of $CaCO_3$ nanoparticles via adsorption of anionic surfactant”, *Langmuir* 26 (**2010**) 12567-12574.

35. Yi Liu, Reid Barlow Grigg, Robert Kenneth Svec, "$CO_2$ foam behavior: Influence of temperature, pressure, and concentration of surfactant", paper SPE 94307 presented at the SPE Production and Operations Symposium held in Oklahoma city, OK, USA, April 17-19, **2005**.
36. Yi Liu, Reid Barlow Grigg, Robert Kenneth Svec, "Foam mobility and adsorption in carbonate core", paper SPE 99756 presented at the SPE/DOE Symposium on Improved Oil Recovery held in Tulsa, Oklahoma, USA, April 22-26, **2006**.
37. Guoqiang Yin, Reid B. Grigg, Yi Svec "Oil recovery and surfactant adsorption during $CO_2$-foam flooding", paper OTC 19787 presented at the Offshore Technology Conference held in Houston, Texas, USA May 4-7 **2009**.
38. J. Yu, N. Liu, L. Liang, R. Lee "Generation of nanoparticle-stabilized supercritical $CO_2$ foams", paper CMTC-150849 presented at the Carbon Management Technology Conference held in Orlando, Florida, USA, 7-9 February **2012**.
39. D. W. Green, G. Paul Willhite "Enhanced oil recovery", SPE Textbook Series vol. 6, Society of Petroleum Engineers **1998**.
40. R.B. Grigg, M.D. Gregory, J.D. Purkaple "Effect of pressure on improved oilflood recovery from tertiary gas injection", *SPE Reservoir Engineering*, 12 (**1997**) 179-187.
41. J. Yu, C. An, D. Mo, N. Liu, R. Lee "Study of adsorption and transportation behavior of nanoparticles in three different porous media", paper SPE-153337 presented at the Eighteenth SPE Improved Oil Recovery Symposium held in Tulsa, Oklahoma, USA, 14-18 April **2012**.
42. J.S. Kim, Y. Dong, W.R. Rossen "Steady-state flow behavior of $CO_2$ foam" *SPE Journal* 10 (**2005**) 405-415.
43. Hua Guo, Pacelli L.J. Zitha, Rien Faber, Marten Buijise "A novel alkaline/surfactant/foam enhanced oil recovery process" *SPE Journal* 17 (**2012**) 1186-1195.
44. Yi Liu, Reid B. Grigg, Baojun Bai "Salinity, pH, and surfactant concentration effects on $CO_2$-foam", paper SPE 93095 presented at the SPE International Symposium on oilfield Chemistry held in Houston, Texas, USA, 2-4 February **2005**.

45. A. Cervantes Martinez, E. Rio, G. Delon, A. Saint-Jalmes, D. Langevin, B.P. Binks "On the origin of the remarkable stability of aqueous foams stabilised by nanoparticles: link with microscopic surface properties", *Soft Matter* 4 (**2008**) 1531-1535.
46. Baojun Bai, Reid B. Grigg "Kinetics and Equilibria of Calcium Lignosulfonate Adsorption and Desorption onto Limestone", paper SPE 93098 presented at the SPE International Symposium on oilfield Chemistry held in Houston, Texas, USA, 2-4 February **2005**.
47. Reid B. Grigg, Baojun Bai, Yi Liu "Competitive adsorption of a hybrid surfactant system onto five Minerals, Berea Sandstone, and Limestone" paper SPE 90612 the SPE Annual Technical Conference and Exhibition held in Houston, Texas, USA, 26–29 September **2004**.